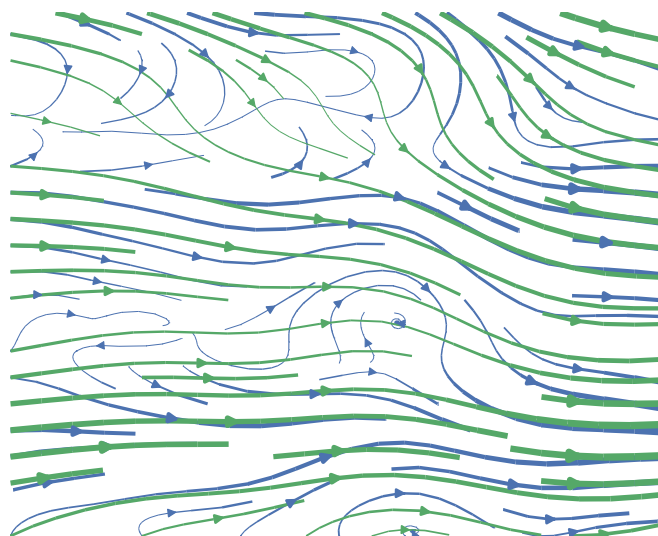


Friedrich-Schiller-Universität Jena

**Filtered Density Functions for
Uncertainty Assessments of Transport in
Groundwater**

Dissertation

Lennart Schüler



Filtered Density Functions for Uncertainty Assessments of Transport in Groundwater

Dissertation

zur Erlangung des akademischen Grades doctor rerum naturalium
(Dr. rer. nat.)

vorgelegt dem Rat der Chemisch-Geowissenschaftlichen Fakultät der
Friedrich-Schiller-Universität Jena

von Dipl.-Phys. Lennart Schüler
geboren am 28. August 1985 in Lübeck

Gutachter:

1. _____

2. _____

Tag der öffentlichen Verteidigung: _____

Zusammenfassung

Schätzungsweise fünfzig Prozent des globalen Trinkwassers wird dem Grundwasser entnommen. Dementsprechend ist das Grundwasser eine sehr wichtige natürliche Ressource. Allerdings wird die Qualität des Grundwassers durch eine Vielzahl von Schadstoffen aus unterschiedlichen Quellen gefährdet. Risikoanalysen werden auf geohydrologische Systeme angewendet um abzuschätzen, ob Ökosysteme oder Menschen durch Verunreinigungen des Grundwassers gefährdet sind. In diesem Zusammenhang ist das Risiko nicht nur von den Auswirkungen der Schadstoffe auf Ökosysteme oder auf den menschlichen Körper abhängig, sondern auch von der Ausbreitung der Schadstoffe im Grundwasser. Zum Beispiel ob eine Schadstoffwolke einen Brunnen kontaminieren könnte. Die Eigenschaften des Untergrunds, wie etwa die Leitfähigkeit, haben einen starken Einfluss auf die Grundwasserströmung und damit auch auf den Transport von gelösten Stoffen. Der Mangel an Daten zusammen mit der Heterogenität des Untergrunds sind der Grund dafür, dass die Unsicherheit bei der Vorhersage des Schadstofftransports oft so groß ist, dass sie nicht vernachlässigt werden kann. Infolgedessen muss diese Unsicherheit in Risikobewertungen berücksichtigt werden. Dies ist durch eine geostatistische Repräsentation des Untergrunds möglich, welche zu einer wahrscheinlichkeitstheoretischen Beschreibung der Transportprozesse führt.

Die Methode der Wahrscheinlichkeitsdichtefunktionen (PDF) bietet eine Möglichkeit nicht nur den Transport von Schadstoffen, sondern auch die Unsicherheiten in einem integrierten Framework zu berechnen. Eine Transportgleichung der Konzentrations-PDF wird dazu aufgestellt und gelöst. Statistische Momente, wie die mittlere Konzentration oder die Konzentrationsvarianz, können direkt aus der PDF berechnet werden. Allerdings haben PDF-Methoden einen Nachteil, wenn sie auf den Grundwassertransport angewendet werden. Um die Parameter für die PDF-Transportgleichung aus den Eigenschaften des Untergrunds zu berechnen, müssen stochastische Mittel unter der Annahme der statistischen Homogenität der Leitfähigkeitsfelder berechnet werden. Dies ist problematisch, da die statistische Homogenität durch das konditionieren von räumlichen Zufallfeldern auf Messdaten zerstört wird. Des Weiteren hat jedes Messgerät ein spezifisches Stützvolumen über welches die gewonnenen Daten gemittelt werden. Diese unterschiedlichen Stützvolumen führen wegen der Heterogenitäten im Untergrund zu unterschiedlichen Messergebnissen. Dadurch wird es schwierig diese Messdaten mit numerischen Methoden, wie die PDF-Methoden, zu vergleichen. Wenn räumlich gemittelte Größen statt der stochastisch gemittelten Größen verwendet werden, kann eine Alternative zu PDF-Methoden benutzt werden, die Methode der gefilterten Wahrscheinlichkeitsdichtefunktionen (FDF). Sie beruhen nicht auf der Annahme der statistischen Homogenität und durch

die räumliche Mittelung (auch räumlicher Filter genannt) können die FDF auf die spezifischen Stützvolumen der unterschiedliche Messmethoden zugeschnitten werden.

Das Ziel der hier präsentierten Forschung ist es, solch eine FDF-Methode für die Vorhersage des Schadstofftransports im Grundwasser zu entwickeln. Dazu sind drei Schritte notwendig. Ein effizientes und akkurates numerisches Lösungsverfahren für FDF-Gleichungen muss entwickelt werden. In einem zweiten Schritt müssen die Parameter der FDF-Gleichungen durch räumliche Filter berechnet werden. Schließlich muss ein geeignetes Mischungsmodell gefunden werden um das Schließungsproblem des Mischungsterms zu lösen. Dieser Term ist von besonderem Interesse da er einen direkten Einfluss auf die zeitliche Entwicklung der Unsicherheit hat.

PDF- und FDF-Gleichungen besitzen dieselbe mathematische Struktur. Deshalb kann zunächst ein numerisches Lösungsverfahren für PDF-Gleichungen entwickelt und getestet werden, deren Parameter einfacher zu berechnen sind. Die hohe Dimensionalität der PDFs stellt eine große Herausforderung für numerische Lösungsverfahren dar. Lagrangesche Partikelmethoden werden in diesem Fall im Allgemeinen gegenüber gitterbasierten Lösungsverfahren bevorzugt, da sie im Falle von reaktiven Mehrkomponenten-Transportproblemen nicht unter dem Fluch der Dimensionalität leiden. Allerdings kann es passieren, dass durch die Anzahl der Partikel, die für eine akzeptable Genauigkeit benötigt wird, die Rechenzeit für praktische Anwendungen zu groß wird. Deshalb wird der Global Random Walk (GRW) Algorithmus in dieser Arbeit verwendet, welcher eine Verallgemeinerung der Particle-Tracking-Verfahren darstellt. Es werden nicht einzelne Partikel sequentiell simuliert, sondern es werden die Bewegungen von beliebig vielen Partikeln auf einem regulären Gitter berechnet. Allerdings lösen solche Particle-Tracking-Verfahren Itô-Gleichungen, die mit Fokker-Planck-Gleichungen in Zusammenhang stehen. Im Allgemeinen unterscheiden sich PDF-Gleichungen von den numerisch gelösten Fokker-Planck-Gleichungen. Aus diesem Grund werden Konsistenzbedingungen hergeleitet, welche dazu führen, dass durch die angewendeten numerischen Verfahren tatsächlich die gesuchten PDF-Lösungen gefunden werden. Mit diesen Konsistenzbedingungen ist der GRW-Algorithmus gut geeignet um PDF-Gleichungen numerisch zu lösen. Das Geschwindigkeitsfeld wird durch den Kraichnan-Algorithmus erzeugt, wohingegen die Dispersionskoeffizienten durch einzelne Partikeltrajektorien in den Geschwindigkeitsfeldern effizient abgeschätzt werden können. Verschiedene Mischungsmodelle werden verwendet um die PDF-Gleichung zu schließen.

Da die Konsistenzbedingungen dafür sorgen, dass die numerischen Verfahren die gesuchten PDF-Lösungen approximieren, können anschließend die stochastischen Mittelungen durch räumliche Filter ersetzt werden, um für die FDF-Methoden benutzt zu werden. Wird ein räumlicher Filter direkt auf die Kraichnan-Formel angewendet, erhält man einen gefilterten Kraichnan-

Algorithmus, der sich lediglich durch einen Konstanten Faktor von dem ungefilterten unterscheidet. Dadurch lässt sich der gefilterte Algorithmus sehr einfach und effizient implementieren. Für moderate Heterogenitäten des Geschwindigkeitsfeldes können die Ensemble-Dispersionskoeffizienten aus einzelnen Trajektorien des Transportprozesses berechnet werden. Die Ensemble-Dispersionskoeffizienten sind abhängig von der Filtergröße und aus deren Differenzen können die gesuchten coarse-grained Diffusionskoeffizienten berechnet werden. Einzig das vielversprechendste Mischungsmodell aus den Untersuchungen mit den PDF-Gleichungen wird für die FDF-Gleichungen verwendet. Dieses Mischungsmodell hängt von einer Längenskala ab, welche im Falle von PDF-Gleichungen der Korrelationslänge des Leitfähigkeitsfelds entspricht. Für FDF-Gleichungen wird die Filtergröße zur Korrelationslänge addiert, um eine Längenskala zu erhalten, welche von der Filtergröße abhängt. Mit den gefilterten Parametern des Geschwindigkeitsfelds und der Dispersionskoeffizienten und dem Mischungsmodell kann der GRW-Algorithmus zur Lösung von FDF-Gleichungen verwendet werden. Wird die mittlere Konzentration durch Monte-Carlo-Referenzsimulationen, durch PDF- und durch FDF-Simulationen berechnet, so gibt es ab einer bestimmten Filtergröße keine signifikante Diskrepanz zwischen den Ergebnissen. Allerdings hängt die mittlere Konzentration nicht von dem Mischungsmodell ab. Vergleicht man die PDFs aus den drei genannten Verfahren, so sind die Ergebnisse weniger vielversprechend. Obwohl das Verschmälern der PDF nicht vom Mischungsmodell wiedergegeben wird, wird der Transport der PDF im Konzentrationsraum richtig vorhergesagt und die kumulativen Verteilungsfunktionen entsprechen der Referenzsimulation.

Da das Verhalten der PDF im Konzentrationsraum vollständig durch das Mischungsmodell beschrieben wird, wenn Reaktionsterme vernachlässigt werden, wird nach einem besseren Mischungsmodell gesucht. Wenn die Klasse der IEM-Mischungsmodelle auf die PDF-Gleichung angewendet wird und die Varianz-Transportgleichung aus dieser bestimmten PDF-Gleichung hergeleitet wird, so findet man eine Verbindung zwischen diesen beiden Gleichungen. Denn beide hängen von einem freien Parameter des Mischungsmodells ab, der beeinflusst wie schnell Varianz abgebaut wird. Die Varianzgleichung ist viel einfacher zu handhaben. Es wird sogar eine analytische Lösung hergeleitet, welche ebenfalls von dem freien Parameter abhängt. Durch physikalisch gestützte Argumente wird das zeitabhängige TIEM-Mischungsmodell hergeleitet, welches deutlich verbesserte Ergebnisse für die Konzentrationsvarianz liefert. Das TIEM-Modell wird anschließend auf PDF-Gleichungen übertragen und liefert auch dafür bessere Ergebnisse.

Zusammenfassend liefert diese Arbeit einen Beitrag zur Entwicklung der FDF-Methoden angewendet auf den Transport im Grundwasser.

Abstract

It is estimated that fifty percent of the drinking water is extracted from groundwater sources, making them a very important source of the natural resource water. But the groundwater quality is threatened by a multitude of contaminants. Risk assessments are applied to geohydrological systems in order to estimate if an ecosystem or the human health is at risk through groundwater pollution. In this context, ecosystem or human health risks not only depend on the impact of the contaminants on the ecosystem or the human body, but also on the spreading and propagation of contaminants in the groundwater. For example, the risk of a well being polluted depends on the spreading. Properties of the subsurface like the hydraulic conductivity have a strong impact on the groundwater flow and therefore also on the transport of solutes. The scarcity of data together with the heterogeneity of the subsurface can cause the uncertainty of the transport predictions to be so large that they cannot be neglected. Consequently, the uncertainty needs to be included in the risk assessments. This is possible by using a geostatistical representation of the subsurface, which results in a probabilistic description of the transport processes.

Probability density function (PDF) methods provide an integrated framework to predict the transport of solutes in which uncertainties are incorporated seamlessly. In these PDF methods, a time evolution equation for the PDF is formulated and solved. Statistical moments like the mean concentration or the concentration variance can be calculated from the concentration PDF. But PDF methods have an important drawback when applying them to groundwater transport. Deriving the parameters for the PDF transport equation from subsurface properties like the hydraulic conductivity, requires stochastic averages under the assumption of a statistically homogeneous conductivity field. This is problematic, because conditioning spatial random fields on measurements destroys the statistical homogeneity. Furthermore, every measurement device has a specific support volume over which the measuring technique averages heterogeneities. These different support volumes lead to different data, which makes it difficult to compare this data to numerical simulations, like PDF simulations. Using spatially averaged quantities instead of stochastic averages, an alternative to PDF methods is found: the filtered density function (FDF) methods. They do not rely on statistically homogeneous conductivity fields and through the spatial averaging (also known as spatial filtering) they can be tailored towards the specific support volume of a measuring technique.

The aim of the research presented here is to develop such an FDF method for predicting the transport of contaminants in groundwater. Therefore, three steps are necessary. An efficient and accurate numerical solver for

FDF equations needs to be developed. In a second step, the parameters contained by the equations have to be filtered. And finally, an appropriate mixing model needs to be found for approximating the unclosed mixing term. The mixing term is of particular interest because it has a direct impact on the uncertainty evolution.

PDF and FDF equations have the same mathematical structure. Hence, a numerical solver is first developed and tested for PDF equations, with easier to obtain parameters. The high dimensionality of PDFs pose a challenge to numerical solvers. Lagrangian particle methods avoid the curse of dimensionality for multi-component reactive transport and are generally favoured over grid based solvers. However, in such approaches a computationally unfeasible amount of particles may be required for an acceptable accuracy. Therefore, the global random walk (GRW) algorithm is used in this work. It is a generalisation of particle tracking methods. It does not simulate single particles sequentially, but instead simulates the movements of arbitrarily large numbers of particles on regular lattices. However, these numerical particle methods solve Itô equations which actually correspond to Fokker-Planck equations. In general, PDF equations differ from the numerically solved Fokker-Planck equations. Thus, consistency conditions are derived which equate the Fokker-Planck equations being solved to the PDF equations of interest. With these consistency conditions, the GRW algorithm proves to be well-suited to solve PDF equations. The velocity field is generated by the Kraichnan algorithm, whereas the dispersion coefficients are efficiently estimated from single particle trajectories in the velocity field. Different mixing models are used to close the PDF transport equation.

With the consistency conditions ensuring that the simulations indeed solve the correct equations, the stochastic averages are now replaced by spatial filters for the use with FDF methods. Applying such a filter directly to the Kraichnan formula results in a filtered Kraichnan algorithm, which only differs from the original one by a constant factor, making it very easy to implement and very efficient to compute. For moderate heterogeneity of the velocity field, the ensemble dispersion coefficients are estimated on single trajectories of transport process. The ensemble dispersion coefficients depend on the filter size and from these differences, the coarse-grained diffusion coefficients can be calculated. Only the most satisfactory mixing model from the investigations with PDF equations is used for the FDF equation. This mixing model depends on a length scale, which is the correlation length of the hydraulic conductivity. For FDF equations, the filter size is added to the correlation length for a filter size dependent length scale. With the filtered velocity, dispersion, and mixing parameters, the GRW algorithm is used to solve the FDF equation. Comparing the mean concentration calculated from Monte Carlo reference simulations, PDF simulations, and FDF simulations, the results practically coincide from a certain filter size on. However, the mean concentration does not depend on the mixing model and

comparing the PDFs computed from Monte Carlo simulations, PDF simulations, and FDF simulations, the results are less promising. Though the narrowing of the PDF is not captured by the mixing model, its transport in concentration space is correctly predicted and the cumulative distribution functions compare well with the reference solution.

Because the behaviour of the PDF in concentration space is completely described by the mixing model, if reaction terms are neglected, more effort is put into finding a better one. If a certain class of mixing models, the IEM mixing models, is applied to the PDF equation and the variance transport equation is derived from this particular PDF equation, a connection is found between these two equations. Both depend on the same free parameter which describes how fast variance is destroyed. The variance equation is much easier to handle, even an analytical solution is derived, which depends on the free parameter. This way, different time dependent parameters can be tested much easier. By using physical arguments, the time dependent TIEM mixing model is found, which gives much better results for the concentration variance. Transferring the TIEM model to PDF equations also results in improved results.

In summary, this work contributes towards the development of an FDF framework applied to the transport in groundwater.

Contents

Zusammenfassung	I
Abstract	IV
1 Introduction	1
1.1 Motivation and Outline	2
1.2 Groundwater Flow and the Transport therein	4
1.2.1 From the Pore-Scale to a Continuum Description	4
1.2.2 Transport Equations	5
1.3 Probability Density Functions	8
1.4 Global Random Walk Algorithm	9
1.5 Random Velocity Field Generation	13
2 Probability Density Functions	15
2.1 Introduction	16
2.2 PDF Equations	19
2.3 Derivation of the PDF Transport Equation	21
2.3.1 Delta Function Method	21
2.3.2 Test Function Method	24
2.4 The Fokker-Planck Approach to PDF Equations	26
2.4.1 Direct Fokker-Planck Approach	26
2.4.2 Reverse Fokker-Planck Approach	30
2.4.3 Numerical Solutions	31
2.5 PDF Simulations	32
2.5.1 Weighting Function	34
2.5.2 Upscaled Diffusion Coefficients	34
2.5.3 Mixing Models and Results	37
2.6 Conclusions	43
3 Filtered Density Functions	45
3.1 Introduction	46
3.2 FDF Equations	48
3.3 Filtering Velocity fields	49
3.4 Coarse-Grained Transport Simulations	51

3.4.1	Coarse-Graining Dispersion Coefficients	53
3.4.2	Coarse-Grained Concentration Simulations	58
3.4.3	FDF Mixing Model	59
3.5	FDF Simulations	59
3.6	Conclusions	63
4	A Time Dependent Mixing Model	65
4.1	Introduction	66
4.2	Physical Background and Methods	68
4.2.1	PDF Transport Equations	69
4.2.2	Mean and Variance Transport Equations	69
4.2.3	Analytical Solutions of the Moment Equations	72
4.3	Time Dependent Extension of the IEM Model	76
4.4	Simulations	79
4.4.1	Variance Modelling	79
4.4.2	PDF Modelling	85
4.5	Conclusions and Future Perspectives	86
5	Summary and Outlook	89
	Bibliography	92
	Acknowledgements	102
	Selbstständigkeitserklärung	104
	Curriculum Vitae	105

Chapter 1

Introduction

Motivation and Outline

Water is one of the most important natural resources, not only for human beings but for all life on earth. Since 2010, the access to clean and drinkable water is even mandated as a human right (*United Nations, 2010*). Besides easily accessible freshwater from surface sources like rivers and lakes, water stored in the subsurface is a major contribution to the globally available and usable freshwater. It is estimated that fifty percent of the drinkable water is extracted from groundwater sources. In some countries it contributes up to hundred percent of the drinking-water supply of a country (*Zetkser and Everett, 2004*). But the quality of the groundwater is threatened by a multitude of risks. There is always the risk of a leakage for example in geological nuclear or chemical waste repositories. However, one does not have to search so deep underground for potential contaminant sources. Waste dumps can leak toxic substances into the subsurface. Industrial and domestic waste can be disposed of illegally or the deposition can simply be unregulated and infiltrate the subsurface as a result. Furthermore, leakages and spills of industrial waste can contaminate the groundwater (*WWAP, 2012*).

Measuring contaminants in the groundwater is very expensive, laborious, and time intensive (*WWAP, 2012*). One reason for the intricateness of the measurements is that the subsurface is often highly heterogeneous. The variability of the properties of the subsurface influencing the transport of contaminants in groundwater ranges from the order of magnitude of individual grains to large geological structures like facies, fractures, and sediment layers. Without unfeasibly highly resolved measurements, the measurement uncertainty stays relatively large with respect to the actual measurements. Therefore, it is necessary to include the uncertainty in risk analyses and in the prediction of the transport of contaminants in groundwater. The importance of an uncertainty analysis is amplified by following fact. When human health risks are assessed in a hydrological system, the risks are influenced by the uncertainties of contaminant measurements in the subsurface (*de Barros et al., 2011a*). Moreover, the increasing impact of human activities on groundwater systems increases additional uncertainties (*WWAP, 2012*).

The scarcity of data and the uncertainty together with the variability of the subsurface make the prediction of the contaminant transport in groundwater a demanding task. It is well known from work published in the last decades that a major source of uncertainty associated with predicting contaminant concentrations is the lack of detailed information about the spatial heterogeneity of the hydraulic conductivity in the subsurface (see e.g. *Gelhar and Axness (1983); Burr et al. (1994)*). A long standing approach to deal with this uncertainty is the stochastic parameterisation of the hydraulic conductivity through random space functions with statistics inferred from field and laboratory data. Via flow and transport equations, the contaminant

concentrations being modelled are random functions too. Their statistics may be inferred from Monte Carlo ensembles of transport simulations, done for realisations of the random hydraulic conductivity or by stochastic perturbation approaches. Statistical moments like the mean and the variance can be extracted from these random functions, giving a first estimate of the expected concentration at a point in space and time. The variance can help to assess the reliability of the mean concentration in predicting the true concentration.

However, more information is needed for a complete risk assessment. The complete statistical information of a random function is contained in its probability density function (PDF). Thus, also higher moments like the skewness or the kurtosis can be extracted from the PDF. Environmental agencies regulate risk thresholds by prescribing an exceedance probability which depends on the concentration PDF and cannot be calculated from the moments alone (*Andričević and Cvetković, 1996*). Therefore, the concentration PDF is a central quantity in risk assessment. This is one of the reasons why the PDF method has received an increased attention during the last decade (*Suciu et al., 2016*). Transport equations can be formulated for PDFs. They not only depend on the time and the position, like the mean concentration for example, but also on the concentration of each species being considered. This dependence makes PDF equations highly dimensional and due to computational limitations they cannot be solved by conventional grid based Eulerian numerical methods. Instead, it is common to use particle based Lagrangian methods to solve PDF equations (*Pope, 1985; Fox, 2003; Suciu et al., 2016*). These particle methods are based on the similarity between PDF equations and Fokker-Planck equations. However, taking a closer look at these two types of equations, one finds that they actually describe the time evolution of two different random variables, or in other words two different random functions and thus different processes. In Chapter 2, consistency conditions will be derived, relating PDF equations to Fokker-Planck equations. Based on these conditions, an efficient numerical solver for PDF equations will be presented.

Upscaling equations to coarser scales through spatial filtering has a long history in subsurface hydrology (*Wen and Gómez-Hernández, 1996; Renard and Marsily, 1997; Rubin et al., 1999; Attinger, 2003*). Upscaling equations separates the dynamics of the scales larger than the filter size from sub-filter effects, which are modelled. The results of measurements in the subsurface depend on the support volume they inherently have (*Gelhar, 1977*). In order to interpret these measurements and to use them in or to compare them to numerical simulations, upscaling procedures are needed. Furthermore, if an aquifer is to be modelled on a field-scale, even if enough measurements were available to parameterise such a model, a highly resolved model quickly becomes computationally unfeasible. Thus, upscaling a numerical model also helps to reduce the computing time. Therefore, it comes naturally to

adapt such filtering techniques to PDF equations. In turbulence theory and combustion physics this has already been done, resulting in so-called filtered density function (FDF) methods. However, these FDF methods have only recently been applied to groundwater transport problems in a paper on which this work is based upon (*Suciu et al., 2016*). FDF methods are applied to groundwater transport problems in Chapter 3. Therefore, the parameters of the FDF equation need to be upscaled from fine-grained descriptions.

The crux of PDF/FDF methods is finding an appropriate mixing model, which describes the temporal evolution of the uncertainty, to put it simply. As will be shown in Chapters 2 and 3, mixing models which are used successfully for transport in turbulent flows, do not necessarily perform well when applied to groundwater transport. Chapter 4 deals with the problem of finding an adequate mixing model for the subsurface transport. If a certain class of mixing models is applied and the variance transport equation is derived from the PDF equation, then different variations of this class of mixing models can be tested with the much easier to handle variance equation. Subsequently, a promising mixing model can be transferred back to the PDF equation. As shown in this work, better mixing models for PDFs applied to groundwater transport can indeed be found this way.

Groundwater Flow and the Transport therein

This section gives an overview of the theories used to describe the flow and transport in the subsurface.

From the Pore-Scale to a Continuum Description

It is assumed that the subsurface can be described as a porous medium. Such a porous medium is characterised by the subdivision of the medium into a solid matrix and the pore space. The pore space is occupied by fluids, which flow through this space. The subdivision holds down to a minimal characteristic length scale.

In principle, the flow and transport in the subsurface can be modelled in this pore space. The flow and transport equations are relatively easy to solve, because in general the viscous forces dominate the advective inertial forces, which means that the flow can be described in a linearised form, the Stokes flow (*Bear and Cheng, 2010*). The true difficulty in modelling the flow and transport in the pore space arises from the boundaries, which are composed of the solid matrix and can form very complicated geometries. Neither measuring nor describing the pore geometries is feasible on a catchment scale. Therefore, an upscaling procedure is needed in order to derive an averaged description.

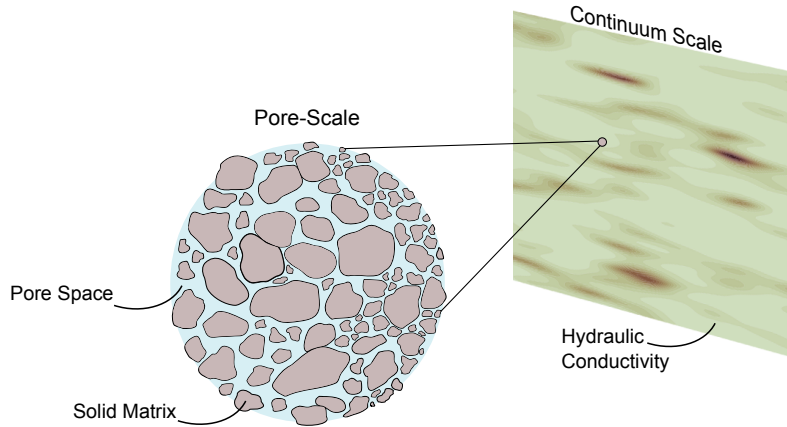


Figure 1.1: An illustration of the upscaling process from the pore-scale to the continuum scale.

One possible way of upscaling equations from the pore-scale to the continuum scale is by introducing so-called representative elementary volumes (REV) ([Bear, 1972](#)). An REV must contain both, parts of the solid matrix and parts of the pore space. A spatial average over the REV for all points of the pore-scale domain is performed in order to derive upscaled equations.

The size of an REV is chosen in such a way that it is small enough to be assumed to be a point on the continuum scale and to include both, parts of the solid matrix and parts of the pore space. But it is chosen large enough that an average over the fluctuations of a quantity gives a statistically meaningful average over its volume. An illustration of this upscaling procedure is given in [Figure 1.1](#).

A second approach to deriving equations on the continuum scale is the method of homogenisation. This approach is used when heterogeneities appear on two or more clearly distinct scales. A periodic structure at the smaller scale is a prerequisite. But it has been shown, that homogenisation also works well for small-scale structures that are not truly periodic ([Bear and Cheng, 2010](#)).

Transport Equations

The equation describing the fluid flow in porous media on the continuum scale was first derived empirically for one dimension by [Darcy \(1856\)](#). But later it was derived mathematically rigorously from the Navier-Stokes equations (e.g. [Bear and Cheng, 2010](#)). For a three-dimensional domain and for a fluid of constant density, Darcy's law can be formulated as

$$\mathbf{q} = -\mathbf{K} \cdot \nabla h. \quad (1.1)$$

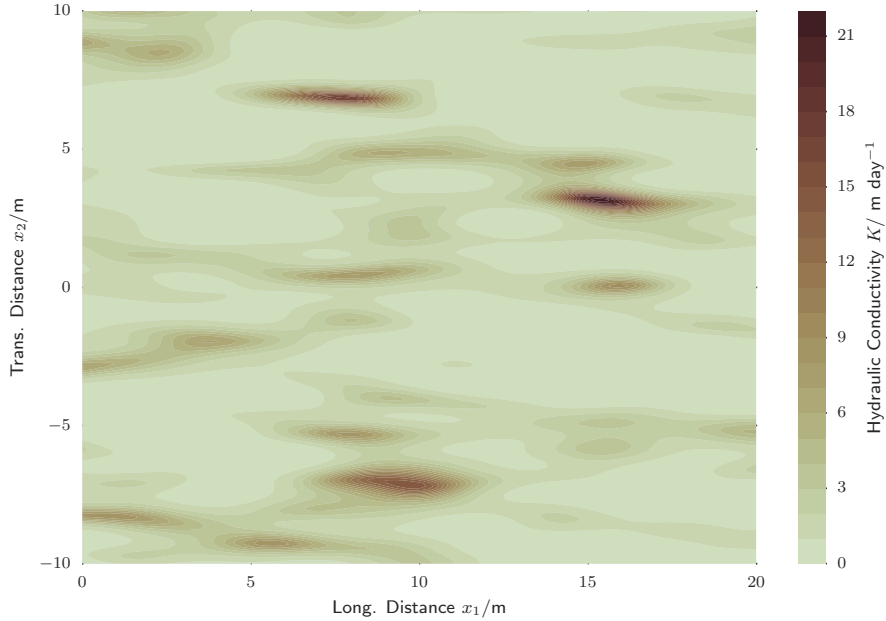


Figure 1.2: The hydraulic conductivity K , which appears in Darcy’s law (1.1), realised as an anisotropic log-normal random field.

The flux \mathbf{q} is the discharge per unit area. ∇h is the piezometric head gradient, with $h = z + \frac{p}{\rho g}$ and z being the elevation at which the piezometric head is being considered. The variables p and ρ are the fluid’s pressure and mass density and g is the acceleration of gravity. The coefficient of proportionality \mathbf{K} is the hydraulic conductivity and describes how much resistance the fluid experiences when flowing through the upscaled continuum of a porous medium. In general it is a tensor and reduces to a scalar only in case of an isotropic medium. The hydraulic conductivity depends on the solid matrix of the porous medium and on the fluid properties, namely its density and its dynamic viscosity. In nature, the hydraulic conductivity varies over 14 orders of magnitude (*Bear et al., 1968*) and can have very heterogeneous spatial distributions. See Figure 1.2 for an artificial example, which was generated by the Kraichnan algorithm presented in Section 1.5.

Solutes are transported by the groundwater. Its flux is described by Darcy’s law (1.1), but for the transport the fluid velocity is of interest. Therefore, the so-called seepage velocity is introduced:

$$\mathbf{V} = \frac{\mathbf{q}}{\phi}, \quad (1.2)$$

with ϕ being the porosity of the porous medium. \mathbf{V} is the mass-averaged velocity of the fluid.

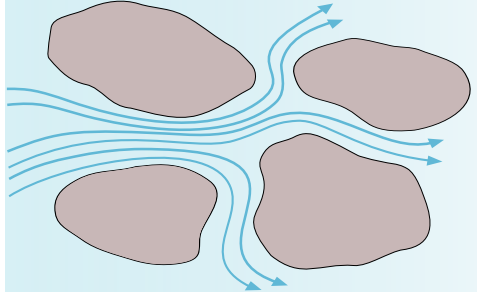


Figure 1.3: The separation of water parcels, illustrated as streamlines, is enhanced by the solid matrix.

Two assumptions are made in order to derive the well-known advection-dispersion-reaction equation. The first one is the well justified assumption of the incompressibility of the groundwater flow $\mathbf{V}(\mathbf{x})$:

$$\nabla \cdot \mathbf{V} = 0. \quad (1.3)$$

The second one is the assumption of a Fickian transport, with the local dispersion tensor \mathbf{D} . The concept of mechanical dispersion needs to be introduced. Going back to the pore-scale, it can be understood why spatial fluctuations of the subsurface properties make the transport of solutes heterogeneous too. Water parcels transporting a contaminant and travelling very closely together can be separated and follow different and distinct flow paths. As a consequence, an enhanced spreading of the plume is observed. This mechanism of separating water parcels without the influence of diffusion is called mechanical dispersion. Such a separation is illustrated on the pore-scale in figure 1.3. However, in the upscaled transport equation this enhanced spreading is described by an additional diffusion-like term. In general, it is much stronger than the molecular diffusion.

The advection-dispersion-reaction equation for N_α solutes with concentrations $C_\alpha(\mathbf{x}, t)$, $\alpha = 1 \dots N_\alpha$ and the reaction rates S_α can now be formulated as:

$$\partial_t C_\alpha + V_i \partial_{x_i} C_\alpha = D_{ij} \partial_{x_i} \partial_{x_j} C_\alpha + S_\alpha. \quad (1.4)$$

The left hand side of equation (1.4) is the material derivative and the two terms on the right hand side are due to the Fickian dispersion and the reactions. The local dispersion is assumed to be diagonal with $D_{11} = D_L$ being the longitudinal component, $D_{ii} = D_T$ for $i > 1$ being the transversal components, and $D_{ij} = 0$ for $i \neq j$. The Einstein summation convention will be used throughout this work.

Probability Density Functions

A short introduction to probability density functions will be given in this section. Due to the scarcity of data in subsurface systems, processes like the transport of solutes are modelled by random functions. Throughout this work, random functions will be denoted by capital letters, e.g. the random concentration of a solute $C(\mathbf{x}, t)$. If the concentration c is measured at point \mathbf{x}_0 and time t_0 , the random concentration takes the value of the so-called sample point $C(\mathbf{x}_0, t_0) = c$. The sample point is an independent variable and thus not a random variable. Such sample points will be denoted by the same letter as their corresponding random function, but with a lowercase letter.

The cumulative distribution function (CDF) $F(c)$ is defined by the probability that a random variable is less than a given value c :

$$F(c) = \Pr(C < c). \quad (1.5)$$

From this definition it is clear that the probability for a value to fall into an interval can be calculated from

$$\Pr(c_1 < C < c_2) = F(c_2) - F(c_1). \quad (1.6)$$

The CDF $F(c)$ is a monotonically increasing function bound to the interval $[0, 1]$.

The probability density function (PDF) $f(c)$ of the random variable C is the derivative of the CDF:

$$f(c) = \frac{dF(c)}{dc}. \quad (1.7)$$

By integrating the PDF from c_1 to c_2 , its meaning becomes clear:

$$\int_{c_1}^{c_2} f(c)dc = F(c_2) - F(c_1) = \Pr(c_1 \leq C < c_2). \quad (1.8)$$

And for an infinitesimal interval:

$$\Pr(c \leq C < c + dc) = f(c)dc. \quad (1.9)$$

Thus, the integral of the PDF over an interval gives the probability that its corresponding function takes a value from this interval.

A PDF has three important characteristics. Its integral over the complete sample space is normed to unity, it is a non-negative function and it vanishes as its argument tends to infinity.

The mean (or expectation) of a random variable C is defined by

$$\langle C \rangle = \int_{\Omega_c} cf(c)dc, \quad (1.10)$$

with Ω_c being the sample space. A function $Y(C)$ of a random variable is also random. Its mean is defined very similarly to the mean (1.10) of the random variable it depends upon:

$$\langle Y(C) \rangle = \int_{\Omega_c} Y(c) f(c) dc. \quad (1.11)$$

In experiments or in numerical simulations, these integrals are approximated by finite sums. Therefore, an ensemble of possible states is measured or computed, by which the ensemble average is defined as

$$\langle C \rangle_N = \frac{1}{N} \sum_{n=1}^N C^{(n)}. \quad (1.12)$$

Besides the mean, all higher statistical moments of a random variable, like the variance, the skewness, and so on, are defined by an integral over the PDF. The n th central moment of C is defined by

$$\mu_n = \int_{\Omega_c} (c - \langle C \rangle)^n f(c) dc. \quad (1.13)$$

This makes the PDF a variable with a large amount of statistical information. It contains all one-point statistical information of its variable. In general, the PDF cannot be reconstructed from only a finite number of moments. In this context, “one-point” means that the PDF only contains the statistical information at one point and thus does not describe the complete statistics of the random field. Spatial correlations or gradients cannot be obtained from a one-point PDF.

By substituting $Y(c)$ in equation (1.11) by the Dirac delta function $Y(c) = \delta(C - c)$, the PDF can be identified with the expectation of the Dirac delta function:

$$f(c) = \langle \delta(C - c) \rangle. \quad (1.14)$$

This identity is important for the derivation of many fundamental results of the PDF methods, which will be presented in Chapter 2. In this context the Dirac delta function is also called the fine-grained PDF.

Figure 1.4 shows a Gaussian PDF and its FDF as green dashed lines. In blue, 20 fine-grained PDFs are shown, which approximate the PDF by the ensemble average (1.12). In the plot beneath, the fine-grained PDFs are summed up and thus approximate the CDF as a step function.

Global Random Walk Algorithm

The global random walk (GRW) method is the numerical solver used throughout this work. It is a generalisation of particle tracking methods. Although

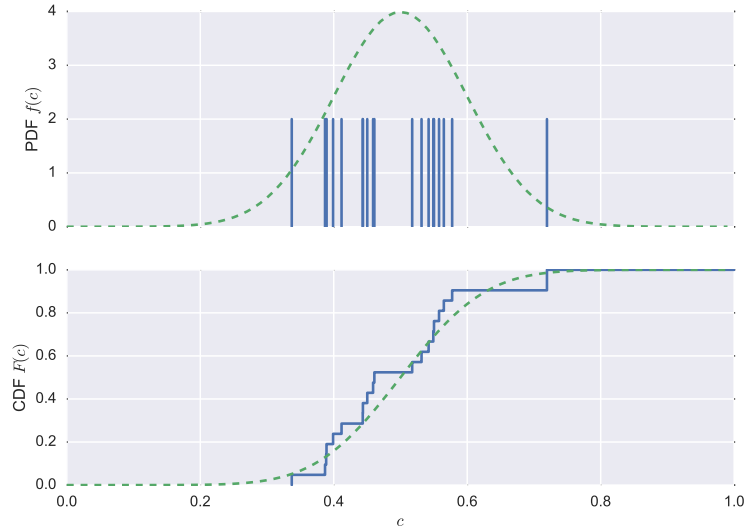


Figure 1.4: The PDF and the CDF are shown as green dashed lines. The PDF is the ensemble average of fine-grained PDFs, which are Dirac delta functions. Here, 20 fine-grained PDFs are symbolised as blue vertical lines.

they are well-suited to calculate global coefficients, like ensemble dispersion coefficients with only a few hundred particles (*Dentz et al., 2002; Schwarze et al., 2001*), they suffer from high computational costs if accurate local quantities are of interest (*Schüler et al., 2016*). The GRW method decreases the computational time and at the same time increases the accuracy (*Vamoş et al., 2003*). The method does not simulate single particles sequentially, but instead simulates the movements of many particles simultaneously projected onto a regular grid and thus simulates the movement of particle numbers. The cell sizes of the grid on which the particles move and the discretised time steps are chosen based on physical parameters such as the diffusion coefficient and the drift velocity. The algorithm can be interpreted as a superposition of many weak solutions of Itô equations projected onto a regular grid (*Suciu, 2014*).

The algorithm described here is adapted to two-dimensional problems, but it can easily be extended to higher dimensions. The particles move on a regular grid with the particle position being $(x_i, x_j) = (i\delta x_1, j\delta x_2)$, with $\delta x_1 \delta x_2$ being the grid cell size. The particles located at position x_i jump to $x_i - d_1 \delta x_1$ and to $x_i + d_1 \delta x_1$ and analogous for the second axis from x_j to $x_j - d_2 \delta x_2$ and to $x_j + d_2 \delta x_2$, with d_1 and d_2 being natural numbers which are related to the diffusion coefficient. Similarly, particles at x_i are drifted to $x_i + v_1 \delta x_1$ and from x_j to $x_j + v_2 \delta x_2$ with v_1 and v_2 being natural numbers related to the velocity field. The exact relations will be introduced later.

The number of particles at position (x_i, x_j) and at time $t_k = k\delta t$ is denoted by $n(i, j, k)$, where δt is the discretised time step. The number of particles moving at time t_k from position x_i to x_l on the i -axis and from position x_j to x_m on the j -axis is described by $\delta n(l|i, m|j, k)$. The movement of the particles is now calculated as a sum of all possible jumps:

$$\begin{aligned} n(i, j, k) &= \delta n(i + v_1|i, j + v_2|j, k) \\ &\quad + \delta n(i + v_1 + d_1|i, j + v_2|j, k) \\ &\quad + \delta n(i + v_1 - d_1|i, j + v_2|j, k) \\ &\quad + \delta n(i + v_1|i, j + v_2 + d_2|j, k) \\ &\quad + \delta n(i + v_1|i, j + v_2 - d_2|j, k), \end{aligned} \quad (1.15)$$

$$n(l, m, k + 1) = \delta n(l, m, k) + \sum_{i \neq l, j \neq m} \delta n(l|i, m|j, k) \quad (1.16)$$

As a start, these particle jumps are illustrated in one dimension and only for diffusion in Figure 1.5 over three time steps. The two-dimensional particle jumps with advection (blue arrow) and diffusion (green arrows) are illustrated in Figure 1.6 over one time step. The particle movements δn are binomial random functions and can be efficiently approximated by

$$\delta n(i + v_1 - d_1|i, j + v_2|j, k) = \begin{cases} r_1 n(i, j, k)/2 & \text{if } n \text{ is even,} \\ r_1 n(i, j, k)/2 + \theta & \text{if } n \text{ is odd} \end{cases} \quad (1.17)$$

$$\delta n(i + v_1 + d_1|i, j + v_2|j, k) = n(i, j, k) - \delta n(i + v_1 - d_1|i, j + v_2|j, k), \quad (1.18)$$

where θ is a random variable which takes the values 0 and 1 with equal probability and equivalently for jumps in j -direction. The coefficients r_i makes it possible to simulate arbitrary diffusion coefficients, which cannot be mapped by the discrete d_i alone.

In order to obtain meaningful results, the particle velocities, composed of a drift and a diffusion part, need to be related to physical quantities, namely the diffusion coefficient and the velocity.

The grid cell size $\delta x_1 \delta x_2$ and the time steps δt are related to the diffusion coefficient through r_i by

$$D = r_i \frac{(d_i \delta x_i)^2}{2\delta t}. \quad (1.19)$$

The advective motion of the particles through a random velocity field is described by a set of integers (v_1, v_2) , which are defined by

$$v_i = \left\lfloor \frac{\delta t}{\delta x_i} V_i(x_i) \right\rfloor, \quad (1.20)$$

with $\lfloor \cdot \rfloor$ being the floor function.

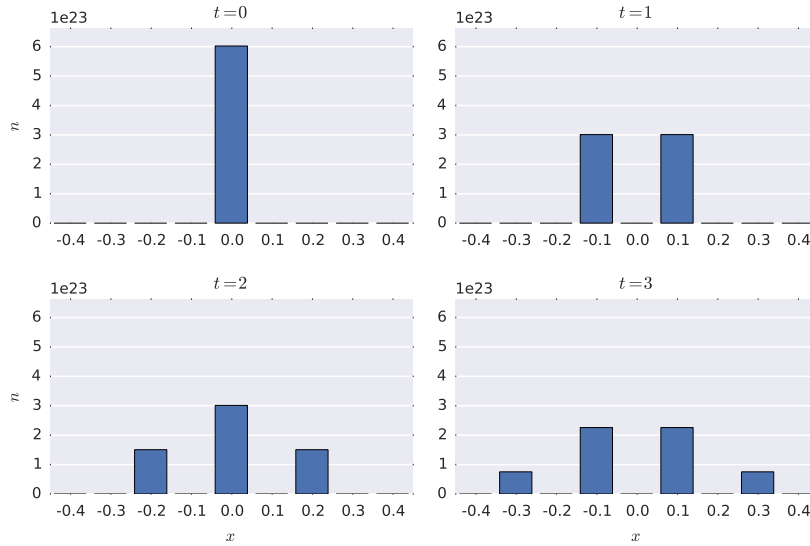


Figure 1.5: An illustration of one-dimensional GRW particle movements only due to diffusion over three time steps.

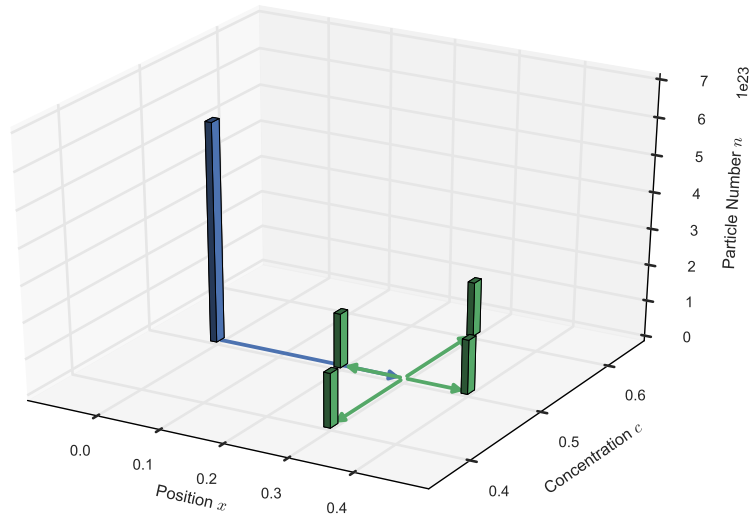


Figure 1.6: An illustration of the GRW particle movements over one time step. The blue arrow indicates the drift and the green arrows indicate the diffusion.

The concentration is calculated from the particle distribution with

$$c(x_i, x_j, t_k) = \frac{1}{l\delta x} \sum_{i'=-l/2}^{l/2} \sum_{j'=-l/2}^{l/2} n(i+i', j+j', k), \quad (1.21)$$

where l is a coefficient, which takes into account that for specific implementations of the algorithm, only every second cell is populated with particles, in which case it is set to $l = 2$. Otherwise it is $l = 1$.

Random Velocity Field Generation

A Gaussian random velocity field $\mathbf{V}(\mathbf{x})$, corresponding to a log-normal hydraulic conductivity $Y(\mathbf{x}) = \ln K(\mathbf{x})$, can be generated in a first order approximation by the Kraichnan method ([Kraichnan, 1970](#)) as a randomised spectral representation given by the formula

$$V_i(\mathbf{x}) = \langle V_1 \rangle \delta_{i1} + \sigma_Y \langle V_1 \rangle \sqrt{\frac{2}{N}} \sum_{j=1}^N p_i(\mathbf{k}^{(j)}) \cos(\mathbf{k}^{(j)} \cdot \mathbf{x} + \phi^{(j)}), \quad (1.22)$$

where $i = 1, \dots, d$ and d is the spatial dimension of the problem and

$$\mathbf{p}(\mathbf{k}) = \mathbf{e}_1 - \frac{\mathbf{k}k_1}{\mathbf{k}^2} \quad (1.23)$$

is a projector ensuring the incompressibility of the velocity field ([Schwarze et al., 2001](#); [Dentz et al., 2002](#)). It is assumed that the mean velocity $\langle \mathbf{V} \rangle = \langle V \rangle \delta_{i1}$ is aligned with the first unit vector \mathbf{e}_1 . The simple representation (1.22) is obtained by choosing the probability density of the random vector $\mathbf{k}^{(j)}$ as given by the Fourier transform of the correlation function of the statistically homogeneous Gaussian random field Y divided by the variance σ_Y^2 (see e.g. [Kurbanmuradov and Sabelfeld, 2010](#)). In the present study, a Gaussian correlation of the Y field is considered. In the general anisotropic case, it is given by

$$\langle Y(\mathbf{x})Y(\mathbf{x} + \mathbf{r}) \rangle = \sigma_Y^2 \exp\left(-\frac{\mathbf{r}^2}{\lambda_Y^2}\right), \quad (1.24)$$

with λ_Y being the correlation length. The random vectors $\mathbf{k}^{(j)}$ are thus distributed according to the PDF

$$f(\mathbf{k}^{(j)}) = \prod_{i=1}^d \sqrt{\pi} \lambda_{Y_i} \exp\left[-\pi^2 \left(k_i^{(j)} \lambda_{Y_i}\right)^2\right] = \prod_{i=1}^d f(k_i^{(j)}), \quad (1.25)$$

that is, they have mutually independent components. With the change of variables $k_i^{(j)} = \eta^{(j)} / (\sqrt{2}\pi \lambda_{Y_i})$, where $\eta^{(j)}$ are standard normally distributed

random variables, the corresponding probability measures of the components become Gaussian, $f(k^{(j)})dk_i^{(j)} = (2\pi)^{-1/2} \exp(-\eta^{(j)2}/2)d\eta^{(j)}$. The random components of $\mathbf{k}^{(j)}$ are therefore extracted from Gaussian distributions with vanishing mean and variances $1/(2\pi^2\lambda_{Y_i}^2)$.

The phases $\phi^{(j)}$, also being independent random numbers, are drawn from a uniform distribution in the interval $[0, 2\pi)$. Randomised spectral representations like (1.22), are particular cases of more general randomisation formulas using sums of cosine and sine functions (*Kurbanmuradov and Sabelfeld, 2010; Heße et al., 2014*). In this case, the general representation is obtained when $\sqrt{2} \cos(\mathbf{k}^{(j)} \cdot \mathbf{x} + \phi^{(j)})$ in (1.22) is replaced by $\xi^{(j)} \cos(2\pi\mathbf{k}^{(j)} \cdot \mathbf{x}) + \zeta^{(j)} \sin(2\pi\mathbf{k}^{(j)} \cdot \mathbf{x})$, where $\xi^{(j)}$ and $\zeta^{(j)}$ are standard normal variables, mutually independent, and independent of $\mathbf{k}^{(j)}$. Tests have shown that the two representations are equally accurate, with the only difference that the general formula is about two times slower.

When dropping the first term of equation (1.22), as well as $\langle V_1 \rangle$ and the projector $\mathbf{p}(\mathbf{k}^{(j)})$ from the second term, (1.22) reduces to the randomisation formula for the fluctuations of the Y field.

Chapter 2

Probability Density Functions

This chapter is mainly based on the paper

Suciu, N., L. Schüler, S. Attinger, and P. Knabner (2016), Towards a filtered density function approach for reactive transport in groundwater, *Adv. Water Resour.*, 90, 83-98, doi:10.1016/j.advwatres.2016.02.016,

with parts based on the papers

Suciu, N., F. A. Radu, S. Attinger, L. Schüler, and P. Knabner (2015), A Fokker-Planck approach for probability distributions of species concentrations transported in heterogeneous media, *J. Comput. Appl. Math.*, 289, 241-252, doi:10.1016/j.cam.2015.01.030

and

Suciu, N., L. Schüler, S. Attinger, C. Vamos, and P. Knabner (2015), Consistency issues in PDF methods, *An. St. Univ. Ovidius Constanta, Ser. Mat.*, 23(3), 187-208, doi:10.1515/auom-2015-0055.

Introduction

Geological formations are heterogeneous and their properties are normally not measurable everywhere. This lack of knowledge implies uncertainty in aquifer parameters like hydraulic conductivity. As a consequence, quantifying the transport of solutes through these formations is also uncertain. This uncertainty is dealt with by using a probabilistic description of the involved processes. Going beyond the mean values and also considering the variance is a good starting point to take the uncertainty into account. But in the case of risk assessments, the need to predict extreme values of contaminant concentrations becomes important. However, such occurrences cannot be described by the variance alone. Hence, the need to describe the solute concentrations by their complete probability density function (PDF) arises.

PDF methods were developed in the context of modelling turbulent reacting flows as a powerful tool to close highly non-linear terms arising from averaged chemical reaction rates (*Lundgren, 1969; Pope, 1985, 2000; Fox, 2003; Haworth, 2010*). If the reaction rates only depend on the set of species concentrations, even highly non-linear reactions can simply be included in the formulation without the need to approximate them. The PDF approach is based on solving evolution equations for the one-dimensional (one-point one-time) joint PDF of sets of variables describing the state of the system. These variables are for example flow velocity, chemical composition, turbulent frequency, temperature, or enthalpy. The PDF evolution equations can be derived by different methods (*Pope, 1976, 1985*), starting from local balance equations governing the flow and the evolution of the thermochemical state of the system. The PDF equations are unclosed because they contain terms which cannot be determined by the one-point PDF alone (*Pope, 1985*). But the chemical source terms in the PDF equations are closed, in strong contrast to other approaches, like the Reynolds-averaged flow equations, where chemical source terms pose major problems (*Borghia, 1988; Fox, 2003*). The unclosed terms which require modelling are those describing the turbulent frequency, the scalar mixing by molecular diffusion, and the effects of turbulent velocity fluctuations, if the velocity is not included as a state variable (*Fox, 2003; Haworth and Pope, 2011*). A recent review of scalar mixing models is given by *Celis and Figueira da Silva (2015)*.

When modelling mass transport through highly heterogeneous natural groundwater systems, the randomness is introduced by the stochastic parametrisation of the hydraulic conductivity, which accounts for the parameter uncertainty due to a lack of measurements. This stochasticity implies the randomness of the Darcy flow velocity and of the dependent variables of the transport equations (*Schwede et al., 2008*). The randomness in modelling groundwater flows can be enhanced by considering uncertain sources in the flow equations, like random recharge (*Pasetto et al., 2011*) or by random parametrisations of storage coefficients for transient flows (*Alzraiee et al.,*

2014). However, the uncertainty of the hydraulic conductivity is an omnipresent source of randomness and it is the focus of this work. While in earlier stochastic approaches the focus was mainly on the mean and in some cases the variance of the concentration, during the last decade the need to model the concentration PDF received an increased attention (*Schwede et al.*, 2008; *Sanchez-Vila et al.*, 2009; *Dentz and Tartakovsky*, 2010; *Meyer et al.*, 2010; *Cirpka et al.*, 2011; *Venturi et al.*, 2013; *Suciu*, 2014; *Suciu et al.*, 2015a).

Concentration PDFs of conserved scalars may be inferred without solving PDF evolution equations in case of small or moderate fluctuations of the hydraulic conductivity. In this case they are modelled as log-normal random functions with finite correlation lengths. Then, a Gaussian shape of the concentration may be assumed or inferred, which is completely determined by its first two moments. The statistics of these moments, specified under various assumptions in a first-order perturbation approach, are finally “mapped” onto the concentration PDF via numerical (*Schwede et al.*, 2008) or analytical techniques (*Dentz and Tartakovsky*, 2010; *Cirpka et al.*, 2011) using the Gaussian functional shape of the concentration.

Another favourable situation is that of stratified transport, when the Gaussian concentration can be expressed explicitly as a function of the hydraulic conductivity, with the only assumption of negligible transverse dispersion. This leads to an explicit functional dependence of the concentration PDF on the hydraulic conductivity (*Sanchez-Vila et al.*, 2009). This approach also provides the PDF of reacting chemical species if their concentrations are fully defined by monotonous functions of conserved scalars (*Sanchez-Vila et al.*, 2009).

For advective-reactive transport, PDFs of reacting species can be computed by solving evolution equations similar to those used in turbulence (*Venturi et al.*, 2013). Such PDF equations do not contain mixing terms, because molecular diffusion is neglected. The only closure problem concerns terms including velocity fluctuations, which are modelled as effective, or up-scaled, diffusion coefficients, leading to Fokker-Planck evolution equations (*Venturi et al.*, 2013; *Suciu et al.*, 2015a).

By considering the velocity among the state variables, joint velocity-concentration PDF equations similar to turbulence problems can be derived and no closure for velocity fluctuations is necessary. Mixing is modelled similarly to turbulence approaches and the concentration PDF is obtained by integrating the joint velocity-concentration PDF over the velocity state space (*Meyer et al.*, 2010). Evolution equations of the concentration PDF weighted by a conserved scalar, which generalises the mass density function used in turbulence (*Pope*, 1985), can be formulated as Fokker-Planck equations (*Suciu et al.*, 2015a). Closures are provided by stochastically up-scaled diffusion coefficients (*Suciu*, 2014; *Suciu et al.*, 2015a) and by mixing models, which are formulated as a diffusion in concentration space. The parameters for this diffusion process can be inferred from measured or simulated

concentration time series (*Suciu et al., 2015b*).

Throughout this work, the term “mixing” will be used with a precise meaning, as in turbulence literature (*Celis and Figueira da Silva, 2015*), which, although related, is different from its meaning in stochastic subsurface hydrology, where it is associated with the effective dispersion coefficient (*Dentz et al., 2000*). The latter is the diffusion coefficient of the stochastic process modelling the transport, centred on the actual plume centre of mass. It differs from the diffusion coefficient of the process centred on the centre of mass averaged over the ensemble of velocity realisations, i.e. the ensemble dispersion coefficient describing the spreading of the solute plume (*Dentz et al., 2000*), by the diffusion coefficient of the centre of mass process (*Suciu, 2014*, equation (3.3)). The molecular diffusion coefficient and a term describing the hydrodynamic dispersion by unresolved velocity fluctuations constitute the local dispersion. It enters additively into both the effective and the ensemble dispersion coefficients. All these are processes in physical space. Instead, a mixing model generically consists of an advection and a diffusion process in concentration space. The mixing models provide closures for the conditional average of the diffusion flux, determined by the local dispersion coefficients (*Suciu et al., 2016*) and are related in this way to the transport processes in physical space.

When comparing the PDF approach applied to groundwater flows and to turbulent flows, there are three major differences. The first one concerns the number of parameters. While only a few parameters are required to solve PDF equations of turbulent flows (*Sabel'nikov et al., 2006; Colucci et al., 1998; Jaber et al., 1999*), upscaling flow and transport processes in groundwater, by either spatial or stochastic averaging, requires fields of parameters: the hydraulic conductivity (*Beckie et al., 1996a; Efendiev and Durlofsky, 2003*) or the velocity field (*Heße et al., 2009; Suciu, 2014*). The second difference, related to the first one, is the origin of the randomness. Turbulent flows are governed by the deterministic Navier-Stokes equations. But for large Reynolds numbers the flow velocity behaves like a random variable due to the sensitive dependence of the solution on initial and boundary conditions. This mathematical aspect corresponds to an experimental lack of reproducibility of the measurements in turbulent systems (*Pope, 1985*). In groundwater systems, the spatial variability of the hydraulic conductivity cannot be completely described. Therefore, stochastic parameterisations by random space functions are used to account for this uncertainty. The flow equations are thus solved in a probabilistic sense (*Cirpka et al., 2011*). In this case, randomness is caused by the uncertainty of the parameter fields propagated through the flow and transport equations, which have to be modelled as stochastic equations. The third difference is given by the available experimental data. In turbulence, detailed velocity, temperature, and concentration profiles are available from measurements. Whereas for groundwater flows, the data is scarce and depends on the support volume

of the used measuring technique.

A closer look at PDF equations will be taken in Section 2.2, followed by the detailed derivation of these equations in Section 2.3. Next, relationships between PDF equations and Fokker-Planck equations are examined in Section 2.4. These relationships are of interest, because efficient numerical solvers for Fokker-Planck equations exist. These numerical solvers are presented in Section 2.5, together with the results of numerical simulations of a transport problem in groundwater. Finally, this chapter is concluded in Section 2.6.

PDF Equations

In this chapter, a statistically homogeneous random velocity field $\mathbf{V}(\mathbf{x})$ with divergence-free samples is considered. This field is a solution of the continuity and Darcy equations with a random parameterisation of the hydraulic conductivity. Furthermore, the effects of local hydrodynamic dispersion and molecular diffusion on transport in a saturated aquifer system are modelled by an isotropic diffusion process specified by a constant diffusion coefficient D . A system of reacting chemical species described by the concentrations $C_\alpha(\mathbf{x}, t) \in \Omega_c$, $\mathbf{x} \in \Omega_x$, $t \in \mathbb{R}_+$, $\alpha = 1, \dots, N_\alpha$ is transported through the aquifer according to the system of balance equations

$$\partial_t C_\alpha + V_i \partial_{x_i} C_\alpha = D \partial_{x_i} \partial_{x_i} C_\alpha + S_\alpha, \quad (2.1)$$

where $\mathbf{S}(\mathbf{C})$ denotes the reaction rates. Since the velocity field $\mathbf{V}(\mathbf{x})$ is a random function, the concentration vector $\mathbf{C}(\mathbf{x}, t)$ is a random field as well.

The marginal one-point one-time PDF $f(\mathbf{c}; \mathbf{x}, t)$ of the random concentration \mathbf{C} solving equation (2.1) satisfies the PDF evolution equation

$$\partial_t f + \partial_{x_i} (\mathcal{V}_i f) - \partial_{x_i} \partial_{x_j} (\mathcal{D}_{ij} f) = -\partial_{c_\alpha} \partial_{c_\beta} (\mathcal{M}_{\alpha\beta} f) - \partial_{c_\alpha} (S_\alpha f), \quad (2.2)$$

where \mathcal{V} and \mathcal{D} are the stochastically upscaled drift vector and the diffusion tensor, respectively, and \mathcal{M} is the conditional dissipation rate accounting for mixing by diffusion (*Suciu et al., 2015a,b*). As a common convention, a semicolon is used in writing the concentration PDF $f(\mathbf{c}; \mathbf{x}, t)$ to emphasize the distinction between the value \mathbf{c} taken by the random function $\mathbf{C}(\mathbf{x}, t)$ in the state space Ω_c and the values \mathbf{x} and t of its independent variables in $\Omega_x \times \mathbb{R}_+$ (*Pope, 1985; Minier and Peirano, 2001*).

The two mostly used approaches to derive the PDF equation (2.2) are the delta function method and the test function method and will be presented in detail in Section 2.3. The first one starts with the definition of the PDF given by the ensemble average of delta functions depending on random fields and is shown in Section 2.3.1. For instance the concentration PDF is given by $f(\mathbf{c}; \mathbf{x}, t) = \langle \delta(\mathbf{C}(\mathbf{x}, t) - \mathbf{c}) \rangle$. Such singular space functions were shown to

define consistent probability distributions ([Suciu, 2014](#)) and formal calculus involving them corresponds to rigorous operations with Dirac functionals ([Klimenko and Bilger, 1999](#); [Suciu et al., 2015b,a](#)). The PDF equation is obtained by evaluating $\partial_t f$ from formal derivatives of δ functions ([Pope, 1976](#); [Sanchez-Vila et al., 2009](#); [Haworth, 2010](#); [Suciu et al., 2015b](#)). In the test function approach, presented in Section 2.3.2, the ensemble average of the operator $\partial_t + V_i \partial_{x_i}$ applied to a test function of state variables Q , with suitable properties, is evaluated in two different ways: first, by interchanging derivatives and the stochastic average and using the incompressibility of the velocity field. And second, by multiplying the right hand side of the concentration transport equation (2.1) by Q and taking the ensemble average. The PDF equation follows by equating the two expressions for $\langle \partial_t Q + V_i \partial_{x_i} Q \rangle$, performing integration by parts, and considering the vanishing of Q at the boundaries of Ω_c ([Pope, 1985](#); [Fox, 2003](#); [Haworth, 2010](#); [Suciu et al., 2015a](#)).

Because of the high dimensionality of the PDF equations (time and space dimensions and the N_α dimensions of the concentration space Ω_c) solutions by standard discretisation methods (finite-differences or finite-elements) are impracticable and computationally unfeasible ([Pope, 1985](#); [Haworth, 2010](#)). Therefore, numerical solutions are usually obtained by Monte Carlo methods. ‘‘Eulerian particle methods’’ simulate the finite-difference solution of the PDF equation by locating an ensemble of N notional particles at each point of a Eulerian grid. These particles have assigned representative values of the state variable, e.g. concentration, initially distributed according to the initial PDF. The particles move on the grid following rules consistent with the finite-difference scheme. Averaging over ensembles of particles converges to the expectation estimated by the finite-difference scheme as N tends to infinity ([Pope, 1981](#)). Even if they are computationally simpler than other particle methods in use, Eulerian particle methods are numerically dissipative and have low spatial accuracy ([Möbus et al., 2001](#); [Haworth, 2010](#)). Another Monte Carlo approach is the ‘‘stochastic Eulerian field method’’ which uses a representation of the PDF by an ensemble of stochastically equivalent space-time random fields, with the same one-point one-time PDF as the solution of the PDF equation ([Mustata et al., 2006](#); [Jones et al., 2012](#); [Dodoulas and Navarro-Martinez, 2013](#)). Stochastic fields are governed by partial differential equations with a linear multiplicative noise term, interpreted either in Itô ([Valiño, 1998](#)) or Stratonovich ([Sabel’nikov and Souldard, 2005](#)) form. The computational effort of solving a partial differential equation for each field renders the method of stochastic Eulerian field less competitive than other Monte Carlo methods when large numbers of fields are required ([Haworth, 2010](#)). ‘‘Lagrangian particle methods’’ use systems of stochastic particles moving in continuous space, according to grid-free particle tracking procedures. Eventually, grids are used to compute averages and to interpolate the output of averaged transport equations to the

particles positions. Lagrangian methods are now the dominant numerical approach for PDF equations. The performance of the above Monte Carlo approaches, with several variants, is analysed by [Haworth \(2010\)](#). The Lagrangian particle methods are further examined in Section 2.4.1. Using the “reverse Fokker-Planck approach”, introduced in Section 2.4.2, GRW particle methods can be used as an alternative to the Lagrangian particle methods, better suited to groundwater problems. The details of the numerical solutions of the reverse Fokker-Planck approach are shown in Section 2.4.3. The results of these simulations are presented in Section 2.5. And finally, Section 2.6 concludes this chapter.

Derivation of the PDF Transport Equation

In this section, the concentration PDF transport equation (2.2) will be derived, first by using the delta function method ([Suciu et al., 2015b](#)) in Section 2.3.1 and then by using the test function method ([Suciu et al., 2015a](#)) in Section 2.3.2.

Delta Function Method

The starting point of the derivation is the so-called fine-grained PDF, which is defined by the multidimensional Dirac delta function, see Section 1.3:

$$\rho(\mathbf{c}; \mathbf{x}, t) = \delta(\mathbf{C}(\mathbf{x}, t) - \mathbf{c}) = \prod_{\alpha=1}^{N_{\alpha}} \delta(C_{\alpha}(\mathbf{x}, t) - c_{\alpha}). \quad (2.3)$$

Then, the concentration PDF is given by the expectation of the fine-grained PDF

$$f(\mathbf{c}; \mathbf{x}, t) = \langle \delta(\mathbf{C}(\mathbf{x}, t) - \mathbf{c}) \rangle. \quad (2.4)$$

The PDF transport equation describes the PDF time evolution and as such, the time derivative of the definition of the PDF (2.4) is taken. Doing so involves derivatives of δ functions. Such a derivative is defined by

$$\int_{-\infty}^{\infty} \delta'(y_0 - y)g(y)dy = - \int_{-\infty}^{\infty} \delta(y_0 - y)g'(y)dy, \quad (2.5)$$

which can be written in a compact notation as $\delta'(g) = -\delta(g') = -g'(y_0)$. If $y_0 = h(x)$ is a function, the derivative can be generalised by

$$\begin{aligned} \partial_x \int_{-\infty}^{\infty} \delta(h(x) - y)g(y)dy &= g'(h(x))\partial_x h(x) \\ &= h'(x) \int_{-\infty}^{\infty} \delta(h(x) - y)g'(y)dy \\ &= -h'(x) \int_{-\infty}^{\infty} \delta'(h(x) - y)g(y)dy. \end{aligned} \quad (2.6)$$

This relation too can be formulated in a compact form as

$$\partial_x \delta(h(x) - y) = -h'(x) \partial_y \delta(h(x) - y). \quad (2.7)$$

Applying these relationships to the concentration PDF yields

$$\begin{aligned} \partial_t f(\mathbf{c}; \mathbf{x}, t) &= \langle \partial_t \delta(\mathbf{C}(\mathbf{x}, t) - \mathbf{c}) \rangle \\ &= - \langle \partial_t C_\alpha(\mathbf{x}, t) \partial_{c_\alpha} \delta(\mathbf{C}(\mathbf{x}, t) - \mathbf{c}) \rangle \\ &= - \partial_{c_\alpha} \langle \partial_t C_\alpha(\mathbf{x}, t) \delta(\mathbf{C}(\mathbf{x}, t) - \mathbf{c}) \rangle. \end{aligned} \quad (2.8)$$

In order to calculate derivatives, more knowledge than the one-point PDF $f(\mathbf{x}, t)$ is needed, because a derivative is the limit of the difference quotients of the dependent and independent variable. This limiting quotient is a two-point quantity. Quantities which cannot be described by one-point PDFs alone can be described by so-called conditional PDFs. To see that, a generic random function $\mathbf{Z}(\mathbf{x}, t)$ which is not fully described by one-point statistics alone is considered. Let $Q(\mathbf{Z}(\mathbf{x}, t))$ be an arbitrary random function. Then the following average can be considered

$$\begin{aligned} \langle Q(\mathbf{Z}(\mathbf{x}, t)) \delta(\mathbf{C}(\mathbf{x}, t) - \mathbf{c}) \rangle &= \left\langle \delta(\mathbf{C}(\mathbf{x}, t) - \mathbf{c}) \int_{-\infty}^{\infty} Q(\mathbf{z}) \delta(\mathbf{Z}(\mathbf{x}, t) - \mathbf{z}) d\mathbf{z} \right\rangle \\ &= \int_{-\infty}^{\infty} Q(\mathbf{z}) \langle \delta(\mathbf{Z}(\mathbf{x}, t) - \mathbf{z}) \delta(\mathbf{C}(\mathbf{x}, t) - \mathbf{c}) \rangle d\mathbf{z} \\ &= \int_{-\infty}^{\infty} Q(\mathbf{z}) f(\mathbf{c}, \mathbf{z}; \mathbf{x}, t) d\mathbf{z} \\ &= f(\mathbf{c}; \mathbf{x}, t) \int_{-\infty}^{\infty} Q(\mathbf{z}) f(\mathbf{z}|\mathbf{c}; \mathbf{x}, t) d\mathbf{z}, \end{aligned} \quad (2.9)$$

where $f(\mathbf{c}, \mathbf{z}; \mathbf{x}, t) = \langle \delta(\mathbf{Z}(\mathbf{x}, t) - \mathbf{z}) \delta(\mathbf{C}(\mathbf{x}, t) - \mathbf{c}) \rangle$ defines the joint PDF in the \mathbf{c} - \mathbf{z} sample space. This is similar to the PDF defined by (2.4) in the \mathbf{c} sample space. In the last line of (2.9) the conditional PDF is introduced, which is defined by

$$f(\mathbf{z}|\mathbf{c}; \mathbf{x}, t) = \frac{f(\mathbf{c}, \mathbf{z}; \mathbf{x}, t)}{f(\mathbf{c}; \mathbf{x}, t)}. \quad (2.10)$$

One important conclusion is the relation

$$\langle Q(\mathbf{Z}(\mathbf{x}, t)) \delta(\mathbf{C}(\mathbf{x}, t) - \mathbf{c}) \rangle = \langle Q(\mathbf{Z}(\mathbf{x}, t)|\mathbf{c}) f(\mathbf{c}; \mathbf{x}, t) \rangle, \quad (2.11)$$

which is the expectation of the random function $Q(\mathbf{Z}(\mathbf{x}, t))$ conditional of a fixed value of the concentration vector \mathbf{c} multiplied by the one-point PDF $f(\mathbf{c}; \mathbf{x}, t)$ and which will be used throughout the following derivations.

Now, the concentration transport equation (2.1) can be inserted into the time derivative of the PDF (2.8), yielding

$$\partial_t f(\mathbf{c}; \mathbf{x}, t) = \partial_{c_\alpha} \left\{ \langle [V_i \partial_{x_i} C_\alpha | \mathbf{c}] - \langle D \partial_{x_i} \partial_{x_j} C_\alpha | \mathbf{c} \rangle - S_\alpha(\mathbf{c}) \right\} f(\mathbf{c}; \mathbf{x}, t). \quad (2.12)$$

It should be noted that the last term in equation (2.12), which is the reaction term, appears in a closed form, which implies that its conditional expectation is just the value of \mathbf{S} evaluated for the sample value \mathbf{c} :

$$\langle S_\alpha(\mathbf{C}(\mathbf{x}, t)) | \mathbf{c} \rangle = \int_{-\infty}^{\infty} S_\alpha(\mathbf{c}) f(\mathbf{z} | \mathbf{c}; \mathbf{x}, t) d\mathbf{z} = S_\alpha(\mathbf{c}) \int_{-\infty}^{\infty} f(\mathbf{z} | \mathbf{c}; \mathbf{x}, t) d\mathbf{z} = S_\alpha(\mathbf{c}). \quad (2.13)$$

The other two terms are not closed and require further attention.

The advective term can be transformed to

$$\begin{aligned} \partial_{c_\alpha} [\langle V_i \partial_{x_i} C_\alpha | \mathbf{c} \rangle f(\mathbf{c}; \mathbf{x}, t)] &= \partial_{c_\alpha} \langle V_i \partial_{x_i} C_\alpha \delta(\mathbf{C}(\mathbf{x}, t) - \mathbf{c}) \rangle \\ &= -\partial_{x_i} [\langle V_i | \mathbf{c} \rangle f(\mathbf{c}; \mathbf{x}, t)], \end{aligned} \quad (2.14)$$

where the first equality follows from (2.11) and for the final result, the relationship (2.7) and the incompressibility $\partial_{x_i} V_i = 0$ were used. By decomposing the velocity into a mean part $\langle \mathbf{V} \rangle$ and a fluctuating part $\mathbf{V}' = \mathbf{V} - \langle \mathbf{V} \rangle$ and by using the gradient diffusion closure (Pope, 1985; Fox, 2003; Haworth, 2010)

$$\langle \mathbf{V}' | \mathbf{c} \rangle f(\mathbf{c}; \mathbf{x}, t) = -\mathbf{D}^* \nabla f(\mathbf{c}; \mathbf{x}, t), \quad (2.15)$$

equation (2.14) becomes

$$-\partial_{x_i} [\langle V_i | \mathbf{c} \rangle f(\mathbf{c}; \mathbf{x}, t)] = -\partial_{x_i} [\langle V_i \rangle f(\mathbf{c}; \mathbf{x}, t)] + \partial_{x_i} [D_{ij}^* \partial_{x_j} f(\mathbf{c}; \mathbf{x}, t)]. \quad (2.16)$$

The upscaled diffusion tensor \mathbf{D}^* is calculated by turbulence models (Pope, 2000) or by stochastic upscaling of diffusion in random velocity fields (Suciu, 2014; Attinger et al., 1999).

The second unclosed term in equation (2.12) is the conditional expectation of the molecular diffusion in the concentration equation (2.1). It will be shown that this term is related to the divergence of the diffusive flux in physical space of the PDF $f(\mathbf{c}; \mathbf{x}, t)$, with the same diffusion coefficient D as in equation (2.1). Since by (2.4), the PDF is given by the expectation of δ functions, the divergence of the diffusive flux of $f(\mathbf{c}; \mathbf{x}, t)$ is determined by

$$\begin{aligned} D \partial_{x_i} \partial_{x_i} f(\mathbf{c}; \mathbf{x}, t) &= D \partial_{x_i} \partial_{x_i} \langle \delta(\mathbf{C}(\mathbf{x}, t) - \mathbf{c}) \rangle \\ &= D \partial_{x_i} \langle -\partial_{x_i} C_\alpha(\mathbf{x}, t) \partial_{c_\alpha} \delta(\mathbf{C}(\mathbf{x}, t) - \mathbf{c}) \rangle \\ &= -D \langle \partial_{x_i} \partial_{x_i} C_\alpha(\mathbf{x}, t) \partial_{c_\alpha} \delta(\mathbf{C}(\mathbf{x}, t) - \mathbf{c}) + \partial_{x_i} C_\alpha(\mathbf{x}, t) \partial_{c_\alpha} \partial_{x_i} \delta(\mathbf{C}(\mathbf{x}, t) - \mathbf{c}) \rangle \\ &= -\partial_{c_\alpha} \left\langle D \partial_{x_i} \partial_{x_i} C_\alpha(\mathbf{x}, t) \delta(\mathbf{C}(\mathbf{x}, t) - \mathbf{c}) \right\rangle \\ &\quad + \partial_{c_\alpha} \partial_{c_\beta} \langle D \partial_{x_i} C_\alpha \partial_{x_i} C_\beta \delta(\mathbf{C}(\mathbf{x}, t) - \mathbf{c}) \rangle \\ &= -\partial_{c_\alpha} [\langle D \partial_{x_i} \partial_{x_i} C_\alpha | \mathbf{c} \rangle f(\mathbf{c}; \mathbf{x}, t)] \\ &\quad + \partial_{c_\alpha} \partial_{c_\beta} [\langle D \partial_{x_i} C_\alpha \partial_{x_i} C_\beta | \mathbf{c} \rangle f(\mathbf{c}; \mathbf{x}, t)]. \end{aligned} \quad (2.17)$$

With equations (2.16) and (2.17), the velocity, dispersion, and mixing coefficients can be defined as:

$$\mathcal{V}_i = \langle V_i \rangle + \partial_{x_j} D_{ij}^*, \quad (2.18)$$

$$\mathcal{D}_{ij} = D + D_{ij}^*, \quad (2.19)$$

$$\mathcal{M}_{\alpha\beta} = \langle D \partial_{x_i} C_\alpha \partial_{x_i} C_\beta | \mathbf{c} \rangle. \quad (2.20)$$

Inserting these coefficients into equation (2.12), a PDF transport equation is derived and it takes the form of equation (2.2).

Test Function Method

The test function method derives the concentration PDF transport equation (2.2) without using δ functions (Suci *et al.*, 2015a). An arbitrary function $Q(\mathbf{x}, t) = Q(\mathbf{C}(\mathbf{x}, t))$ with compact support in the interior of the concentration space Ω_c is considered, which only depends on space and time variables through the random concentration vector $\mathbf{C}(\mathbf{x}, t)$. Two independent expressions of the ensemble average of the product between a weighting function $\Theta(C(\mathbf{x}, t))$ and the differential operator $A = \partial_t + V_i \partial_{x_i}$ applied to the function Q will be equated, yielding equation (2.2). The function $\Theta(C(\mathbf{x}, t))$ will be discussed in detail in Section 2.4 and for now it is enough to know that it fulfills the continuity equation $\partial_t \Theta + V_i \partial_{x_i} \Theta = 0$ and that it will be used in the following to define weighted PDFs.

The first expression is given by

$$\begin{aligned} \langle \Theta A Q \rangle &= \langle \Theta \partial_t Q + \Theta V_i \partial_{x_i} Q \rangle = \langle \partial_t (\Theta Q) + \partial_{x_i} (V_i \Theta Q) \rangle \\ &= \partial_t \langle \Theta Q \rangle + \langle V_i \rangle \partial_{x_i} \langle \Theta Q \rangle + \partial_{x_i} \langle V_i' \Theta Q \rangle, \end{aligned} \quad (2.21)$$

besides the continuity equation for Θ , the incompressibility of the velocity field $\partial_{x_i} V_i = 0$ and the Reynolds decomposition of the velocity field into its mean part and the fluctuations about the mean $V_i' = V_i - \langle V_i \rangle$ where used here. In order to compute the ensemble average (2.21), more information is needed than provided by the one-point PDF $f(\mathbf{c}; \mathbf{x}, t)$. In this case, the statistics of the velocity field are not fully described. Following Fox (2003, Section 6.2), the unknown statistics are lumped together in a random vector $\mathbf{Z} \in \Omega_z$ and the joint PDF $f(\mathbf{c}, \mathbf{z}; \mathbf{x}, t)$ is considered. The ensemble average of a function $f(\mathbf{C}, \mathbf{Z}) = F_1(\mathbf{C})F_2(\mathbf{Z})$ is then computed by

$$\begin{aligned} \langle F(\mathbf{C}(\mathbf{x}, t), \mathbf{Z}(\mathbf{x}, t)) \rangle &= \int_{\Omega_c} \int_{\Omega_z} F_1(\mathbf{c}) F_2(\mathbf{z}) f(\mathbf{c}, \mathbf{z}; \mathbf{x}, t) d\mathbf{c} d\mathbf{z} \\ &= \int_{\Omega_c} F_1(\mathbf{c}) \langle F_2 | \mathbf{c} \rangle f(\mathbf{c}; \mathbf{x}, t) d\mathbf{c}, \end{aligned} \quad (2.22)$$

where the conditional average is performed with respect to the conditional PDF $f(\mathbf{z} | \mathbf{c}; \mathbf{x}, t) = f(\mathbf{c}, \mathbf{z}; \mathbf{x}, t) / f(\mathbf{c}; \mathbf{x}, t)$:

$$\langle F_2 | \mathbf{c} \rangle = \int_{\Omega_z} F_2(\mathbf{z}) f(\mathbf{z} | \mathbf{c}; \mathbf{x}, t) d\mathbf{z}. \quad (2.23)$$

With equations (2.22) and (2.23), the first expression for the ensemble average (2.21) becomes

$$\begin{aligned} \langle \Theta A Q \rangle &= \\ \int_{\Omega_c} Q(\mathbf{c}) \Theta(\mathbf{c}) \{ \partial_t f(\mathbf{c}; \mathbf{x}, t) + \langle V_i \rangle \partial_{x_i} f(\mathbf{c}; \mathbf{x}, t) + \partial_{x_i} [\langle V_i' | \mathbf{c} \rangle f(\mathbf{c}; \mathbf{x}, t)] \} d\mathbf{c}. \end{aligned} \quad (2.24)$$

The second expression for $\langle \Theta A Q \rangle$ follows from the fact that Q depends on time and space variables through the random concentration $\mathbf{C}(\mathbf{x}, t)$ and AC is given by the right hand side of the concentration transport equation (2.1):

$$\begin{aligned} \langle \Theta A Q \rangle &= \langle \Theta \partial_{c_\alpha} Q A C_\alpha \rangle = \langle \Theta \partial_{c_\alpha} Q [D \partial_{x_i} \partial_{x_i} C_\alpha + S_\alpha(\mathbf{C})] \rangle \\ &= \int_{\Omega_c} \Theta(\mathbf{c}) \partial_{c_\alpha} Q(\mathbf{c}) [\langle D \partial_{x_i} \partial_{x_i} C_\alpha | \mathbf{c} \rangle + S_\alpha(\mathbf{c})] f(\mathbf{c}; \mathbf{x}, t) d\mathbf{c}. \end{aligned} \quad (2.25)$$

To obtain equation (2.25), the chain rule and the averaging procedure (2.22) were used. Integrating by parts yields

$$\begin{aligned} \langle \Theta A Q \rangle &= \int_{\partial\Omega_c} Q(\mathbf{c}) \{ \Theta(\mathbf{c}) [\langle D \partial_{x_i} \partial_{x_i} C_\alpha | \mathbf{c} \rangle + S_\alpha] f(\mathbf{c}; \mathbf{x}, t) \} n_\alpha d\Gamma_c \\ &\quad - \int_{\Omega_c} Q(\mathbf{c}) \partial_{c_\alpha} \{ \Theta(\mathbf{c}) [\langle D \partial_{x_i} \partial_{x_i} C_\alpha | \mathbf{c} \rangle + S_\alpha(\mathbf{c})] f(\mathbf{c}; \mathbf{x}, t) \} d\mathbf{c}, \end{aligned} \quad (2.26)$$

where \mathbf{n} is the outward pointing unit vector normal to the boundary $\partial\Omega_c$ of the concentration space Ω_c and $d\Gamma_c$ is the surface element. Since the function $Q(\mathbf{c})$ has a compact support in Ω_c , it vanishes on the boundary $\partial\Omega_c$ and with it the first integral vanishes too, so finally following equation is obtained:

$$\langle \Theta A Q \rangle = - \int_{\Omega_c} Q(\mathbf{c}) \partial_{c_\alpha} \{ \Theta(\mathbf{c}) [\langle D \partial_{x_i} \partial_{x_i} C_\alpha | \mathbf{c} \rangle + S_\alpha(\mathbf{c})] f(\mathbf{c}; \mathbf{x}, t) \} d\mathbf{c}. \quad (2.27)$$

Since expressions (2.24) and (2.27) should give the same result for any function Q with compact support, equating them yields the evolution equation

$$\partial_t \mathcal{F} + \langle V_i \rangle \partial_{x_i} \mathcal{F} = - \partial_{x_i} [\langle V_i' | \mathbf{c} \rangle \mathcal{F}] - \partial_{c_\alpha} [\langle D \partial_{x_i} \partial_{x_i} C_\alpha | \mathbf{c} \rangle \mathcal{F}] - \partial_{c_\alpha} (S_\alpha \mathcal{F}), \quad (2.28)$$

where $\mathcal{F} = \Theta f$. Equation (2.28) is still unclosed and the conditional average of the velocity fluctuations and that of the diffusive flux on the right hand side require modelling. The same gradient-diffusion closure (2.15) as used in Section 2.3.1 is used to close the first term. Doing so yields the diffusion term $\partial_{x_i} D_{ij}^* \partial_{x_j} \mathcal{F}$. To put equation (2.28) into a Fokker-Planck form, the term $\partial_{x_i} \mathcal{F} \partial_{x_j} D_{ij}^*$ is added on both sides, which also implies defining the new drift coefficients $\mathcal{V}_i = \langle V_i \rangle + \partial_{x_j} D_{ij}^*$, which is identical to (2.18). The

final remaining unclosed term is treated in the same way as in Section 2.3.1, equation (2.17). Now, the upscaled diffusion coefficient is defined as (2.19) and the conditional dissipation tensor is defined as (2.20). Then, the result is equation (2.2).

The Fokker-Planck Approach to PDF Equations

Direct Fokker-Planck Approach

Following the work of *Suciu et al.* (2016), the relationship between concentration PDFs and Fokker-Planck equations are examined in this section. Lagrangian particle methods are based on the similarity between PDF equations of type (2.2) and Fokker-Planck equations. It is common to compare (*Colucci et al.*, 1998; *Jaberi et al.*, 1999; *Meyer et al.*, 2010), or even to assimilate (*Wacławczyk et al.*, 2008) PDF equations to Fokker-Planck equations and to use the associated Itô equations as a model for Lagrangian particles. Furthermore, numerical solutions of equation (2.2) are constructed by imposing a uniform distribution of Lagrangian particles during the simulations. To understand this constraint, the concentration PDF problem is considered and it is noted that the corresponding PDF fulfills the normalisation condition $\int_{\Omega_c} f(\mathbf{c}; \mathbf{x}, t) d\mathbf{c} = 1$. On the other side, if equation (2.2) were a Fokker-Planck equation, its solution would be a PDF $p(\mathbf{c}, \mathbf{x}, t)$ defined in the concentration-position state space $\Omega = \Omega_c \times \Omega_x$ (*Suciu et al.*, 2015a), which yields $\int_{\Omega_c} p(\mathbf{c}, \mathbf{x}, t) d\mathbf{c} = p_x(\mathbf{x}, t)$ by integration over Ω_c , where $p_x(\mathbf{x}, t)$ is the position PDF of the Lagrangian particles. A uniform particle distribution $p_x(\mathbf{x}, t) = \text{const}$, would suffice to make $p(\mathbf{c}, \mathbf{x}, t)$ proportional to $f(\mathbf{c}; \mathbf{x}, t)$, which allows estimating the concentration PDF from the solution of the Fokker-Planck equation. As will be shown in the following, a general relation between the two PDFs $f(\mathbf{c}; \mathbf{x}, t)$ and $p(\mathbf{c}, \mathbf{x}, t)$, which renders them consistent with the same normalisation condition may be established if a suitable weighting function Θ exists such that $\int_{\Omega_c} \Theta(\mathbf{c}) f(\mathbf{c}; \mathbf{x}, t) d\mathbf{c} = p_x(\mathbf{x}, t)$.

In operator splitting schemes the transport of the PDF in physical space is treated in separate advection and diffusion steps (*Pope*, 1981). These two steps solve equation (2.2) with the right-hand side set to zero (*Pope*, 1985). This equation has the form of a Fokker-Planck equation describing the position PDF of a passive scalar. The corresponding Itô equation used to simulate the transport step in Lagrangian particle methods (*Wang et al.*, 2010) has the form

$$dX_i(t) = \mathcal{V}_i(\mathbf{X}, t)dt + d\tilde{W}_i(\mathbf{X}, t), \quad (2.29)$$

where $\{X_i, i = 1, 2, 3\}$ are trajectories of an Itô diffusion process and \tilde{W}_i is a Wiener process with expectation $E\{\tilde{W}_i(\mathbf{X}, t)\} = 0$ and variance $E\{\tilde{W}_i^2(\mathbf{X}, t)\} = 2 \int_0^t \mathcal{D}_{ii}(\mathbf{X}, t')dt'$. The other fractional steps of the Lagrangian approach

([Pope, 1985](#); [Wang et al., 2010](#)) correspond to the transport in concentration space and may be formulated in a general way as

$$dC_\alpha(t) = M_\alpha(C_\alpha(t))dt + S_\alpha(\mathbf{C}(t))dt, \quad (2.30)$$

where $C_\alpha(t) = C_\alpha(\mathbf{X}(t))$ and the coefficients M_α are provided by mixing models for the term containing the dissipation rate $\mathcal{M}_{\alpha\beta}$ in equation (2.2) ([Suciu et al., 2015a](#)).

To design a Monte Carlo method based on equations (2.29) and (2.30), a correspondence between the two mathematical objects involved have to be established. These objects are the stochastic process $\{\mathbf{C}(t), \mathbf{X}(t)\}$, indexed by a single index t , and the multi-index random function $\mathbf{C}(\mathbf{x}, t)$. To do so, it is pointed out that the Itô equation (2.29) and the corresponding Fokker-Planck equation ([Kloeden and Platen, 1999](#)) for the position PDF

$$\partial_t p_x + \partial_{x_i}(\mathcal{V}_i p_x) = \partial_{x_i} \partial_{x_j}(\mathcal{D}_{ij} p_x), \quad (2.31)$$

do not depend on concentrations (i.e. on the process $C_\alpha(t)$ or on the state space variable \mathbf{c}). Therefore, they may be used to describe any conserved scalar transported in the same system (with the same parameters \mathcal{V}_i and \mathcal{D}_{ij}) under the same initial conditions. Equation (2.31) also coincides with the equation satisfied by the ensemble averaged ([Meyer et al., 2010](#)) scalar, which can be derived by multiplying the PDF equation (2.2) without the reaction term by the scalar and by taking the ensemble average. It follows that for any conserved scalar $\Theta(\mathbf{x}, t)$ solving equation (2.1) without reaction terms, the ensemble averaged $\langle \Theta \rangle$ solves the Fokker-Planck equation (2.31) and thus

$$\frac{\langle \Theta \rangle(\mathbf{x}, t)}{\Theta^*} = p_x(\mathbf{x}, t), \quad \text{where } \Theta^* = \int_{\Omega_x} \langle \Theta \rangle(\mathbf{x}, t) d\mathbf{x}. \quad (2.32)$$

Next, a conserved scalar depending on (\mathbf{x}, t) through concentrations of chemical species, $\Theta(\mathbf{x}, t) = \Theta(\mathbf{C}(\mathbf{x}, t))$ is considered. Making use of the definition of the PDF via delta functions (2.4), equation (2.32) is rewritten as

$$\begin{aligned} \frac{\langle \Theta(\mathbf{C}(\mathbf{x}, t)) \rangle}{\Theta^*} &= \frac{1}{\Theta^*} \left\langle \int_{\Omega_c} \Theta(\mathbf{c}) \delta(\mathbf{C}(\mathbf{x}, t) - \mathbf{c}) d\mathbf{c} \right\rangle \\ &= \frac{1}{\Theta^*} \int_{\Omega_c} \Theta(\mathbf{c}) f(\mathbf{c}; \mathbf{x}, t) d\mathbf{c} \\ &= \int_{\Omega_c} p(\mathbf{c}, \mathbf{x}, t) d\mathbf{c}. \end{aligned} \quad (2.33)$$

The last equality in (2.33) is ensured by choosing

$$\Theta(\mathbf{c}) f(\mathbf{c}; \mathbf{x}, t) = \Theta^* p(\mathbf{c}, \mathbf{x}, t). \quad (2.34)$$

Relation (2.34) provides a correspondence between the one-point statistics of the random concentration $\mathbf{C}(\mathbf{x}, t)$ and that of the stochastic process $\{\mathbf{C}(t), \mathbf{X}(t)\}$ (Suciu *et al.*, 2016). Hence, the normalised scalar Θ/Θ^* is the weighting function sought after. For the first time, such a correspondence has been introduced in a somewhat heuristic manner by Suciu *et al.* (2015a) and further analysed by Suciu *et al.* (2015b).

With $p(\mathbf{c}|\mathbf{x}, t) = p(\mathbf{c}, \mathbf{x}, t)/p_x(\mathbf{x}, t)$ being the conditional PDF of the concentration given the position of the stochastic process (2.29) - (2.30) and using equation (2.32), relation (2.34) becomes equivalent to

$$\frac{\Theta(\mathbf{c})}{\langle \Theta \rangle(\mathbf{x}, t)} f(\mathbf{c}; \mathbf{x}, t) = p(\mathbf{c}|\mathbf{x}, t). \quad (2.35)$$

Thus, relation (2.34) not only solves the normalisation issue, but according to (2.35) it also determines the one-point statistics of the weighted concentration PDF by that of the stochastic process (2.29) - (2.30). It is worth mentioning that the PDF $f(\mathbf{c}; \mathbf{x}, t)$ of the random concentration cannot be uniquely determined by relation (2.34). Instead, based on (2.35), the system of Itô equations (2.29) - (2.30) can be used to compute the concentration PDF weighted by a normalised conserved scalar.

The conserved scalar Θ can be chosen as the sum of all species concentrations composing the reaction system $\Theta = \sum_{\alpha=1}^{N_\alpha} C_\alpha$. This sum is conserved in closed systems as a consequence of mass conservation of the total amount of chemical elements contained in the reacting species molecules (Suciu *et al.*, 2015b). That this is indeed the case has been proven by Suciu *et al.* (2016) by a slight extension of the method used by Bilger (1976) to construct conserved scalars as concentrations of chemical elements. Let $r_{\alpha k}$ be the weight (e.g. the mass fraction) of the chemical element indexed by k in the composition of the molecules α and let C_k be the total concentration of the element k . Obviously, the elemental masses sum to unity: $\sum_{k=1}^{N_k} r_{\alpha k} = 1$ and $C_k = \sum_{\alpha=1}^{N_\alpha} r_{\alpha k} C_\alpha$. It follows that

$$\sum_{k=1}^{N_k} C_k = \sum_{k=1}^{N_k} \sum_{\alpha=1}^{N_\alpha} r_{\alpha k} C_\alpha = \sum_{\alpha=1}^{N_\alpha} C_\alpha \sum_{k=1}^{N_k} r_{\alpha k} = \sum_{\alpha=1}^{N_\alpha} C_\alpha, \quad (2.36)$$

that is, the sum of elemental concentrations equals the sum of species concentrations. Since elemental concentrations are conserved under chemical reactions, the sum of species concentrations is a conserved scalar. Furthermore, summing up the concentration equations (2.1) with species independent coefficients, one obtains the relation $\sum_{\alpha=1}^{N_\alpha} S_\alpha = 0$, which expresses the conservation of mass of the reacting system, if C_α are mass concentrations.

In particular, if the transport problem is formulated in terms of mass concentrations $C_\alpha = \rho_\alpha$ and all the components of the fluid system are included among the N_α species, it is $\Theta = \sum_{\alpha=1}^{N_\alpha} \rho_\alpha = \rho$, where ρ is the fluid

density. Then, according to equation (2.32), $\Theta^* = M$ is the total mass of fluid in Ω_x , $\langle \rho \rangle(\mathbf{x}, t) = Mp_x(\mathbf{x}, t)$, and the correspondence relation (2.34) takes the form

$$\rho(\mathbf{c})f(\mathbf{c}; \mathbf{x}, t) = Mp(\mathbf{c}, \mathbf{x}, t), \quad (2.37)$$

which relates the mass density function $\mathcal{F}(\mathbf{c}, \mathbf{x}; t) = \rho(\mathbf{c})f(\mathbf{c}; \mathbf{x}, t)$ to the PDF $p(\mathbf{c}, \mathbf{x}, t)$ of the system of stochastic particles used in Lagrangian Monte Carlo solution algorithms (Pope, 1985).

With the correspondence relation (2.34) inserted, equation (2.28) can also be interpreted as a Fokker-Planck equation for the PDF $p(\mathbf{c}, \mathbf{x}, t)$ governing the concentration position process:

$$\begin{aligned} & \partial_t p(\mathbf{c}, \mathbf{x}, t) + \langle V_i \rangle \partial_{x_i} p(\mathbf{c}, \mathbf{x}, t) + \partial_{x_i} [\langle V_i' | \mathbf{c} \rangle p(\mathbf{c}, \mathbf{x}, t)] \\ & = - \partial_{c_\alpha} \{ [\langle D \partial_{x_i} \partial_{x_i} C_\alpha | \mathbf{c} \rangle + S_\alpha(\mathbf{c})] p(\mathbf{c}, \mathbf{x}, t) \}. \end{aligned} \quad (2.38)$$

Only if $\Theta = \text{const}$ is assumed, can the same models which lead to the coefficients (2.18), (2.19), and (2.20) be applied. But the assumption $\Theta = \text{const}$, together with equation (2.32) implies a uniform position PDF equal to the inverse of the volume of the physical domain, $\Theta/\Theta^* = p_x(\mathbf{x}, t) \equiv 1/\int_{\Omega_x} d\mathbf{x}$, and from (2.35) one obtains

$$f(\mathbf{c}; \mathbf{x}, t) = p(\mathbf{c} | \mathbf{x}, t). \quad (2.39)$$

Further, with the parameters (2.18) - (2.20) and with equation (2.39) inserted into (2.38), one obtains the PDF equation (2.2) (Suciu *et al.*, 2015a).

In turbulence applications, the D_{ij}^* component of the upscaled diffusion coefficients \mathcal{D}_{ij} defined in (2.19) is an isotropic tensor, called ‘‘turbulent diffusion coefficient’’, which may vary in space and time (Pope, 1985). If only the gradient-diffusion closure is considered in equation (2.38), without transforming the conditional diffusion flux, then $\mathcal{D}_{ij} = D_{ij}^*$ and in the PDF equation (2.2) the mixing term has to be replaced by the first term on the right hand side of equation (2.38) (Pope, 1985, 2000; Fox, 2003). In models for solute plumes migrating in groundwater systems and for statistically homogeneous velocity fields, considered in this study, \mathcal{D}_{ij} are the ensemble dispersion coefficients which govern the evolution of the mean concentration, see (2.31). The corresponding term D_{ij}^* is the contribution of velocity correlations and it is an anisotropic tensor whose components are time-dependent and uniform in space (Suciu, 2014). Then, the drift coefficient (2.18) coincides with the ensemble averaged velocity, $\mathcal{V}_i = \langle V_i \rangle$. For $\Theta = \rho = \text{const}$, equation (2.2) with coefficients given by (2.18) - (2.20) and the relation (2.39) provide the framework of the PDF approach for constant density flows (Fox, 2003; Meyer *et al.*, 2010; Colucci *et al.*, 1998; Wacławczyk *et al.*, 2008). It is noted that it is only in this simple situation of a constant weighting factor Θ that the PDF equation (2.2) can be treated as a Fokker-Planck equation.

Within the direct Fokker-Planck approach, the coefficients of equation (2.38) are determined by those of the transport equations (2.1) through

unclosed conditional averages. The joint concentration-position PDF solving this equation can be numerically approximated by the associated Itô equations (2.29) and (2.30) and interpreted as a weighted concentration PDF by using the correspondence relation (2.34). Relations between joint concentration-position PDFs of Itô processes and density weighted concentration PDFs (2.37) are the core of the Lagrangian particle Monte Carlo approaches. These approaches were introduced by somewhat involved arguments using the concept of “fluid particles” (Pope, 1985; Minier and Peirano, 2001; Fox, 2003), which is rather questionable for systems undergoing diffusion (Suciu et al., 2015a).

Reverse Fokker-Planck Approach

Following Suciu et al. (2016), the issue of choosing the weighting function Θ for reactive transport in groundwater is discussed in this section. The balance equation for the solvent is considered together with those for $N_{\alpha-1}$ reacting species concentrations. Then, by summing up these equations, not only the sum of the reaction rates but also that of the diffusion fluxes vanishes. Then, it follows that the solution $\Theta = \sum_{\alpha=1}^{N_{\alpha}} C_{\alpha}$ of the continuity equation

$$\partial_t \Theta + V_i \partial_{x_i} \Theta = 0 \quad (2.40)$$

is precisely the density ρ of the fluid system (Herz, 2014). Considering the balance equations for all the components of the fluid is a natural choice in PDF approaches for reacting gas mixtures (Pope, 1985), where different components may have comparable weights. Including the carrying fluid among species components of a dilute solution transported in groundwater may cause difficulties in solving PDF problems. Even if the complicated balance equation for the solvent may be avoided by using the $N_{\alpha-1}$ equations (2.1) and the continuity equation (2.40) (Herz, 2014), the numerical solution of the system of Itô equations (2.29) - (2.30) would be complicated by the need to consider the initial condition for the carrying fluid. If one neglects the variations of the solvent concentration, which is tantamount to considering constant density flows, in a direct Fokker-Planck approach, then equation (2.32) imposes a uniform position PDF. In turn, a space-time constant solution of the position PDF equation (2.31) requires some relations between the spatial derivatives of the drift and diffusion coefficients (Suciu et al., 2015a), which may not be fulfilled in case of statistically inhomogeneous velocity fields (Morales-Casique et al., 2006a). Such issues can be avoided in a Fokker-Planck approach which does not require the fulfillment of the continuity equation (2.40).

Such an alternative Fokker-Planck approach has already been suggested by Suciu (2014). Instead of specifying the system of Itô equations by the (modelled) coefficients of the Fokker-Planck equation (2.38), modelled Itô equations may be used to derive a Fokker-Planck equation. In the case

considered here, given the system of Itô equations (2.29) - (2.30), the corresponding Fokker-Planck equation is (Kloeden and Platen, 1999)

$$\partial_t p + \partial_{x_i}(\mathcal{V}_i p) + \partial_{c_\alpha}(M_\alpha p) = \partial_{x_i} \partial_{x_j}(\mathcal{D}_{ij} p) - \partial_{c_\alpha}(S_\alpha p). \quad (2.41)$$

According to the correspondence relation (2.34), the solution p of the Fokker-Planck equation (2.41) coincides with the concentration PDF f weighted by a conserved scalar Θ solving the concentration equation (2.1) without reaction terms, but not necessarily solving the continuity equation (2.40). This “reverse” Fokker-Planck approach could be a valid option in modelling groundwater systems, for which dispersion coefficients \mathcal{D}_{ij} are provided by various theoretical (Rubin *et al.*, 1999; Cirpka *et al.*, 2011; De Barros and Rubin, 2011) or numerical (Efendiev *et al.*, 2000; Suciu, 2014) methods and mixing models may be inferred from measurements (Suciu *et al.*, 2015b). Similar reverse approaches have been used in a hydrological context to obtain the Fokker-Planck equation for the concentration PDF of a process generated by a given mixing model for fixed positions in physical space (Bellin and Tonina, 2007), and, in a general setting, to formulate the evolution equation for the velocity-concentration PDF (Meyer *et al.*, 2010). Also, similar to this approach is the derivation of the evolution equation for the mass density function from a diffusion model for the velocity of discrete particles dispersed in turbulent flows presented by Minier *et al.* (2014). The novelty of the reverse Fokker-Planck approach presented in this work is that it does not require the conserved scalar Θ to be a solution of the continuity equation.

Numerical Solutions

A straightforward solution to the system of Itô equations (2.29) and (2.30) is given by a grid-free particle tracking in the concentration-position state space $\Omega_c \times \Omega_x$. A particle follows a trajectory which starts at an initial position $(\mathbf{c}_0, \mathbf{x}_0)$ drawn from the initial PDF $p(\mathbf{c}, \mathbf{x}, 0)$. N particles initialised in the same way are used to form a statistical ensemble. The approximation of $p(\mathbf{c}, \mathbf{x}, t)$ at $t > 0$ is given by the particle distribution in computational cells around (\mathbf{c}, \mathbf{x}) . As an example, a two-dimensional passive transport in groundwater with initial concentration $C(\mathbf{x}, 0) = 1$ in a rectangular initial support in the (x_1, x_2) plane is considered. The initial PDF $p(c, \mathbf{x}, 0)$ is approximated by a uniform distribution of particles in the same rectangle lifted in a plane parallel to the (x_1, x_2) plane which intersects the concentration axis at $c = 1$. The actual joint concentration-position PDF $p(c, \mathbf{x}, t)$ is then approximated at the centre of the cubic cells of a regular lattice in the (c, x_1, x_2) space by the number of particles n in each cell, through the particle number density n/N .

In Lagrangian particle approaches, the solution algorithm differs from the straightforward solution to the system of Itô equations. A “notional

particle” carries a “composition” $\mathbf{c} = \{c_1, \dots, c_{N_\alpha}\}$ of species concentrations in physical space. The Itô equation (2.29) is solved for N notional particles and Itô equation (2.30), solved for each particle, updates its composition (Pope, 1985; Fox, 2003). For a fixed initial position \mathbf{x}_0 of a notional particle, the composition \mathbf{c}_0 , consistent with the initial PDF $p(\mathbf{c}, \mathbf{x}, 0)$, has to be extracted from the conditional PDF $p(\mathbf{c}|\mathbf{x}, 0)$. It follows that the initial distribution of notional particles has to approximate the position PDF $p_x(\mathbf{x}, 0)$, to ensure that the joint event “extracting \mathbf{c}_0 and \mathbf{x}_0 ” belongs to the ensemble with the PDF $p(\mathbf{c}|\mathbf{x}, 0)p_x(\mathbf{x}, 0) = p(\mathbf{c}, \mathbf{x}, 0)$. The algorithm is mainly useful when one wants to impose a uniform position PDF p_x which allows representing the concentration PDF through conditional PDFs of the Itô process by using equation (2.39). As an illustration, for the case of two-dimensional passive transport discussed above, the notional particles are initially uniformly distributed and their concentrations are set to unity for particles inside the rectangular support of the initial concentration and to zero outside (Meyer et al., 2010). The concentration PDF $p(\mathbf{c}, \mathbf{x}, t)$ may be approximated by histograms obtained from ensembles of particles in cells, further smoothed by spline functions (Pope, 1985), taking spatially constant values in the cells (Meyer et al., 2010), or in a weak sense, through estimations of cell averaged quantities (Minier and Peirano, 2001).

Both particle tracking and Lagrangian particle methods suffer from the increase of the computational costs with the number of particles and from numerical diffusion generated by interpolation of cell averages to the particles’ positions (Klimenko, 2007; Suciú et al., 2015a). Such inconveniences are overcome by using a global random walk (GRW) algorithm as presented in Section 1.4. Unlike sequential particle tracking procedures, in GRW algorithms all N particles used to construct a numerical estimate of the probability density solving the Fokker-Planck equation are distributed on the lattice, according to the initial PDF, at the beginning of the simulation. The particles from each lattice site are then globally spread over new positions on the lattice determined by drift and diffusion coefficients, according to binomial distributions. This numerical procedure is free of numerical diffusion by construction. Moreover, the GRW algorithm is practically insensitive to the increase of the number of particles (Suciú, 2014). Since mean values are defined at lattice sites, the GRW solutions are not affected by the artificial diffusion caused by cell averaging and interpolation in particle tracking and Lagrangian particle approaches.

PDF Simulations

A two-dimensional problem for passive transport in saturated aquifers, previously considered for investigations on ergodicity, memory effects, and asymptotic behaviour (Suciú, 2014; Suciú et al., 2006, 2009, 2016), is chosen

to illustrate the principles and utilities of the PDF approach in subsurface hydrology.

Within the frame of the reverse Fokker-Planck approach presented in Section 2.4.2, the PDF solutions will be computed from the one-time PDF of a two-dimensional Itô process, governed by a particular form of equations (2.29) and (2.30):

$$dX(t) = \mathcal{V}dt + \sqrt{2\mathcal{D}}dW_1(t), \quad (2.42)$$

$$dC(t) = \mathcal{V}_c dt + \sqrt{2\mathcal{D}_c}dW_2(t), \quad (2.43)$$

where $C(t) = C(X(t))$ and $W_1(t), W_2(t)$ are two independent standard Wiener processes (Suciu, 2014). The particular form of the Fokker-Planck equation (2.41) derived from the Itô equations (2.42) and (2.43) is

$$\partial_t p + \mathcal{V}\partial_x p + \mathcal{V}_c\partial_c p = \mathcal{D}\partial_x^2 p + \mathcal{D}_c\partial_c^2 p. \quad (2.44)$$

The PDF $f(c; x, t)$ is estimated from the solution $p(c, x, t)$ of the Fokker-Planck equation (2.44) via relationship (2.35) with $\Theta(c) = c$, which makes it to

$$\frac{\mathbf{c}}{\langle C \rangle(\mathbf{x}, t)} f(\mathbf{c}; \mathbf{x}, t) = p(\mathbf{c}|\mathbf{x}, t). \quad (2.45)$$

This choice will be evaluated in Section 2.5.1.

Samples of a Gaussian random velocity field are numerically generated with the Kraichnan formula (1.22), as presented in Section 1.5. The variance of the underlying hydraulic conductivity field is set to $\sigma_Y^2 = 0.1$, the correlation length to $\lambda_Y = 1$ m with a corresponding integral scale of $I_Y = 0.09$ m and the mean velocity to $\langle \mathbf{V} \rangle = (1, 0)^T \text{m d}^{-1}$. The local dispersion is described by an isotropic and constant diffusion coefficient $D = 0.01 \text{m}^2 \text{d}^{-1}$. With these parameters, the longitudinal ensemble dispersion coefficient (Suciu et al., 2006) takes the long time asymptotic value of $D_{11}^{\text{ens}} = D + \langle V_1 \rangle I_Y = 0.1 \text{m}^2 \text{d}^{-1}$ so that $D_{11}^{\text{ens}}/D = 10$. The initial plume is chosen as a slab of size $1 \text{m} \times 100 \text{m}$, which corresponds to a transversal dimension of 100 correlation scales of the random hydraulic conductivity field. Statistical ensembles are obtained by repeating simulations for $R = 256$ to $R = 3072$ realisations of the velocity field. The larger ensemble of 3072 realisations is computed with an exponential correlation of the log-conductivity field, with the same correlation length and variance as the Gaussian correlation considered here (Suciu et al., 2006).

As an observable affected by uncertainty, the cross-section concentration at the plume centre of mass is considered. It is obtained by summing the number of particles $n(x_1, x_2, t)$ over transversal slabs $\Delta x_1 \times L_{x_2}$, where $\Delta x_1 = 1$ m and L_{x_2} is the transversal length of the computational domain. This concentration

$$C(x, t) = \int_0^{L_{x_2}} c(x_1, x_2, t) dx_2, \quad (2.46)$$

is estimated on the trajectory $x_1 = \langle V_1 \rangle t$ of the ensemble averaged flow velocity at intervals of one day.

Reference estimates of the concentration PDFs and dispersion coefficients are obtained from the ensembles of Monte Carlo simulations presented by *Suciu et al. (2006)*, as well as from new simulations performed during this work.

The transport of the cross-section averaged concentration C is essentially one-dimensional. For now, the assertion is made that the upscaled velocity is the ensemble averaged longitudinal velocity $\mathcal{V} = \langle V_1 \rangle = 1 \text{ m d}^{-1}$ and the upscaled diffusion coefficient is the time-dependent longitudinal ensemble dispersion coefficient $D_{11}^{\text{ens}}(t)$ (*Suciu, 2014*). These assertions allow the reduction of the dimensionality of the PDF problem by one. Their validity will be demonstrated numerically in Section 2.5.3.

Weighting Function

The Monte Carlo results presented in Figures 2.1 and 2.2 show that there is no significant difference between the concentration PDFs $f(c; x, t)$ and the weighted PDFs $cf(c; x, t)/\langle C \rangle$. This is a consequence of the large transversal slab source, for which the transport is almost ergodic (*Suciu, 2014; Suciu et al., 2006*), that is $C \approx \langle C \rangle$. Therefore, relation (2.35) may be approximated by (2.39). In Section 2.5.3, the concentration PDF $f(c; x, t)$ will be estimated by the conditional PDF $p(c|x, t) = p(c, x, t)/p_x(x, t)$. The latter is obtained by GRW simulations consisting of superpositions of about 10^{25} solutions of the Itô equations (2.42) and (2.43) projected onto a regular grid. The computational particles are initially distributed on the c -axis at $x = 0$ proportionally to the concentration PDF estimated by Monte Carlo simulations at $t = 1 \text{ d}$. Contours of the particle numbers of such a simulation are shown in Figure 2.3.

Upscaled Diffusion Coefficients

Thanks to their self-averaging property, upscaled diffusion coefficients can be efficiently estimated from computations on single trajectories of the advection-diffusion process (*Suciu and Vamoş, 2009; Suciu, 2014; Suciu et al., 2016*, Appendix B) specified in Section 2.5. Such estimations were validated numerically for diffusion in velocity fields with finite correlation lengths (*Suciu and Vamoş, 2009*). One expects these estimations also to be valid in the case of power law correlated velocities as long as their covariance sampled on trajectories is ergodic (*Suciu, 2014*).

In the following, the method of the self-averaging estimation is introduced. A component of the ensemble process $\{X_t, t \geq 0\}$ is considered. It has a zero mean starting from $X_0 = 0$, obtained by subtracting the ensemble mean $\langle X_{i,t} \rangle$ from one of the components $X_{i,t}$, $i = 1, 2$, of the transport pro-

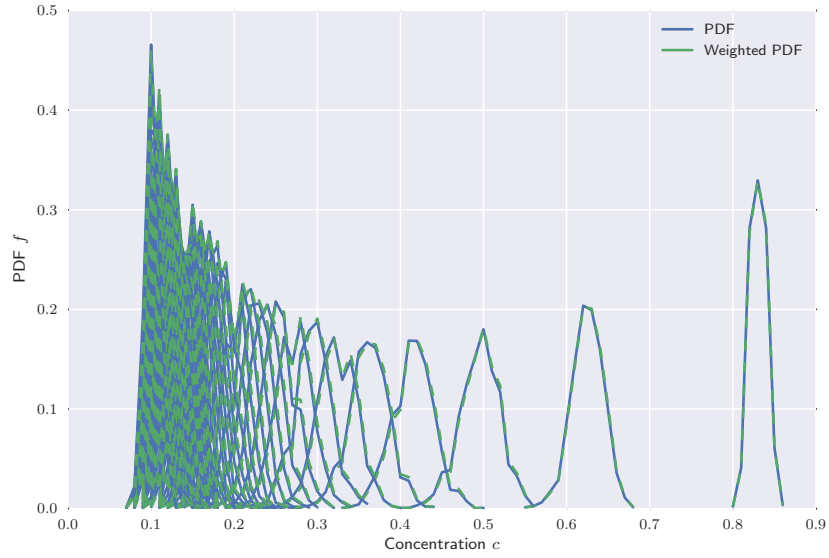


Figure 2.1: Concentration PDFs at $x = \langle V_1 \rangle t$, sampled at 2 days intervals, from $t = 0$ d to 100 d (from right to left), inferred from 3072 GRW simulations of the two dimensional transport problem.

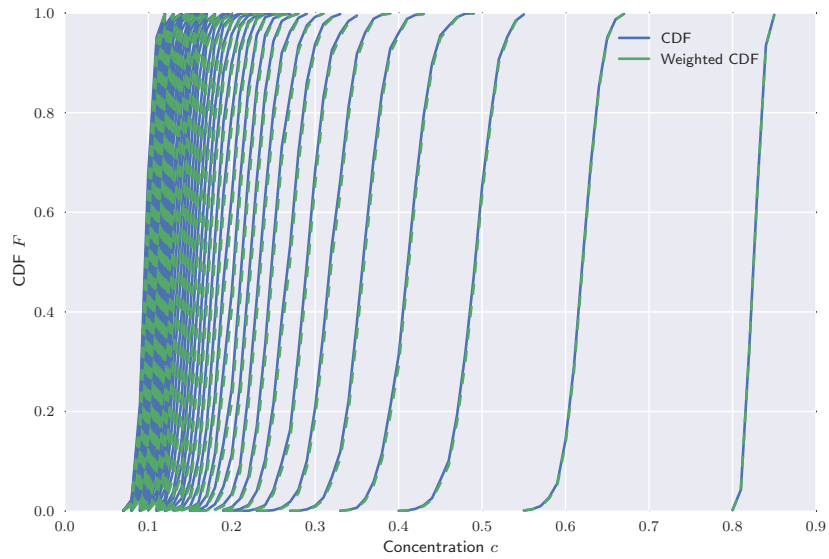


Figure 2.2: The CDFs corresponding to the PDFs presented in Figure 2.1.

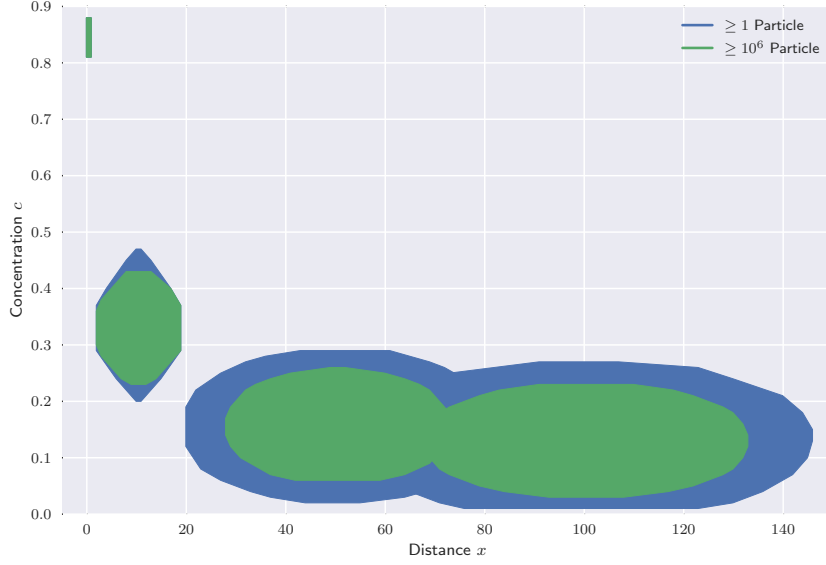


Figure 2.3: Contours of the number of particles in the (x, c) GRW lattice at successive times $t = 0$ d, 10 d, 50 d, and 100 d.

cess. If the continuous time interval $[0, t]$ is partitioned into S subintervals of equal length τ , so that $t = S\tau$, then a position on the trajectory X_t and its square X_t^2 can be expressed in terms of increments $\delta X_s = X_{s\tau} - X_{(s-1)\tau}$ as

$$X_t = \sum_{s=1}^S \delta X_s, \quad X_t^2 = \sum_{s=1}^S (\delta X_s)^2 + 2 \sum_{r=1}^{S-1} \sum_{s=1}^{S-r} \delta X_s \delta X_{s+r}. \quad (2.47)$$

Further, introducing the time averages

$$\rho(r) = \frac{1}{S-r} \sum_{s=1}^{S-r} \delta X_s \delta X_{s+r}, \quad (2.48)$$

X_t^2 can be rewritten as

$$X_t^2 = S\rho(0) + 2 \sum_{r=1}^{S-1} (S-r)\rho(r). \quad (2.49)$$

Since the averages ρ defined by (2.48) are similar to stochastic correlations, equation (2.49) is a single-realisation form of the Taylor formula for processes with stationary variance (Suciú, 2014).

The process of the increments δX_s is determined through advective displacements by the velocity field sampled on trajectories (Suciú and Vamos, 2014).

2009), which has ergodic covariances in a first order approximation (Suciú, 2014). Therefore, one expects that the ergodic estimation (2.48) converges to the correlation of δX_s , so that (2.49) yields a good approximation of the variance of X_t . Then, the diffusion coefficient can be estimated on a single sample of X_t as $\tilde{D} = X_t^2/(2S\tau)$. With this, equation (2.49) yields

$$\tilde{D} = \frac{1}{2\tau}\rho(0) + \frac{1}{\tau} \sum_{r=1}^{S-1} \left(1 - \frac{r}{S}\right) \rho(r). \quad (2.50)$$

Since the time averages ρ are poor ergodic estimates of the correlations as r gets closer to S , a rigorous ergodicity statement is not possible in this case. Nevertheless, the reliability of the self-averaging estimator (2.50) has been demonstrated by numerical experiments (Suciú and Vamoş, 2009). In practice, acceptable results are obtained if the estimation time $S\tau$ is larger than the total simulation time T . For the PDF simulations with $T = 100$ d presented here, $S\tau = 400$ d is chosen. For an increased accuracy, the ergodic estimations (2.48) of the correlations ρ are further averaged over 10^6 paths S sampled on the same trajectory. With these parameters, the computation time of the estimation (2.50) of the diffusion coefficient is about 4 min. For comparison, on the same computing platform, the computation of an ensemble of GRW simulations which provides the time variation of the ensemble dispersion coefficients over 100 d requires about 10 min and 256 processors.

The longitudinal ensemble dispersion coefficient estimated by (2.50), as well as those given by Monte Carlo GRW simulations of two-dimensional transport (Suciú et al., 2006), are defined as one-half of the mean slope of the time dependent variance of the ensemble process. The diffusion coefficient \mathcal{D} from (2.42), needed in PDF simulations, is defined as one-half of the local variance, which is tantamount to one-half of the derivative of the global variance, since the process has finite first and second spatial moments at finite times (Suciú, 2014). \mathcal{D} is approximated in the GRW-PDF scheme from the input parameter numerically estimated by (2.50) as

$$\mathcal{D}(t) = \frac{1}{\delta t} \left[(t + \delta t)\tilde{D}(t + \delta t) - t\tilde{D}(t) \right], \quad (2.51)$$

where δt is the simulation time step.

Mixing Models and Results

In this section, three different mixing models are examined which account for the transport in concentration space. Because finding mixing models is the final step towards solving PDF equations, the simulation results are presented here too.

The Time Series Mixing Model

In the following, the coefficients \mathcal{V}_c and \mathcal{D}_c occurring in the Itô equation (2.43) are estimated by a stochastic time series analysis (Suciu *et al.*, 2016). An ensemble of 500 time series $C(t) = C(\langle V_1 \rangle t, t)$ of simulated concentrations, previously described by Suciu *et al.* (2015b), is presented in Figure 2.4. As common in time series analyses, t is an integer and represents the count of successive terms, sampled at regular intervals of one day in this case. Since the velocity field is statistically homogeneous, these time series correspond to the concentration C sampled at the plume centre of mass (Suciu *et al.*, 2006). The corresponding increments $dC(t) = C(t+1) - C(t)$, approximating the slope $dC(t)/dt$ of a continuous time series, are shown in Figure 2.5. The residual noise in the time series increments, $\xi(t) = dC(t) - \langle dC(t) \rangle$ is shown in Figure 2.6 and has an approximately exponentially decaying amplitude. After normalising each ξ -sample by its maximum amplitude $\|\xi\| = \max |\xi|$, the standardised noise $\xi/\|\xi\|$ may be approximated by a white noise, as shown in Figure 2.7. In turn, it follows that $\xi(t)$ may be approximated by a so-called heteroskedastic process (Vamoş and Crăciun, 2010) consisting of a white noise with a rapidly decaying amplitude.

The drift coefficient \mathcal{V}_c in the Itô equation (2.43) is inferred from the slope of the ensemble mean concentration $\langle C(t) \rangle$, represented by a thick and dark curve in Figure 2.5. The maximum value of the diffusion coefficient \mathcal{D}_c is specified by an initial amplitude of diffusive jumps in the GRW algorithm of $5\delta c$, where $\delta c = 0.001$ is the space step in concentration space. This value is chosen as close as possible to the standard deviation 0.0053 of the maximum amplitude $\|\xi\|$ of the noise shown in Figure 2.6. The time variation of the diffusion coefficient \mathcal{D}_c which mimics the behaviour of the noise in Figure 2.6 is optimised through a crude calibration of the PDF simulations.

As shown in Figure 2.8, the time series mixing model (TS) presented above accurately describes the transport of the PDF in concentration space, but it fails to reproduce the narrowing of the PDF at large times and small values of the concentration shown in Figure 2.1 (Suciu, 2014; Suciu *et al.*, 2015a,b). The narrowing of the PDF is due to the local dispersion process which smooths the concentration differences so that in the limit of uniform concentration distributions the PDF approaches a δ function in every realisation of the transport process. The narrower the PDF is, the smaller the differences between the concentration realisations and their ensemble average. An appropriate mixing model should therefore account for this “attraction” towards the mean of the concentration. For the TS model, the drift in equation (2.43), shown in Figure 2.4, vanishes relatively quickly and the concentration $C(t) = C(X(t))$ will be almost constant on the trajectory $X(t) = \langle V_1 \rangle t$, with small fluctuations given by the noisy term shown in Figure 2.6. This behaviour of the TS model could be explained by the excessive smoothing in the stochastic time series analysis used to infer its

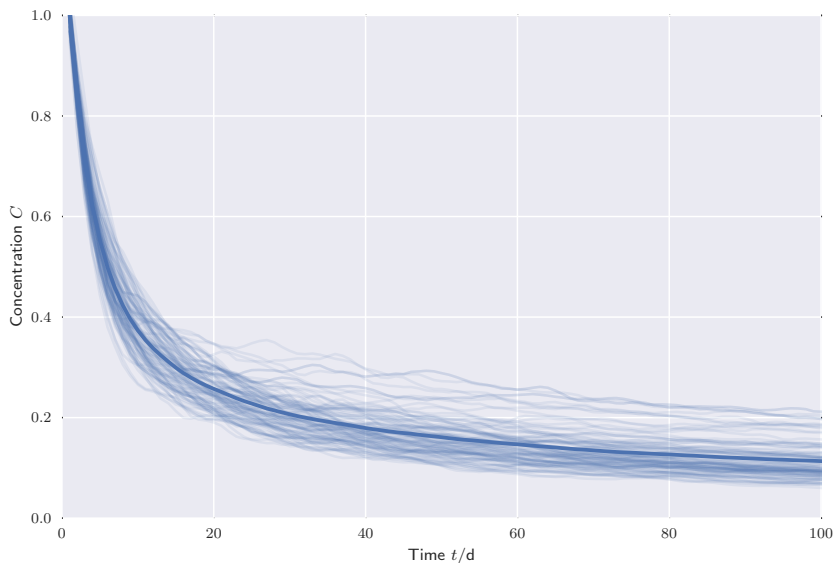


Figure 2.4: Time series of cross-section concentrations $C(t)$ at the centre of mass of the plume, given by Monte Carlo simulations.

parameters. An automatic algorithm to decompose time series into intrinsic components (*Vamoş et al., 2015*) could be used to check whether, besides the trend and the noise shown in Figures 2.5 and 2.6, the concentration time series contains more components which were smoothed out by the stochastic analysis.

The Interaction by Exchange with the Mean Mixing Model

The attraction towards the mean of the concentration realisations is enforced by the Interaction by Exchange with the Mean (IEM) model $\mathcal{V}_c = -\chi(C - \langle C \rangle)$, where χ is the inverse decay time scale of the concentration fluctuations (*Pope, 1985; Colucci et al., 1998*). For a statistically homogeneous Gaussian concentration field of a passive scalar in homogeneous and isotropic turbulence, the IEM model is precisely the expression of the conditional diffusion flux, which it tries to approximate (*Pope, 2000*). Furthermore, since in this case the density is constant and the PDF no longer depends on spatial coordinates, it follows from equations (2.38) and (2.2) that the mixing terms based on the conditional diffusion flux and the conditional dissipation rate are equivalent. The IEM model has the drawback that it preserves the shape of the initial PDF (*Pope, 2000, 1985*). However, the simple IEM model has proven to be useful in many practical PDF problems for turbulent reacting flows (*Colucci et al., 1998; Jaber et al., 1999; Mustata et al., 2006*). For the purpose of the present illustration of the IEM

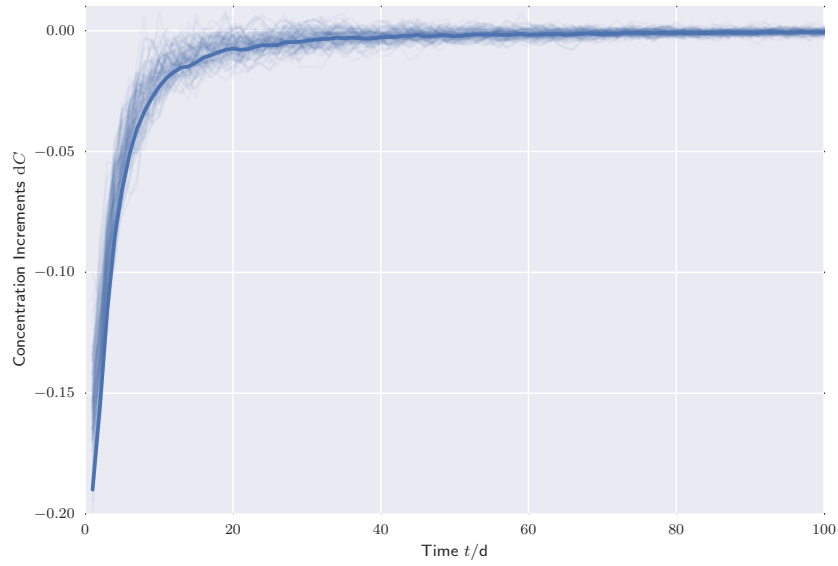


Figure 2.5: Concentration increments $dC(t)$ of the sample time series shown in figure 2.4.

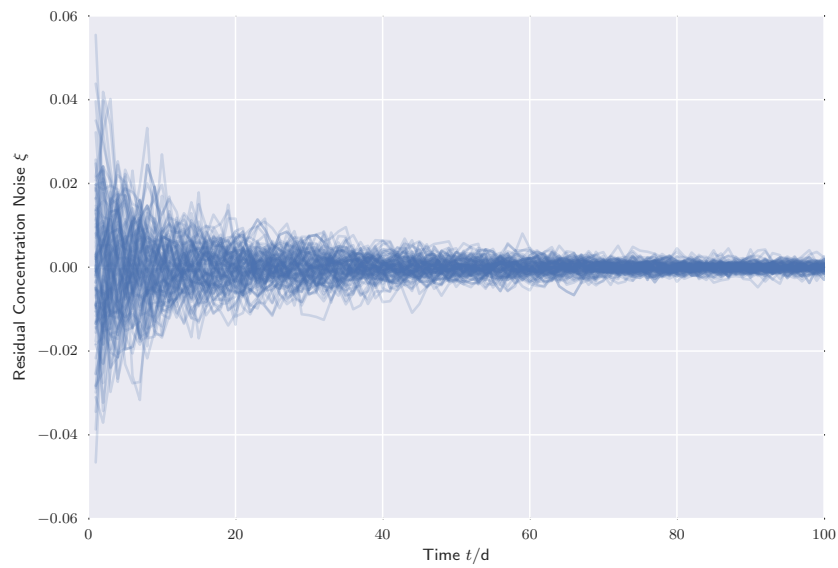


Figure 2.6: The residual concentration noise $\xi(t)$ of the concentration increments $dC(t)$ shown in figure 2.5.

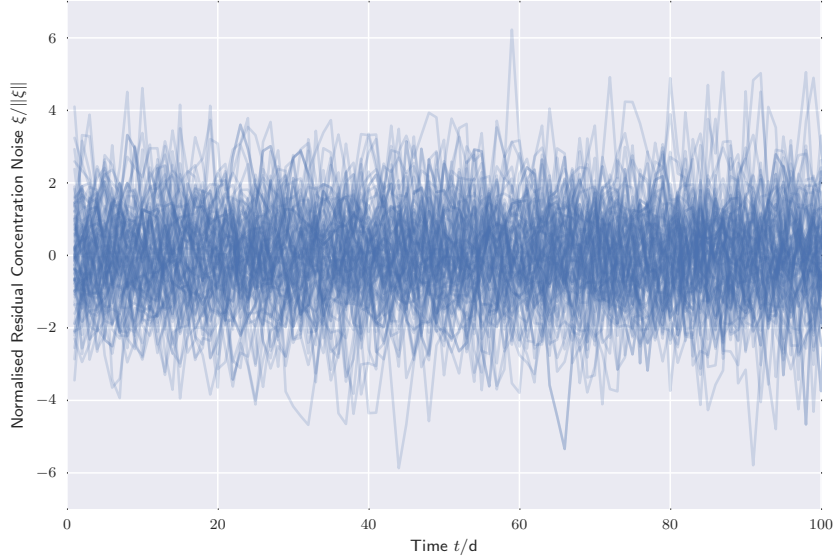


Figure 2.7: The residual concentration noise normalised by the maximum amplitude $\xi(t)/\|\xi\|$.

model, the characteristic frequency χ is defined as an inverse diffusion time, similarly to PDF approaches in turbulence (*Colucci et al., 1998; Jaberi et al., 1999*), in terms of effective dispersion coefficients and a characteristic length scale l . Since the transport process is almost ergodic, the effective and the ensemble coefficients are almost identical (*Suciu, 2014*), so that $\chi = \mathcal{D}/l^2$. The scale l is given by the correlation length λ_Y of the log-hydraulic conductivity field. With these parameters, the IEM model reads

$$\mathcal{V}_c^{\text{IEM}} = -k_\chi \frac{\mathcal{D}}{\lambda_Y^2} (C - \langle C \rangle). \quad (2.52)$$

The dimensionless model constant k_χ is not a universal constant and it is generally determined from comparisons with measurements or reference solutions. In turbulence studies for instance, k_χ ranges between 0.6 and 3.1 (*Pope, 1985*). For the present study, a value of $\kappa = 2$ was found to be appropriate for the PDF simulations.

The Time Series - Interaction by Exchange with the Mean Mixing Model

Since the IEM model is not satisfactory at all, as shown in Figure 2.8, a linear combination of the TS and IEM models is also considered (*Suciu et al., 2016*) and hereafter referred to as the TS-IEM model:

$$\mathcal{V}_c^{\text{TS-IEM}}(t) = \frac{T-t}{T} \mathcal{V}_c^{\text{TS}}(t) + \frac{t}{T} \mathcal{V}_c^{\text{IEM}}(t), \quad (2.53)$$

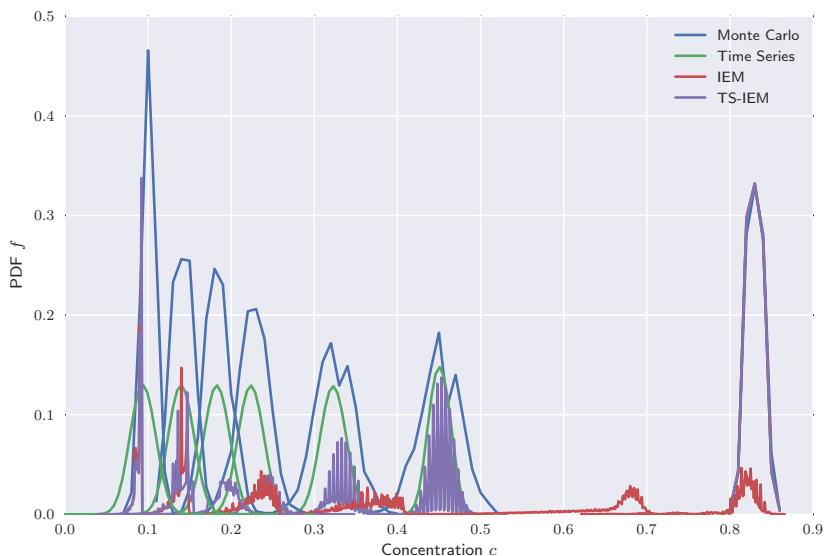


Figure 2.8: GRW solutions of the PDF $f(c; x, t)$ with different mixing models (time series, IEM, and time series IEM) compared to Monte Carlo reference solutions, sampled at position $x = \mathcal{V}t$ at different times $t = 0$ d, 5 d, 10 d, 20 d, 30 d, 50 d, and 100 d (from right to left).

where T denotes the total simulation time. For both IEM and TS-IEM models of the drift \mathcal{V}_c , the diffusion term in the Itô equation (2.43) with the diffusion coefficient \mathcal{D}_c is provided by the TS model. In Figures 2.8 and 2.9 PDF-GRW simulations carried out with the three mixing models are compared. The reference solution and the initial condition for these simulations are those from Monte Carlo ensembles computed with the exponential log-conductivity field. As shown in Figure 2.8, both the IEM model (2.52) and the TS-IEM model (2.53) yield narrow PDFs at small concentrations but they do not reproduce the reference solution. The PDFs are non-smooth for both models and the pure IEM model completely fails to reproduce the transport of the PDF in concentration space. The IEM solution for the cumulative distribution function shown in Figure 2.9 is also totally unsatisfactory, the corresponding curves lagging far behind the reference solution. The TS-IEM solution for the cumulative distribution function compares satisfactorily with the TS and the reference solutions at small to intermediate times, as seen from Figure 2.9.

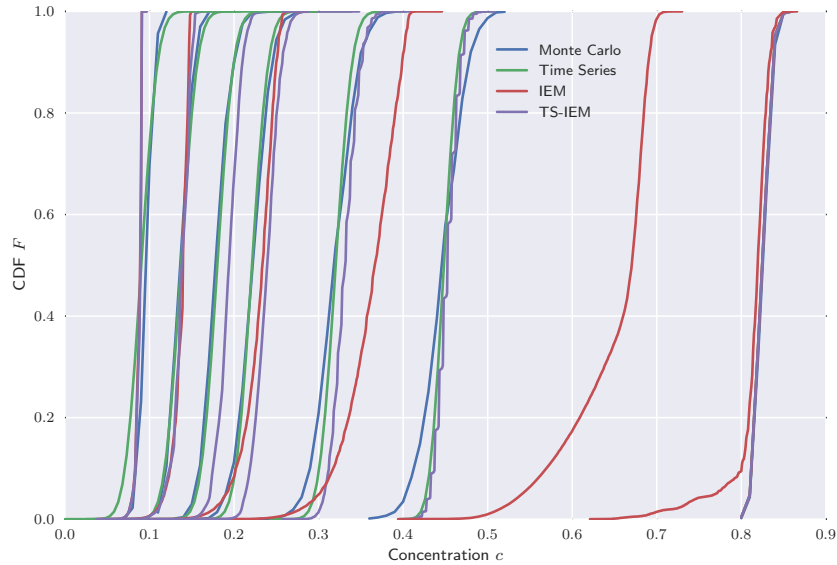


Figure 2.9: The concentration CDFs $F(c; x, t)$ corresponding to the PDFs shown in Figure 2.8.

Conclusions

PDF evolution equations are formulated as Fokker-Planck equations describing processes in the concentration-position space stochastically equivalent to random concentration fields. Within this approach, which is called the “reverse Fokker-Planck approach”, the PDF weighted by a conserved scalar is numerically approximated by the one-time PDF of the Itô process in the concentration-position space described by the Fokker-Planck equation. The conserved scalar which weights the one-point one-time PDF to render it equivalent to the one-time PDF of the concentration-position process is not involved in chemical reactions but, unlike in classical approaches, it does not necessarily solve a continuity equation. For systems of mobile reacting species in groundwater with species-independent diffusion coefficients, the conserved scalar can be chosen as the sum of molecular species concentrations, governed by an advection-diffusion equation.

The numerical solution is provided by the GRW algorithm, which computes the density of an ensemble of computational particles on a lattice embedded in the concentration-position space. The GRW algorithm is stable, free of numerical diffusion, and practically insensitive to the increase of the number of particles. The transport of the system of particles in the physical space is described by drift and diffusion coefficients obtained through stochastic upscaling. For small variances of the log-hydraulic conductivity, the upscaled coefficients can be determined through self-averaging estima-

tions using a single trajectory of diffusion in the velocity field.

One of the most stringent problems in PDF approaches is to design an appropriate mixing model which describes the transport in concentration space of the system of computational particles. For the problem considered here, with the random concentration depending on a single spatial coordinate, an advection-diffusion process in concentration space, inferred from a time series analysis was found to yield a correct solution for the transport of the cumulative distribution towards low concentration values. The time series are taken from simulated concentrations sampled on the mean-flow trajectory. However, this time series model cannot account for the narrowing and the raising peak of the maximum PDF values at large times and small concentrations.

The classical IEM model widely used in turbulence studies, which should in principle recover this large time behaviour, fails to describe the transport in concentration space of the cumulative distribution function. A linear combination of time series and IEM mixing models (TS-IEM) used in the PDF simulations yields an acceptable accuracy only for moderately large times. The numerical computations carried out with the TS-IEM model indicate that improvements can be achieved by choosing an appropriate variation of the characteristic time scale in the coefficient of the IEM component of the model which would result in an enhanced drift in concentration space at early times, which decreases gradually as the spreading of the solute plume progresses. This idea is investigated in Chapter 4.

Chapter 3

Filtered Density Functions

This chapter is based on the paper

Suciu, N., L. Schöler, S. Attinger, and P. Knabner (2016), Towards a filtered density function approach for reactive transport in groundwater, *Adv. Water Resour.*, 90, 83-98, doi:10.1016/j.advwatres.2016.02.016.

Introduction

Filtered density function (FDF) methods provide an alternative to PDF methods. FDF methods use spatially filtered quantities instead of stochastic averages on which PDF methods are based ([Haworth and Pope, 2011](#); [Colucci et al., 1998](#); [Jaberi et al., 1999](#); [McDermott and Pope, 2007](#)). In this context, spatial filtering means spatial averaging. The FDF has the meaning of a PDF of state variables at scales smaller than the filter width ([Heinz, 2007](#); [Dodoulas and Navarro-Martinez, 2013](#)). FDF evolution equations can be derived by similar procedures and have the same structure as PDF equations, with source terms in a closed form ([Haworth, 2010](#); [Haworth and Pope, 2011](#); [Colucci et al., 1998](#)). For an introduction to PDF methods, see Section 2.1. With rare exceptions, the only state variables considered in FDF methods are the scalars describing the thermochemical composition ([Haworth and Pope, 2011](#)). Unlike the PDF, which is a deterministic function, the FDF is a random quantity. Its expectation tends to its PDF only in the limit of a small filter width ([Haworth and Pope, 2011](#)). However, by invoking an ergodic theorem, the ensemble averaging may be seen as a filtering in space with a filter width much smaller than the domain, but larger than the characteristic length of the large-scale motions. Thus, the FDF should approach its PDF in the limit of a large filter width ([Heinz, 2007](#)). Even though this assertion has not been proven theoretically, in some cases the convergence may be demonstrated numerically, as will be shown in Section 3.5.

While several PDF approaches are being developed for modelling transport in groundwater systems ([Meyer et al., 2010](#); [Venturi et al., 2013](#); [Suciu et al., 2015a](#)), FDF methods were not yet used for such systems. In the following, the feasibility and the utility of the FDF approach in stochastic subsurface hydrology will be investigated ([Suciu et al., 2016](#)). First, the striking similarities between large eddy simulations (LES) in turbulence ([Colucci et al., 1998](#); [Jaberi et al., 1999](#); [Dodoulas and Navarro-Martinez, 2013](#)) and some approaches to coarse-scale, or coarse-grained simulations (CGS) in porous media ([Beckie et al., 1996a,b](#); [Efendiev et al., 2000](#); [Efendiev and Durlofsky, 2003](#); [Efendiev and Hou, 2009](#); [Attinger, 2003](#)) should be noted. In both cases, spatial averages of dependent variables are used to coarsen the computational grid, whereas subgrid effects are modelled. The objective is to obtain results comparable to fine grid simulations at reduced computational costs. In case of reactive transport, the upscaled equations obtained by spatial filtering contain unclosed averaged reaction terms. In LES, the closure problem is solved by coupling the filtered equations to FDF evolution equations ([Dodoulas and Navarro-Martinez, 2013](#)). In subsurface hydrology, effective reaction rates closing the problem can only be determined for specific problems under simplifying assumptions ([Heße et al., 2009](#)). FDF approaches can be used to avoid the need to close the filtered reaction terms. CGS can be designed based on numerical upscaling through volume

averages (*Efendiev et al.*, 2000; *Efendiev and Durlafsky*, 2003), multiscale finite element methods (*Efendiev and Hou*, 2009), and by solving filtered equations, similarly to LES (*Beckie et al.*, 1996a,b).

Nevertheless, there are three major differences with respect to LES-FDF modelling for turbulent flows. These differences have already been discussed in detail in Section 2.1 and will therefore only briefly be repeated here. Only a few parameters are needed to solve filtered LES equations, whereas upscaling of flow and transport processes in the groundwater requires whole parameter fields, namely hydraulic conductivity or velocity fields. The second difference is related to the first one and concerns the origin of the randomness. Turbulent flows are governed by the Navier-Stokes equations, which show deterministically chaotic behaviour. This mathematical aspect corresponds to an experimental lack of reproducibility. In groundwater systems stochastic parametrisation is used to account for the uncertainty caused by the scarcity of data. The third difference is given by the available experimental data. In contrast to transport in groundwater, there is an abundance of experimental data of transport in turbulent flows. Consequently, in LES-PDF simulations the objective is to obtain a good agreement with the available measurements, at scales lying between that of the fine-scale simulations, which fully resolve the variability of the turbulent flows, and that of the ensemble averaged solutions of the Navier-Stokes and transport equations, for which the variability of the unresolved scales is modelled by the solution of the PDF equation (*Heinz*, 2007; *Dodoulas and Navarro-Martinez*, 2013). In natural porous media the measurements are sparse and subject to uncertainty. Therefore, as long as the simulation relies on fields of stochastic parameters (hydraulic conductivity or velocity) and no detailed experimental data is available, the aim of the FDF approach should be a probabilistic quantification of the uncertainty for the whole hierarchy of scales. In other words, FDF approaches for modelling transport processes in groundwater systems, besides closing reaction terms, could alleviate the computational costs through estimations of the global FDF from filtered parameter fields and coarse-grained simulations.

In Section 3.2, the FDF equation is discussed in detail. Section 3.3 deals with the spatial filtering of the Kraichnan algorithm, introduced in Section 1.5. Coarse-grained simulations are investigated in Section 3.4, where the details of the upscaling of the parameters is shown. The results of the FDF simulations are presented in Section 3.5, including the numerical results of the convergence of the FDF solution towards the PDF solution with increasing filter width. Section 3.6 concludes this chapter.

FDF Equations

In this section, FDF equations will be discussed in detail. The same system of local transport equations as in Section 2.3 is considered

$$\partial_t C_\alpha + V_i \partial_{x_i} C_\alpha - D \partial_{x_i} \partial_{x_i} C_\alpha = S_\alpha, \quad (3.1)$$

together with the corresponding one-point one-time PDF $f(\mathbf{c}; \mathbf{x}, t)$, which solves

$$\partial_t f + \partial_{x_i} (V_i f) - \partial_{x_i} \partial_{x_j} (D_{ij} f) = -\partial_{c_\alpha} \partial_{c_\beta} (\mathcal{M}_{\alpha\beta} f) - \partial_{c_\alpha} (S_\alpha f). \quad (3.2)$$

The upscaled drift vector \mathbf{V} and diffusion tensor \mathbf{D} and the conditional dissipation rate \mathbf{M} have the same structure as (2.18), (2.19), and (2.20), but with the difference that now the averages have to be understood as spatial averages.

In LES approaches, spatial filters are used to separate the dynamics of the scales larger than the filter width from sub-filter effects. The former are obtained as solutions of filtered equations and the latter, corresponding to unresolved scales, are modelled (Heinz, 2007; Haworth, 2010; Haworth and Pope, 2011). The filtered value of a physical quantity Q is given by the spatial average

$$\langle Q \rangle_\lambda(\mathbf{x}, t) = \int_{\Omega_x} Q(\mathbf{x}', t) G(\mathbf{x}' - \mathbf{x}) d\mathbf{x}', \quad (3.3)$$

with λ being the filter width, which is implicitly defined by the filter function $G(\mathbf{x}' - \mathbf{x})$. The filter $G(\mathbf{x}' - \mathbf{x})$ is spatially invariant, non-negative, and normalised to unity: $\int_{\Omega_x} G(\mathbf{x}' - \mathbf{x}) d\mathbf{x}' = 1$. Furthermore, the filtering operation commutes with differentiation (Waclawczyk et al., 2008). Under these conditions, the FDF can be defined as the filtered fine-grained PDF:

$$f_\lambda(\mathbf{c}; \mathbf{x}, t) = \langle \delta(\mathbf{C}(\mathbf{x}, t) - \mathbf{c}) \rangle_\lambda. \quad (3.4)$$

It has the same characteristics as a PDF defined by the expectation of the fine-grained PDF, see Section 1.3. FDF equations can be derived by the delta function method analogous to PDF equations (Haworth, 2010). The FDF equation has the form of PDF equation (3.2), but its coefficients are now obtained by spatial averages (3.3) instead of ensemble averages. Note that technically, neither the derivation of the PDF equation nor the derivation of the FDF equation require the statistical homogeneity of the random velocity field (Suciu et al., 2015a,b). Nevertheless, there is an important difference between PDF and FDF approaches. While in the case of the PDF approach to transport in groundwater, the statistical homogeneity of the random velocity is essential for the existence of the stochastically upscaled coefficients (Morales-Casique et al., 2006b), spatially filtered upscaled

coefficients to be used in FDF equations can be derived by methods free of homogeneity assumptions (*Efendiev et al., 2000; Efendiev and Durlofsky, 2003*). This opens the perspective of FDF methods applicable to realistic situations, such as transport simulations conditional on measurements of the hydraulic conductivity (*Morales-Casique et al., 2006a*).

The same consistency conditions as for the PDF equations, derived in Section 2.4.1 hold true for FDF equations when the ensemble average of the weighting function $\langle \Theta \rangle$ is replaced by the spatial filter (3.3), resulting in $\langle \Theta \rangle_\lambda$ (*Suciu et al., 2016*).

To facilitate the derivation of the FDF evolution equation, the filtered mass density function is usually written as (*Jaberi et al., 1999; Haworth, 2010*)

$$\mathcal{F}_\lambda(\mathbf{c}; \mathbf{x}, t) = \int_{\Omega_x} \rho(\mathbf{x}', t) \delta(\mathbf{C}(\mathbf{x}', t) - \mathbf{c}) G(\mathbf{x}' - \mathbf{x}) d\mathbf{x}'. \quad (3.5)$$

With $\rho(\mathbf{x}, t) = \rho(\mathbf{C}(\mathbf{x}, t))$ being the density, using the FDF definition by the filtering operation (3.3) applied to $\delta(\mathbf{C}(\mathbf{x}, t) - \mathbf{c})$ and the sifting property $\rho(\mathbf{c})\delta(\mathbf{C}(\mathbf{x}, t) - \mathbf{c}) = \rho(\mathbf{C}(\mathbf{x}, t))\delta(\mathbf{C}(\mathbf{x}, t) - \mathbf{c})$ (*Suciu et al., 2015b*), it is easy to recognise that $\mathcal{F}_\lambda(\mathbf{c}; \mathbf{x}, t) = \rho(\mathbf{c})f_\lambda(\mathbf{c}; \mathbf{x}, t)$. Further, (2.33) still holds when the ensemble average is replaced by filtering and the FDF version of the correspondence relation is given by (2.37), with f replaced by f_λ .

Filtering Velocity fields

The purpose of filtering the velocity field is to smooth out the small-scale fluctuations, which are smaller than a prescribed filter width λ . The choice of the filter function is arbitrary, but it should have a sharp cut-off at the given filter width. One choice would be a rectangular function, but it is not differentiable. Therefore a Gaussian filter function is chosen:

$$G(\mathbf{x}' - \mathbf{x}) = \left(\frac{b}{\pi}\right)^{d/2} \exp[-b(\mathbf{x}' - \mathbf{x})^2], \quad (3.6)$$

where $b = a/\lambda^2$ and $a \in \mathbb{R}^+$. Using the filter function (3.6) in the filtering operation (3.3) applied to the Kraichnan formula (1.22), one obtains

$$\begin{aligned} \langle V_i \rangle_\lambda(\mathbf{x}) &= \int_{-\infty}^{\infty} \left(\frac{b}{\pi}\right)^{d/2} V_i \exp[-b(\mathbf{x}' - \mathbf{x})^2] d\mathbf{x}' \\ &= \langle V_1 \rangle \delta_{i1} + \sigma_Y \langle V_1 \rangle \sqrt{2/N} \sum_{j=1}^N p_i(\mathbf{k}^{(j)}) \\ &\quad \underbrace{\int_{-\infty}^{\infty} \cos(\mathbf{k}^{(j)} \cdot \mathbf{x}' + \phi^{(j)}) \left(\frac{b}{\pi}\right)^{d/2} \exp[-b(\mathbf{x}' - \mathbf{x})^2] d\mathbf{x}'}_{=I}. \end{aligned}$$

The integral I can be simplified by the substitution $\mathbf{q} = \mathbf{x}' - \mathbf{x}$, which results in

$$I = \left(\frac{b}{\pi}\right)^{d/2} \int_{-\infty}^{\infty} \cos\left(\mathbf{k}^{(j)} \cdot \mathbf{q} + \mathbf{k}^{(j)} \cdot \mathbf{x} + \phi^{(j)}\right) \exp(-b\mathbf{q}^2) d\mathbf{q}.$$

The cosine function has an argument with $2d + 1$ terms, of which d depend on a component of the vector \mathbf{q} . The goal now is to separate these d terms from the rest. This separation can be achieved by a trigonometric identity. For fewer terms, this identity is

$$\begin{aligned} \cos(u + v) &= \cos(u) \cos(v) - \sin(u) \sin(v), \\ \cos(u_1 + u_2 + v) &= \cos(u_1) \cos(u_2) \cos(v) - \sin(u_1) \sin(u_2) \cos(v) \\ &\quad - \sin(u_1) \cos(u_2) \sin(v) - \cos(u_1) \sin(u_2) \sin(v) \\ &\quad \dots, \end{aligned}$$

and it can be seen that there is always only one term which has no sine functions. As sine functions are antisymmetric and the exponential function with which they are multiplied under the integral is symmetric, the resulting term is antisymmetric and the evaluated integral over all these terms vanishes. Hence, only the single term with no sine functions gives a non-zero value. Thus, by using the result $\int_{-\infty}^{\infty} dq \cos(uq) \exp(-w^2q^2) = \sqrt{\pi} \exp(-u^2/4w^2)/w$ ([Bronstein et al., 2006](#)), the integral gives

$$\begin{aligned} I &= \left(\frac{b}{\pi}\right)^{d/2} \int_{-\infty}^{\infty} \left[\prod_{\alpha=1}^d \cos(k_{\alpha}^{(j)} q_{\alpha}) \cos(\mathbf{k}^{(j)} \cdot \mathbf{x} + \phi^{(j)}) + \dots \right] \exp(-b\mathbf{q}^2) d\mathbf{q} \\ &= \cos(\mathbf{k}^{(j)} \cdot \mathbf{x} + \phi^{(j)}) \exp\left[-\frac{(\mathbf{k}^{(j)})^2}{4b}\right]. \end{aligned}$$

The final expression for the Gaussian filtered velocity field is

$$\begin{aligned} \langle V_i \rangle_{\lambda}(\mathbf{x}) &= \\ \langle V_1 \rangle \delta_{i1} + \sigma_Y \langle V_1 \rangle \sqrt{2/N} \sum_{j=1}^N p_i(\mathbf{k}^{(j)}) \cos(\mathbf{k}^{(j)} \cdot \mathbf{x} + \phi^{(j)}) \exp\left[-\frac{(\mathbf{k}^{(j)})^2 \lambda^2}{4a}\right]. \end{aligned} \quad (3.7)$$

The same derivation as shown above can be done with a rectangular filter function, e.g. as used by [Colucci et al. \(1998\)](#)

$$G(\mathbf{x}' - \mathbf{x}) = \prod_{i=1}^d \tilde{G}(x'_i - x_i), \quad \text{with } \tilde{G}(x'_i - x_i) = \begin{cases} 1/\lambda & \text{if } |x'_i - x_i| \leq \lambda/2 \\ 0 & \text{else} \end{cases}. \quad (3.8)$$

The result is then

$$\begin{aligned} \langle V_i \rangle_\lambda(\mathbf{x}) = \\ \langle V_1 \rangle \delta_{i1} + \sigma_Y \langle V_1 \rangle \sqrt{2^{2d+1}/N} \sum_{j=1}^N p_i(\mathbf{k}^{(j)}) \cos(\mathbf{k}^{(j)} \cdot \mathbf{x} + \phi^{(j)}) \prod_{m=1}^d \frac{\sin(k_m^{(j)} \lambda/2)}{k_m^{(j)}}. \end{aligned} \quad (3.9)$$

However, for the present computations of filtered velocities, the Gaussian filter function was used with $a = 2$ (*Attinger, 2003*). The only difference compared to the unfiltered velocity equation (1.22) is one factor for each mode, which can be precalculated and saved before the actual simulations start.

The number of Fourier modes is set to $N = 6400$ for all the simulations performed in this study. The isotropic version of the correlation function (1.24) is considered and is specified by the correlation length $\lambda_Y = 1$ m and by the variance $\sigma_Y^2 = 0.1$, which ensures the accuracy of the first-order approximation. With these parameters, integrating (1.24) from zero to infinity along any straight line through the origin of the coordinate system yields the integral scale $I_Y = \sqrt{\pi} \sigma_Y^2 \lambda_Y / 2 \approx 0.09$ m.

The effect of the filtering on the velocity field can be seen in Figure 3.1, where the longitudinal and transversal components of the filtered velocity field $\langle V_1 \rangle_\lambda$ and $\langle V_2 \rangle_\lambda$ approach their ensemble averages $\langle V_1 \rangle = 1 \text{ m d}^{-1}$ and $\langle V_2 \rangle = 0 \text{ m d}^{-1}$, respectively, with increasing filter width. Figure 3.2 compares the streamlines of an unfiltered velocity field generated according to the Kraichnan formula (1.22) to the streamlines of a filtered velocity field generated by the filtered Kraichnan formula (3.7). For this comparison, the variance of the underlying hydraulic conductivity field was set to a value of $\sigma_Y = 3$, for which the small variance assumption used to derive the Kraichnan formula surely breaks down. But this is just a visual comparison of the effect of the filtering on the spatial distribution and the patterns of the streamlines.

Coarse-Grained Transport Simulations

In this section, the effect of filtering the velocity field on the transport behaviour of a solute is investigated. In particular, the dependence of the ensemble dispersion coefficients on the filter size and how to estimate these coefficients from single particle trajectories will be examined in Section 3.4.1. In Section 3.4.2 these coarse-grained ensemble dispersion coefficients are used for simulations on a coarse-grained velocity field to retrieve the mean concentration.

The same simulation setup as for the PDF approach described in Section 2.5 is used here. Thus, also the same parameters are used.

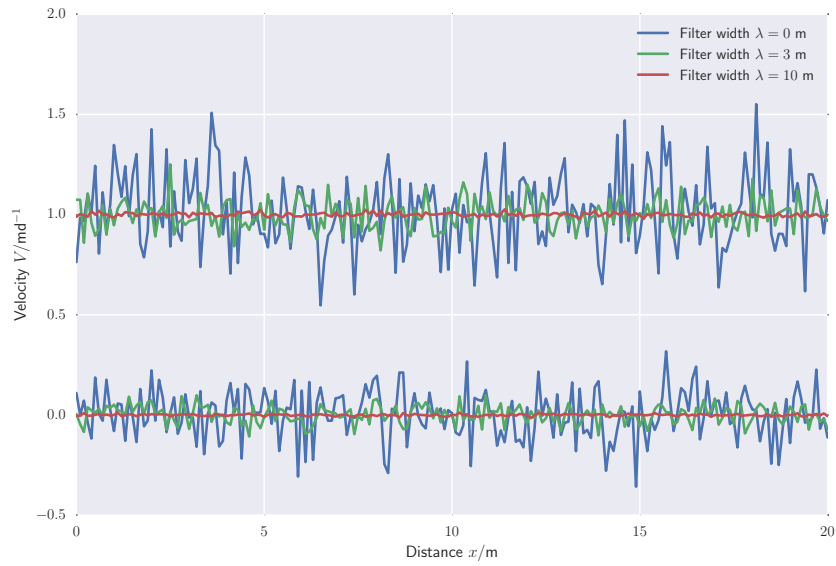


Figure 3.1: The longitudinal and transversal components of a velocity field unfiltered ($\lambda = 0$ m) and with two different sized filters.

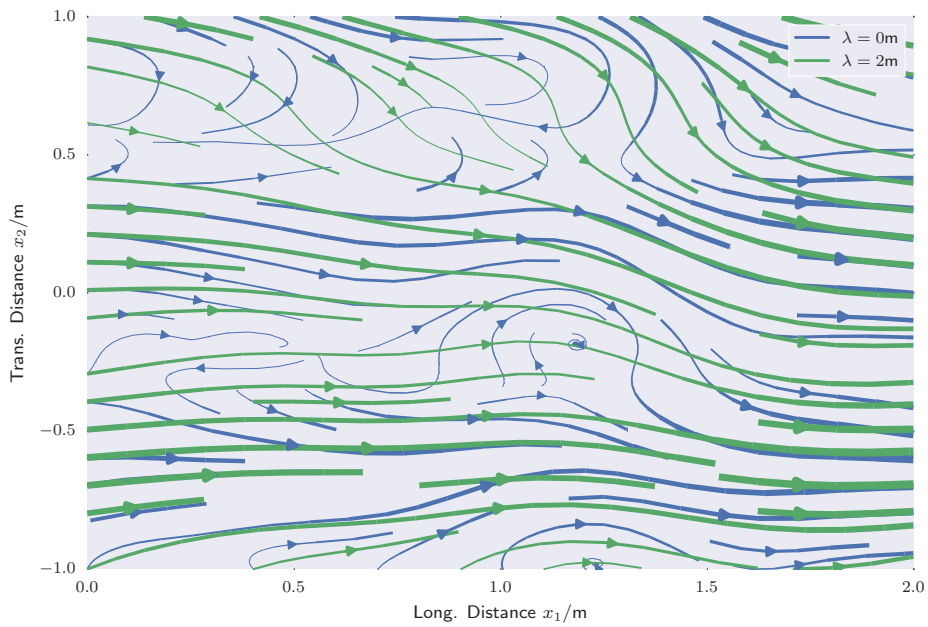


Figure 3.2: The streamlines of a 2-dimensional unfiltered velocity field ($\lambda = 0$ m) and of the same field with a filter of size $\lambda = 2$ m applied.

Coarse-Graining Dispersion Coefficients

Ensemble dispersion coefficients computed for diffusive transport in filtered velocity fields only account for the variability of the velocity at scales larger than the filter width λ . Therefore, as seen in Figure 3.3, the coefficients $D_{11}^{\text{ens}}(t, \lambda)$ are smaller than the coefficients obtained for fine-grained, unfiltered velocity fields (the case $\lambda = 0$ m) and they approach the local dispersion coefficient D as λ increases and the velocity fluctuations are smoothed out. The sub-filter variability is modelled by fictitious diffusion coefficients. When used in a coarse-grained description, such coefficients should retrieve the statistics of the spatial moments in stochastic approaches (Dagan, 1994; Rubin *et al.*, 1999; De Barros and Rubin, 2011) or they should produce results close to those from fine scale simulations in numerical upscaling approaches (Efendiev *et al.*, 2000; Efendiev and Durlofsky, 2003).

Following this paradigm, GRW-CGS of the two dimensional transport problem formulated in Section 2.5 are conducted. Therefore, the filtered velocities $\langle \mathbf{V} \rangle_\lambda$ generated by the filtered Kraichnan formula (3.7) are used. The coarse-grained longitudinal diffusion coefficients are obtained by adding the difference between fine-grained and filtered ensemble dispersion coefficients to the local dispersion coefficient D :

$$D_{11}^{\text{cg}}(t, \lambda) = D + \delta D(t, \lambda), \quad \delta D(t, \lambda) = D_{11}^{\text{ens}}(t) - D_{11}^{\text{ens}}(t, \lambda). \quad (3.10)$$

Because the corrections to the transverse coefficient were found to be negligible, it is set to $D_{22}^{\text{cg}} = D$. By using the representation of the dispersion coefficients in terms of trajectories of Itô processes, it can be seen that the corrections δD in equation (3.10) are entirely due to sub-filter effects only in absence of correlations between the filtered and the sub-filter velocity fields (see paragraph on page 56). Such correlations are generally non-vanishing in upscaling by spatial averages of the flow equations (Beckie *et al.*, 1996b). In analytical estimations by first order approximations in σ_V^2 the condition of vanishing correlations is ensured by integrating over disjoint domains in the Fourier space (Rubin *et al.*, 1999). In the numerical approach presented here, the lack of correlations is ensured by using independent sets of random numbers to generate filtered and fine-grained velocity fields.

The longitudinal ensemble dispersion coefficients are computed with GRW simulations from the variance of the ensemble process

$$X_1^{\text{ens}} = X_1 - \langle X_1 \rangle \quad (3.11)$$

as

$$D_{11}^{\text{ens}} = \frac{\langle (X_1^{\text{ens}})^2 \rangle}{2t}, \quad (3.12)$$

where $\langle \cdot \rangle$ is the average over the $N = 10^{10}$ particles (realisations of the local diffusion process) and over the $R = 256$ realisations of the velocity field.

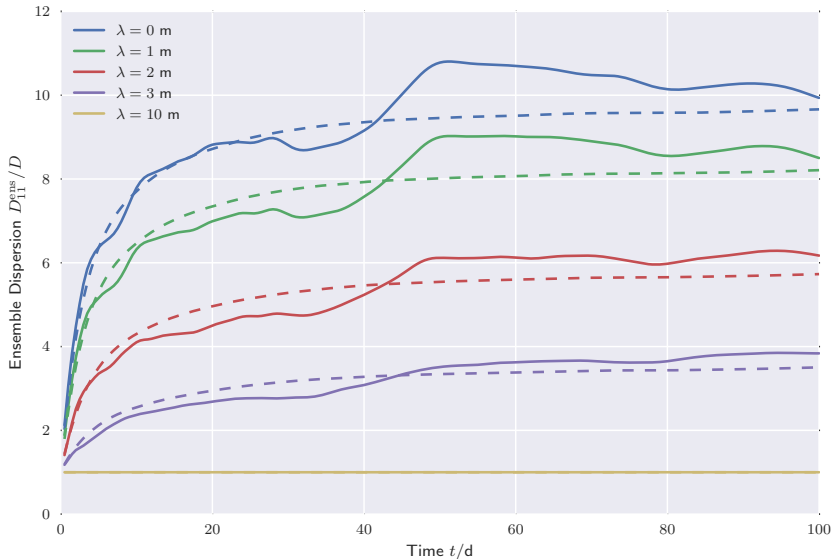


Figure 3.3: Ensemble dispersion coefficients $D_{11}^{\text{ens}}(t, \lambda)$ derived from GRW simulations for single realisations of the filtered velocity field compared to their ensemble average (plotted as dashed curves).

Single-realisation estimations of D_{11}^{ens} are computed by averaging $(X_1^{\text{ens}})^2$ for $R = 1$ over the N particles, while keeping the fully averaged mean $\langle X_1 \rangle$.

In Figure 3.4 it is shown that CGS, performed with filtered velocity fields and coarse-grained diffusion coefficients (3.10) determined from single-realisation coefficients $D_{11}^{\text{ens}}(t, \lambda)$, recover the fine-grained ensemble coefficient computed in a single realisation (corresponding to $\lambda = 0$ m) for large enough filter widths. Figure 3.5 shows that for the same single realisation CGS, but with coarse-grained coefficients (3.10) computed from $D_{11}^{\text{ens}}(t, \lambda)$ averaged over $R = 256$ realisations, for a filter width $\lambda = 4$ m one recovers the ensemble averaged D_{11}^{ens} given by fine-grained simulations ($\lambda = 0$ m). This demonstrates the usefulness of CGS, which reduces the computational costs by a factor of 256, provided that the coarse-grained coefficient $D_{11}^{\text{cg}}(t, \lambda)$ can be obtained without carrying out ensembles of GRW simulations.

In the present numerical setup, the low variance $\sigma_Y^2 = 0.1$ makes it possible to generate velocity fields at given points in space (Section 3.3) and to construct trajectories on which self-averaging estimations of the coefficients $D_{11}^{\text{ens}}(t, \lambda)$ for filtered velocity fields are readily available (Section 2.5.2). These self-averaging estimations, shown in Figure 3.6, are used to infer the coarse-grained coefficients (3.10). With the coefficients $D_{11}^{\text{cg}}(t, \lambda)$ obtained in this way, it was found that GRW simulations for $R = 256$ velocity realisations yield an acceptable recovery of the fine-grained ensemble coefficient D_{11}^{ens} , as shown in Figure 3.7. The suitability of the self-averaging

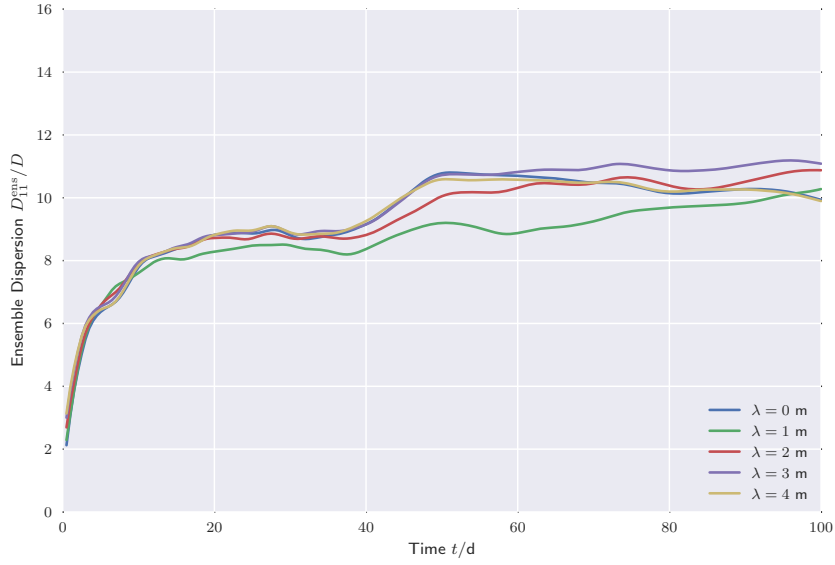


Figure 3.4: Single-realisation coarse-grained simulation estimations of the ensemble dispersion coefficient D_{11}^{ens} for increasing filter width λ , performed with single-realisation coarse-grained diffusion coefficients $D_{11}^{\text{cg}}(t, \lambda)$.

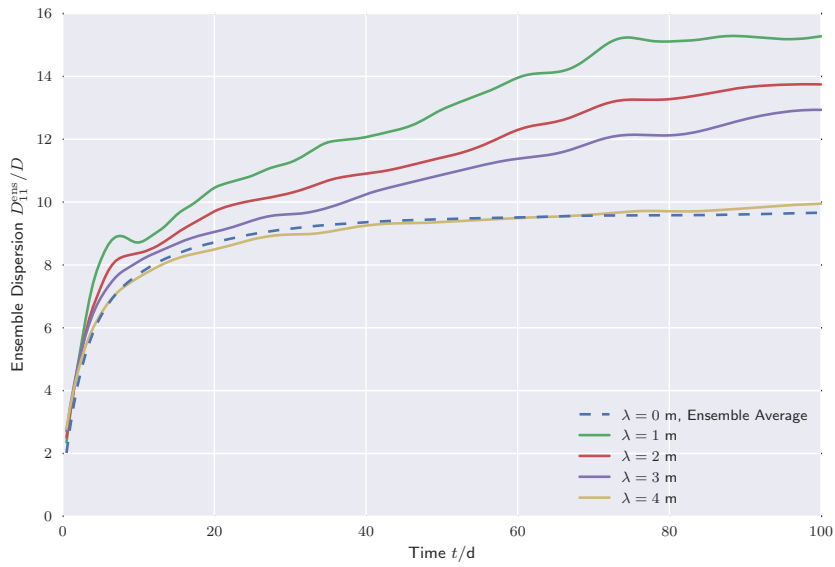


Figure 3.5: Single-realisation coarse-grained simulation estimations of the fine-grained dispersion coefficient D_{11}^{fg} for increasing filter width λ , performed with ensemble averaged coarse-grained diffusion coefficients $D_{11}^{\text{cg}}(t, \lambda)$.

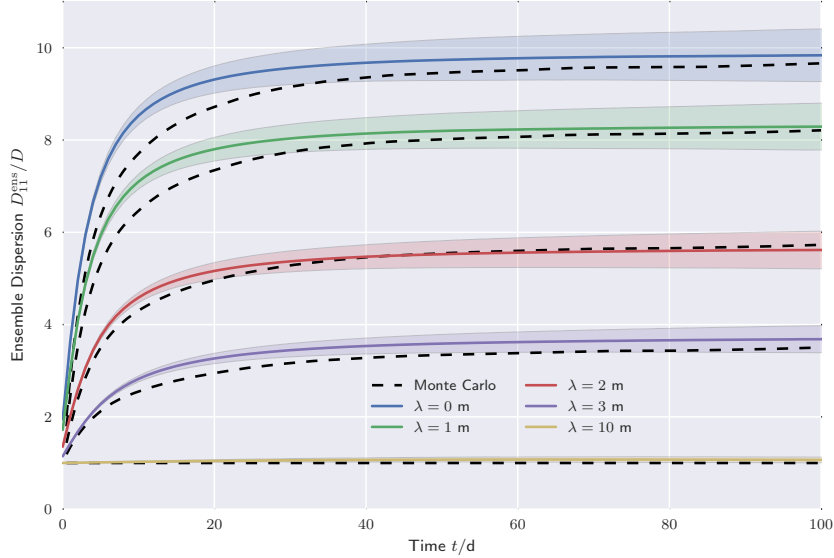


Figure 3.6: Ensemble dispersion coefficients $D_{11}^{\text{ens}}(t, \lambda)$ for filtered velocity fields obtained by self-averaging estimations and corresponding standard deviations (represented by lighter colours). Dashed black lines represent ensemble averaged coefficients $D_{11}^{\text{ens}}(t, \lambda)$ obtained from 256 GRW simulations.

estimations of the coarse-grained coefficients for ensemble average estimates could significantly alleviate the costs in Monte Carlo simulations by using discretisation elements several times coarser than in fine-grained simulations.

Prerequisite for Coarse-Graining Diffusion Coefficients

Decomposing the velocity field into its ensemble mean and fluctuations around this mean $\mathbf{V} = \langle \mathbf{V} \rangle + \mathbf{V}'$ and taking its statistical homogeneity into account, it can be seen that it is related to the filtered velocity by

$$\mathbf{V} = \langle \mathbf{V} \rangle + \langle \mathbf{V}' \rangle_{\lambda} + \mathbf{V}'_{\lambda}, \quad (3.13)$$

where $\langle \mathbf{V}' \rangle_{\lambda}$ is the filtered fluctuation of the fine-grained velocity and \mathbf{V}'_{λ} is the residual sub-filter velocity fluctuation about the filtered velocity $\langle \mathbf{V} \rangle_{\lambda} = \langle \mathbf{V} \rangle + \langle \mathbf{V}' \rangle_{\lambda}$. The longitudinal component of the transport process starting at $\mathbf{X} = \mathbf{0}$ is described by the Itô equation

$$X_1(t) = \int_0^t V_1(t') dt' + W(t), \quad (3.14)$$

where $V_1(t') = V_1(\mathbf{X}(t'))$ and $W(t)$ is a Wiener process of zero mean and variance equal to $2Dt$. For statistically homogeneous velocity fields, the ensemble average of (3.14) is $\langle X_1 \rangle(t) = \langle V_1 \rangle t$. The longitudinal ensemble

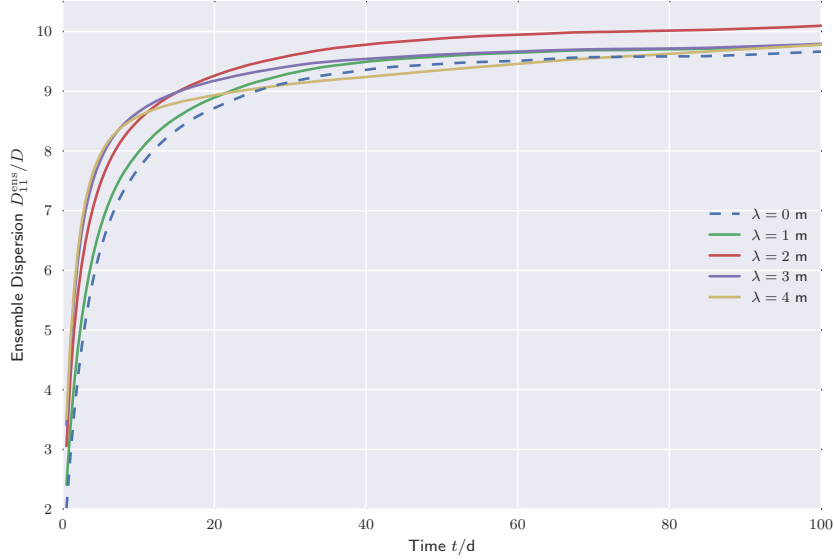


Figure 3.7: Estimations of the fine-grained ensemble averaged coefficient $D_{11}^{\text{ens}}(t)$ for increasing filter width λ , obtained from 256 GRW simulations with filtered velocities and self-averaging estimates of the coarse-grained diffusion coefficients $D_{11}^{\text{cg}}(t, \lambda)$.

process $X_1^{\text{ens}}(t) = X_1(t) - \langle X_1(t) \rangle$ verifies the same equation (3.14), with the velocity component V_1 replaced by its fluctuation V_1' . The half derivative of its variance gives the ensemble dispersion coefficient in the following form (Suciu, 2014):

$$D_{11}^{\text{ens}}(t) = D + \int_0^t \langle V_1'(t) V_1'(t') \rangle dt'. \quad (3.15)$$

From equations (3.13) and (3.14) one obtains the equivalent expression

$$\begin{aligned} D_{11}^{\text{ens}}(t) &= D + \int_0^t \langle \langle V_1' \rangle_\lambda(t) \langle V_1'(t') \rangle_\lambda \rangle dt' \\ &\quad + \int_0^t \langle V_{\lambda,1}'(t) V_{\lambda,1}'(t') \rangle dt' \\ &\quad + \int_0^t \langle \langle V_1' \rangle_\lambda(t) V_{\lambda,1}'(t') \rangle dt' + \int_0^t \langle \langle V_1' \rangle_\lambda(t') V_{\lambda,1}'(t) \rangle dt'. \end{aligned} \quad (3.16)$$

The first line in equation (3.16) corresponds to equation (3.15) with V_1' replaced by $\langle V_1' \rangle_\lambda$, that is to the coefficient $D_{11}^{\text{ens}}(t, \lambda)$ derived for a filtered velocity field. The second line is given by the integral from (3.15) written for the correlation of the sub-filter velocity fluctuations. And last line

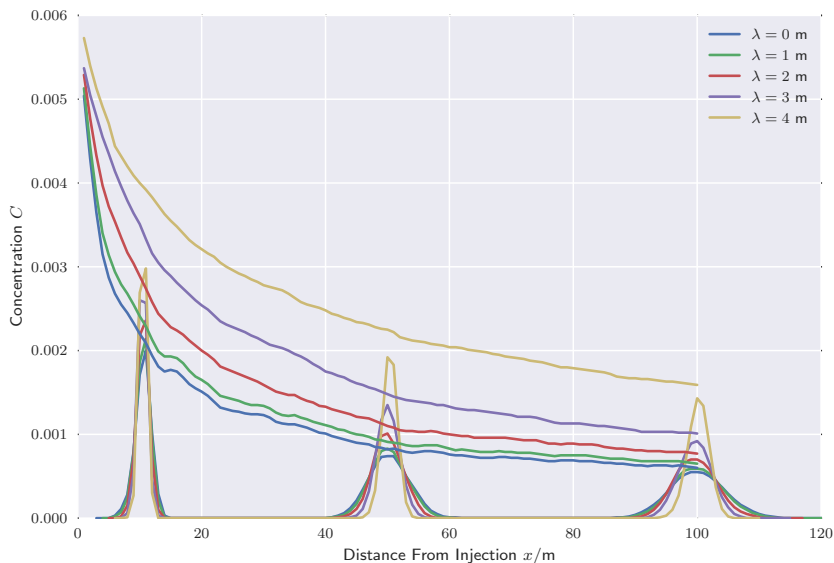


Figure 3.8: Cross section concentration $C(x_1, t)$ recorded at $t = 10$ d, 50 d, and 100 d and the concentration at the expected centre of mass $C(\langle V_1 \rangle t, t)$ (shown as monotonically decreasing curves) given by single-realisation GRW simulations with filtered velocities.

in equation (3.16) describes a contribution to the ensemble coefficient produced by correlations between filtered and sub-filter velocity fluctuations. If this last contribution vanishes, then the contribution from the second line of (3.16) corresponds to the correction $\delta D_{11}^{\text{ens}}(t, \lambda)$ of the coarse-grained diffusion coefficient defined by equation (3.10).

Coarse-Grained Concentration Simulations

The cross-section concentration $C(x_1, t)$ and the concentration at the expected position of the centre of mass $\langle V_1 \rangle t$ are calculated from a single GRW simulation with filtered velocities and with an unchanged local dispersion coefficient D . The result is shown in Figure 3.8. An ensemble of $R = 256$ GRW simulations, using self-averaging estimations of the coarse-grained coefficients $D_{11}^{\text{cg}}(t, \lambda)$ and filtered velocities, recover the fine-grained ensemble averaged cross-section concentration with a good precision, which can be seen in Figure 3.9. This result indicates that the self-averaging estimations of the coarse-grained coefficients $D_{11}^{\text{cg}}(t, \lambda)$ are accurate enough for the purpose of simulating the transport of the PDF/FDF in physical space, which is governed by the same equation as for the mean concentration (2.42).

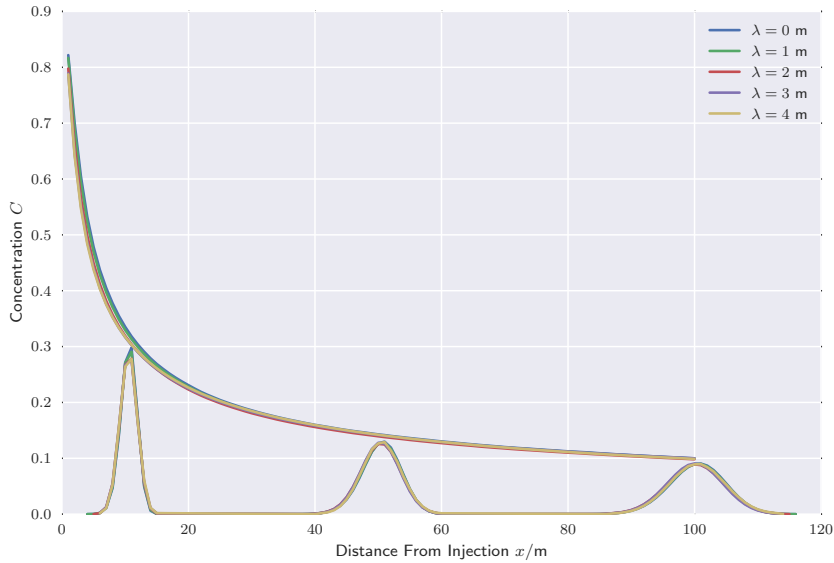


Figure 3.9: Fine-grained ensemble averages corresponding to the concentrations shown in Figure 3.8, recovered from 256 GRW simulations with filtered velocities and self-averaging coarse-grained dispersion coefficients $D_{11}^{cg}(t, \lambda)$.

FDF Mixing Model

When mixing models are used in FDF simulations, the filter width should be taken into account by the mixing model. Thus it is proposed that the correlation length of the hydraulic conductivity λ_Y used as a length scale in the IEM equation (2.52) is replaced by a linear combination of λ_Y and the filter width λ . It is noted that for $\lambda > 0$, the coefficient \mathcal{D} is the coarse-grained diffusion coefficient (3.10). With these parameters, the IEM model reads

$$\mathcal{V}_c^{\text{IEM}} = -k_\chi \frac{\mathcal{D}}{(\lambda_Y + \lambda)^2} (C - \langle C \rangle), \quad (3.17)$$

with $k_\chi = 0.6$. Furthermore, as shown in Section 2.5.3, only the linear combination of the time series and the IEM mixing model (TS-IEM) yields acceptable results. Hence, the TS-IEM model (2.53) with the IEM model taking the filter width into account (3.17), is the only mixing model used for the FDF simulations.

FDF Simulations

GRW-FDF solutions for the problem of passive transport formulated in Section 2.5 and specified for FDF simulations in Section 3.4 are computed with drift coefficients for transport in physical space \mathcal{V} (see equation (2.42))

given by filtered velocity fields $\langle V_1 \rangle_\lambda$. The filtered fields are generated in a first-order approximation by the modified Kraichnan expression (3.7). The corresponding diffusion coefficients, \mathcal{D} in equation (2.42), are computed by equation (2.51) from coarse-grained longitudinal ensemble dispersion coefficients $D_{11}^{\text{cg}}(t, \lambda)$. The coefficients $D_{11}^{\text{cg}}(t, \lambda)$ are obtained by equation (3.10) from the mean values of the self-averaging ensemble dispersion coefficients presented in Figure 3.6.

The GRW-PDF solutions are obtained similarly, with \mathcal{V} given by the ensemble average $\langle V_1 \rangle = 1 \text{ m d}^{-1}$ of the fine-grained velocity field and \mathcal{D} given by the mean value of the self-averaging ensemble dispersion coefficient $D_{11}^{\text{ens}}(t, 0)$ (the case $\lambda = 0 \text{ m}$ in Figure 3.6). The coefficients describing the transport in concentration space, \mathcal{V}_c and \mathcal{D}_c in equation (2.43), are those of the combined TS-IEM model (2.53).

The reference solution and the initial condition for these simulations are estimated from the Monte Carlo ensemble of 256 transport simulations computed for log-conductivities with Gaussian correlation and for $\lambda = 0 \text{ m}$ (Section 3.4). The same ensemble was used to estimate the drift \mathcal{V}_c in the TS model, while using the diffusion coefficient \mathcal{D}_c inferred in Section 2.5.3.

In the present reverse Fokker-Planck approach to PDF/FDF solutions (Section 2.4.2), the weighting factor is the scalar concentration itself, $\Theta(c) = c$. Hence, as follows from relation (2.32), the mean concentration equals the position PDF $\langle C \rangle(x, t) = p_x(x, t)$, which is simply obtained from the GRW-PDF/FDF simulation by summing up the joint concentration-position PDF/FDF $p(c, x, t)$ over the c -axis. The advantage of using the reverse Fokker-Planck approach should be stressed. In a direct approach, the scalar concentration c cannot serve as a weighting factor Θ , because it undergoes diffusion and does not verify the continuity equation (2.40).

Results for the mean concentration $\langle C \rangle_\lambda$ obtained from GRW-FDF simulations using the linear combination of mixing models TS-IEM (2.53) for increasing filter width λ are compared to Monte Carlo results and to GRW-PDF simulations using the TS mixing model in Figure 3.10. It can be seen that the accuracy of the GRW-FDF solutions increases with the filter width λ and for $\lambda \geq 5 \text{ m}$ the results obtained by the three methods practically coincide. It is also remarked that the FDF solution for small λ is less smooth than similar results obtained from single-realisation GRW simulations of the two dimensional transport shown in Figure 3.8. In both cases, one can see a discrepancy between $\langle C \rangle(t)$ or $\langle C \rangle_\lambda(t)$ respectively, both recorded at the expected centre of mass $x = \langle V_1 \rangle t$ and the peaks in the spatial distribution of the concentration located at the position of the actual centre of mass, which is random and generally does not coincide with its expectation.

The mean concentration is the PDF $p_x(x, t)$ of the Itô process (2.42) which solves the Fokker-Planck equation (2.31). Thus, $\langle C \rangle_\lambda$ can also be computed by solving equation (2.31), independently of the FDF problem, like in moment equations approaches (Haworth, 2010). As for the variance, it

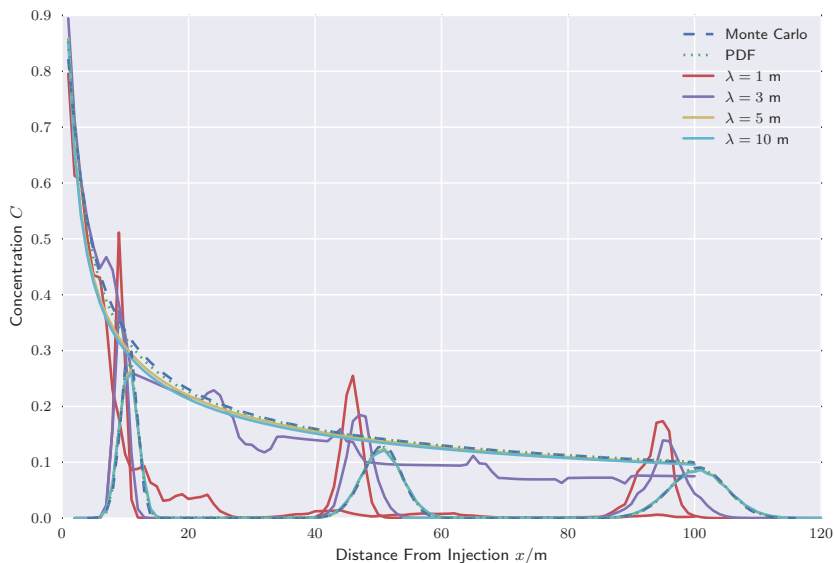


Figure 3.10: $\langle C \rangle_\lambda(x, t)$ recorded at fixed times $t = 10$ d, 50 d, and 100 d and $\langle C \rangle_\lambda(t)$ recorded at $x = \langle V_1 \rangle t$. TS-IEM results for increasing λ are compared to Monte Carlo estimates (MC) and PDF solutions using the TS model (PDF).

requires the computation of $\langle C^2 \rangle_\lambda$, which involves the consistency condition (2.34) and the knowledge of the one point FDF (Suci *et al.*, 2015b). Since, as shown in the following, the estimated FDFs are generally inaccurate, so will be the variance, and it is not estimated.

Cumulative distribution functions sampled on the same trajectory $x = \langle V_1 \rangle t$ are shown in Figure 3.11. At early times $t \leq 20$ d the cumulative distributions obtained by GRW-FDF simulations approach the PDF and the Monte Carlo results with increasing filter width. However, at larger times the FDF solutions are even worse than the PDF solutions for the TS-IEM model shown in Figure 2.8. Figure 3.12 shows that the FDFs are shifted towards small concentrations with increasing time, the smaller λ , the larger the shift. The corresponding cumulative distributions, presented in Figure 3.13 show a similar behaviour, with large deviations from the reference solution for $\lambda = 5$ m and $t \geq 20$ d. For the largest filter width $\lambda = 10$ m, acceptable GRW-FDF estimations of the cumulative distribution can be obtained at small and intermediate times $t < 50$ d.

The behaviour of the TS-IEM model at large times indicates that the left-drift, towards small concentrations, is too large. Since, according to the TS-IEM mixing model (2.53) the IEM model has a dominant contribution at large times, $\mathcal{V}_c^{\text{TS-IEM}}$ can be reduced by reducing $\mathcal{V}_c^{\text{IEM}}$. A larger time scale τ at large times is therefore needed in the IEM model. The convergent

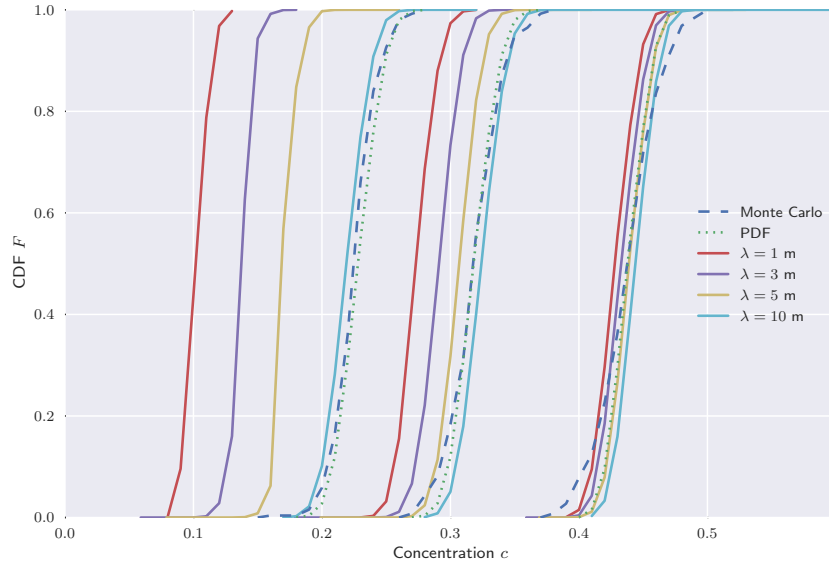


Figure 3.11: Cumulative distribution functions (CDF) for the same cases as in Figure 3.10, estimated at $x = \langle V_1 \rangle t$, for $t = 5$ d, 10 d, and 20 d (from right to left).

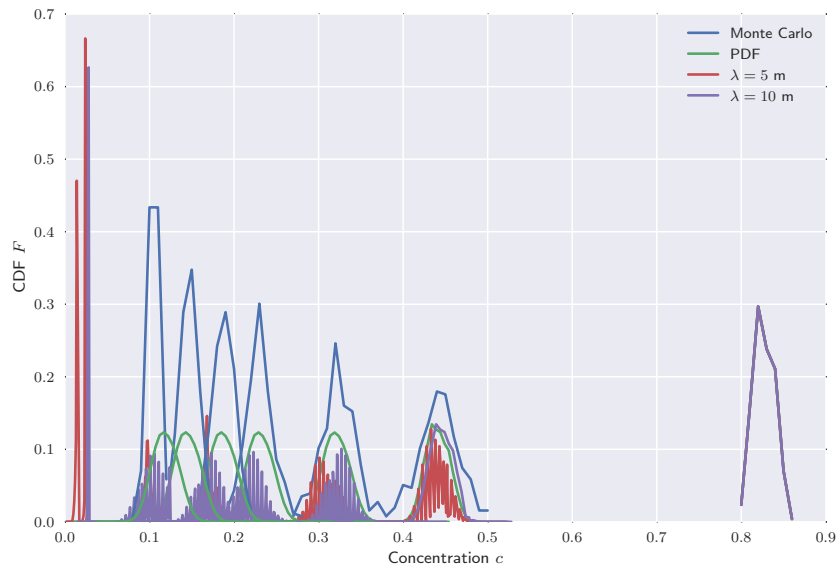


Figure 3.12: GRW-FDF solutions $f(c; x, t)$ for the TS-IEM mixing model, compared to Monte Carlo estimates and PDF solutions with the TS model, sampled at $x = \langle V_1 \rangle t$, for $t = 0$ d, 5 d, 10 d, 20 d, 30 d, 50 d, and 100 d (from right to left).

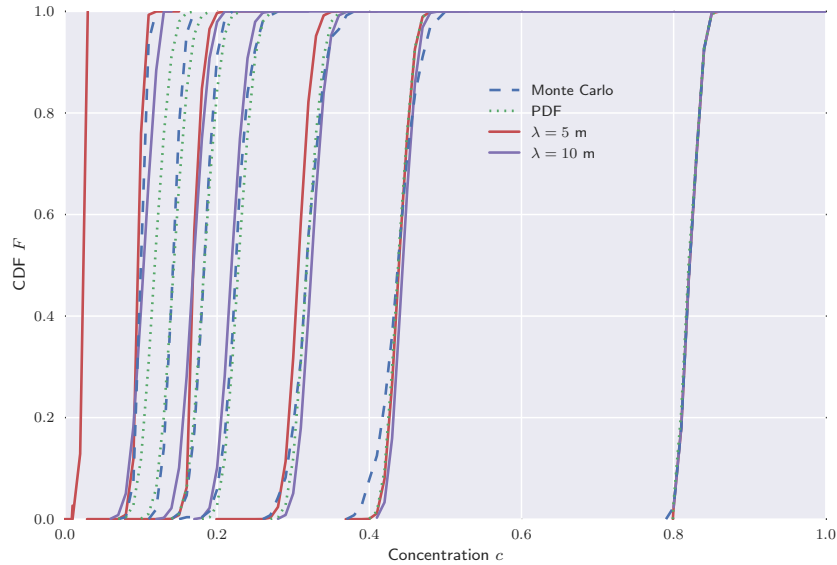


Figure 3.13: Cumulative distribution functions (CDF) corresponding to the PDFs presented in Figure 3.12 for $t = 0$ d, 5 d, 10 d, 20 d, 30 d, and 50 d.

behaviour of the TS-IEM model at intermediate times is ensured by the TS component $\mathcal{V}_c^{\text{TS}}$, which compensates the smallness of $\mathcal{V}_c^{\text{IEM}}$ (see Figure 2.9). The same result can be obtained by an IEM model with a smaller time scale τ at small times. These ideas will be further examined in Chapter 4. The time scale $\tau = L^2/\mathcal{D}$ used in turbulence seems to be inadequate for the PDF/FDF problem considered here. The GRW-FDF solutions presented in this article could be utilized to design the appropriate mixing model for solute plumes migrating in groundwater.

Conclusions

Although they share the same mathematical formalism, CGS-FDF modelling of groundwater systems and LES-FDF modelling of turbulent reacting flows differ in an important aspect. Whereas in turbulence the upscaled transport parameters are not known a priori, for transport in aquifers with the hydraulic conductivity modelled by statistically homogeneous random fields with low variance, the stochastically upscaled model is completely determined, at least in a first-order approximation, by the statistics of the random field. In addition, the coarse-grained diffusion coefficients (3.10), estimated as ensemble averages, converge to the stochastically upscaled diffusion coefficients with increasing filter width and allow recovering the results of the stochastically upscaled model in single-realisation CGS (Figure

3.5). Thus, in CGS-FDF simulations, the solution of equation (2.42) approaches the PDF solution for the mean concentration with increasing filter width. Provided that the same convergence holds for the solution of equation (2.43), which describes the transport of the FDF in concentration space, the CGS-FDF solution converges to the PDF solution. The numerical results presented here partially illustrate this convergence: with high accuracy for the mean concentration, at moderately large times for the cumulative distribution function, but, in absence of an adequate mixing model, only at small times for the filtered density. For sake of clarity and simplicity, chemical reactions were not considered in the numerical illustration of the approach. Because the reaction terms are in a closed form, they only contribute with a supplementary drift in equation (2.43).

If the hydraulic conductivity is no longer statistically homogeneous, the upscaled transport parameters are not known a priori and even the existence of the upscaled transport equation is questionable. In this case, filtered velocities and single-realisation estimates of coarse-grained diffusion coefficients can be used to recover the results obtained for the fully resolved velocity field (Figure 3.4). The CGS-FDF modelling is now similar to the classical LES-FDF approach. Like in turbulence modelling, the ensemble average is replaced by a smoothing in space which still allows an appropriate description of the large scale variability of the velocity field. The PDF will then be the probabilistic description obtained by the spatial smoothing of the fine-scale description of the process, and the aim of FDF modelling will be to recover this global probabilistic description on coarse grids, at affordable computational costs. Volume averaging or multi-grid numerical upscaling procedures can be used to extend the CGS-FDF strategy illustrated in this chapter to problems of reactive transport in conditions of highly variable and statistically inhomogeneous hydraulic conductivity of the groundwater system. Furthermore, the reverse Fokker-Planck approach could also be used to design robust numerical schemes based on the GRW algorithm to solve PDF/FDF problems for other fluid systems, such as those studied in turbulence and combustion theory.

Chapter 4

A Time Dependent Mixing Model

This chapter is based on the paper

Schüler, L., N. Suci, P. Knabner, and S. Attinger, A time dependent mixing model to close PDF equations for transport in heterogeneous aquifers, *Adv. Water Resour.*, under review.

Introduction

The moment approach predicts the evolution of the true concentration distribution by its statistical moments. They are consistent with the geostatistical representation of the heterogeneity of the subsurface. If this heterogeneity is statistically homogeneous, the equation for the first moment, which is the mean concentration, has the following characteristics: The highly heterogeneous and spatially fluctuating groundwater velocity is replaced by an ensemble averaged velocity field and the effect of the fluctuating velocity on the transport is modelled by an enhanced dispersion, called macrodispersion or ensemble dispersion (*Gelhar and Axness, 1983*). This approach has the limitation that the ensemble averaged concentration only describes the mean plume behaviour. But in general, the mean behaviour differs from that of a specific plume in a single aquifer. See Figure 4.1 for a comparison between the mean concentration and a concentration obtained from a simulation in a specific velocity field realisation. Only if the hydraulic conductivity has finite correlation lengths and the plume has sampled a representative part of the aquifer, it becomes ergodic and its transport behaviour can be modelled by the ensemble averaged behaviour, described above. In a first step, possible deviations from the mean behaviour can be quantified by the concentration variance. It is transported by the same processes as the mean concentration, thus it is advected by the averaged velocity field and dispersed by an enhanced macrodispersion. But concentration variance is also generated by mean concentration gradients and simultaneously it is destroyed by dissipative processes, which are created by small-scale fluctuations in the velocity field. In order to calculate the influence of these small-scale fluctuations on the concentration variance, a closure model is needed.

In the field of turbulence modelling, where very similar transport equations are used, different approaches exist for such closure models (e.g. *Tennekes and Lumley, 1972*). Up to this point, the adaption of these approaches to groundwater transport modelling has been hampered by the vastly different flow conditions prevalent in both fields. Contrary to most other problems where turbulent flows are more challenging, the roles are reversed here. The strong mixing induced by turbulent flows causes this closure problem to be easier to tackle. The mixing induced by heterogeneities in the groundwater flow is slower and changes significantly in time and is therefore more difficult to model. As *Dentz et al. (2000)* have shown, the mechanism which generates the physical mixing in a given aquifer realisation is more reliably described by the effective dispersion coefficients in comparison to the ensemble dispersion coefficients, which correspond to the turbulent diffusion coefficients. The effective dispersion is small at early times and increases only slowly with time. Therefore, concentration gradients at early times are steep and may remain steep for prolonged times, which in turn prevents the smoothing of concentration fluctuations and preserves concentration uncer-

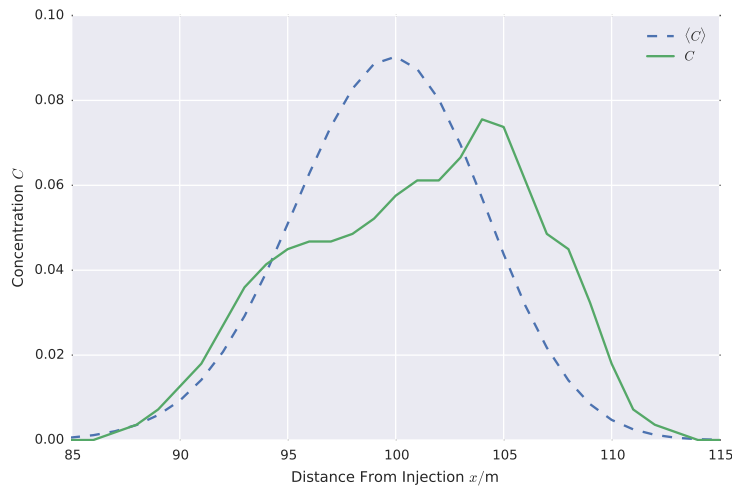


Figure 4.1: A measure is needed to quantify how good the mean concentration $\langle C \rangle$ approximates the actual concentration C , since the difference can be significant.

tainty. [Andričević \(1998\)](#) proposed a mixing mechanism based on a time variable effective length scale which, in principle, could be determined experimentally. [Kapoor and Gelhar \(1994a,b\)](#) derived a transport equation for the concentration variance, including local dispersivity and macrodispersive transport. By neglecting the local dispersivity, the results from [Dagan \(1982\)](#) could be derived. It was concluded that even very small local dispersivities create a qualitatively different behaviour compared to the zero local dispersivity case, as the local dispersivity is the only mechanism which can reduce the variance. They used an approach developed for turbulent flows to model the variance dissipation, created by the local dispersivity. Furthermore, analytical solutions for the long-time behaviour of the concentration variance were derived. These results were confirmed for globally integrated variances by numerical simulations ([Kapoor and Kitanidis, 1997](#)).

If the predictions made by a contaminant transport model are to be used for risk analysis, even more information than the mean concentration and the variance is needed. Risk thresholds, regulated e.g. by an environmental agency ([WWAP, 2012](#)), can only be factored in by the exceedance probability (e.g. [Andričević and Cvetković, 1996](#)). It depends on the complete one-point PDF of the concentration. The concentration variance, as discussed above, can only be used to calculate a first estimation of the exceedance probability ([de Barros et al., 2011b](#)). Even if such estimation would be an acceptable approximation, rare events or extreme values cannot be mapped by the mean concentration and the concentration variance alone. This limitation stems from the fact that by using only the first two

statistical moments, namely the mean and the variance, a Gaussian shape for the concentration PDF is implied. Such a distribution is short-tailed and therefore excludes the possibility of rare events. *Yee and Chan (1997)* analysed a large set of experimental data from tracer tests in the turbulent atmosphere. From this analysis they identified a collapse of higher-order concentration moments, which means that the higher-order moments can be expressed through lower-order moments. *Srzie et al. (2013a)* applied such an analysis to the transport of solutes in groundwater and also found a collapse. This might be a promising way of computing the concentration PDF from the mean concentration and the concentration variance.

In this chapter, the evolution of the concentration variance and the concentration PDF over a long time period is investigated and it is shown that mixing models used before fail to reproduce the variance at all times. To that end, a closed transport equation for the one-point concentration PDF is briefly repeated in Section 4.2.1. Using this equation as a starting point, the transport equations of the first two statistical moments are derived in Section 4.2.2. It is shown that by prescribing a certain mixing model, both the PDF and the variance equations have the same closure problem and thus depend on the same mixing coefficients. The importance of this finding lies in the possibility of testing new mixing models with much simpler concentration variance simulations first and subsequently transferring them to PDF models. Next, analytical solutions of the moment equations are derived in Section 4.2.3 and the dependence of the analytical solution of the concentration variance on the mixing model is highlighted. In Section 4.3 the need for a time dependency of the coefficients of the mixing model is identified and a new time dependent mixing model is proposed. This new model is explicit and in a closed form. It is then verified in Section 4.4 by comparing the previously derived analytical solution of the concentration variance equation with the old and the new mixing model with reference Monte Carlo simulations. Afterwards, the new model is also used in the PDF framework and compared to reference Monte Carlo solutions. Finally, this chapter is concluded in Section 4.5 and a future perspective is shown.

Physical Background and Methods

The reactive transport of a solute in groundwater can be described by equation (1.4). It is assumed that the random velocity field $\mathbf{V}(\mathbf{x})$ is statistically homogeneous and that the local dispersion \mathbf{D} is isotropic. If an ensemble of statistically equivalent solutions of this equation is calculated, the mean behaviour can be calculated from the ensemble average $\langle \mathbf{C} \rangle = \sum_{i=1}^N \mathbf{C}^{(i)} / N$ over N realisations. As a first measure, the variance $\sigma_c^2(\mathbf{x}, t)$ can quantify how good the ensemble average approximates the behaviour in a specific realisation. The mean concentration $\langle \mathbf{C} \rangle(\mathbf{x}, t)$ and the concentration vari-

ance $\sigma_c^2(\mathbf{x}, t)$ are the first and second statistical moments of the one-point one-time concentration PDF $f(\mathbf{c}; \mathbf{x}, t)$:

$$\langle \mathbf{C} \rangle := \int_{\Omega_c} \mathbf{c} f d\mathbf{c} \quad (4.1)$$

$$\sigma_c^2 := \int_{\Omega_c} \mathbf{c}^2 f d\mathbf{c} - \langle \mathbf{C} \rangle^2. \quad (4.2)$$

Thus, if a transport equation for the PDF is derived, transport equations of the mean and variance can be derived too.

PDF Transport Equations

The derivation of the PDF transport equation has already been shown in two different ways in Section 2.3. With the considerations regarding the parameters of the resulting PDF transport equation (2.2) made at the end of Section 2.4.1, the equation can be formulated as

$$\partial_t f + \langle V_i \rangle \partial_{x_i} f - D_{ij}^{\text{ens}} \partial_{x_i} \partial_{x_j} f = -\partial_{c_\alpha} \partial_{c_\beta} (\mathcal{M}_{\alpha\beta} f) - \partial_{c_\alpha} (S_\alpha f), \quad (4.3)$$

The ensemble dispersion coefficient tensor \mathbf{D}^{ens} is diagonal with $D_{11}^{\text{ens}} = D_L^{\text{ens}}$, $D_{ii}^{\text{ens}} = D_T^{\text{ens}}$ for $i > 1$, and $D_{ij}^{\text{ens}} = 0$ for $i \neq j$. In general, the ensemble dispersion coefficients \mathbf{D}^{ens} are time dependent. But in the turbulent regime, these coefficients can be assumed to be constant in time, because mixing is so fast. In aquifers, the asymptotic values can be reached within a few advective time scales (*Dentz et al., 2000*).

The interaction by exchange with the mean (IEM) model for closing the mixing term was first formulated by *Villermaux and Devillon (1972)* and by *Dopazo and O'Brien (1974)* and still remains very popular for modelling reactive and turbulent flows (see e.g. *Colucci et al., 1998*; *Raman and Pitsch, 2007*; *Popov and Pope, 2014*). It was already introduced in Section 2.5.3 and it closes the mixing term by following approximation

$$M = \partial_{c_\alpha} \partial_{c_\beta} (\mathcal{M}_{\alpha\beta} f) = -\partial_{c_\alpha} [\chi (c_\alpha - \langle C_\alpha \rangle) f], \quad (4.4)$$

where χ is a parameter called the mixing frequency when used in PDF methods or the variance decay coefficient (*Kapoor and Gelhar, 1994a*) when used in moment methods. It has to be prescribed and it will be discussed in detail in Section 4.3. This model causes concentration fluctuations to relax towards the local mean concentration in an exponentially decaying way.

Mean and Variance Transport Equations

The transport equation for the mean concentration can be derived from the PDF transport equation (4.3) by multiplying it with \mathbf{c} and integrating over

the entire concentration space ([Schüler et al., 2016](#)). Doing so yields

$$\begin{aligned} & \int_{\Omega_c} c_\alpha \partial_t f \, d\mathbf{c} + \int_{\Omega_c} c_\alpha \langle V_i \rangle \partial_{x_i} f \, d\mathbf{c} - \int_{\Omega_c} c_\alpha D_{ij}^{\text{ens}} \partial_{x_i} \partial_{x_j} f \, d\mathbf{c} \\ &= \int_{\Omega_c} c_\alpha \partial_{c_\alpha} [\chi(c_\alpha - \langle C_\alpha \rangle) f] \, d\mathbf{c} - \int_{\Omega_c} c_\alpha \partial_{c_\alpha} (S_\alpha f) \, d\mathbf{c}. \end{aligned} \quad (4.5)$$

The order of integration and derivation is swapped on the left hand side and on the right hand side the product rule is applied:

$$\begin{aligned} & \partial_t \int_{\Omega_c} c_\alpha f \, d\mathbf{c} + \langle V_i \rangle \partial_{x_i} \int_{\Omega_c} c_\alpha f \, d\mathbf{c} - D_{ij}^{\text{ens}} \partial_{x_i} \partial_{x_j} \int_{\Omega_c} c_\alpha f \, d\mathbf{c} \\ &= \int_{\Omega_c} \{ \partial_{c_\alpha} [c_\alpha \chi(c_\alpha - \langle C_\alpha \rangle) f] - \chi(c_\alpha - \langle C_\alpha \rangle) f \partial_{c_\alpha} c_\alpha \} \, d\mathbf{c} \\ & \quad - \int_{\Omega_c} [\partial_{c_\alpha} (c_\alpha S_\alpha f) - S_\alpha f \partial_{c_\alpha} c_\alpha] \, d\mathbf{c}. \end{aligned} \quad (4.6)$$

On the left hand side, the definition of the mean concentration $\langle \mathbf{C} \rangle = \int_{\Omega_c} \mathbf{c} f \, d\mathbf{c}$ and on the right hand side the mean reaction rate $\langle \mathbf{S} \rangle = \int_{\Omega_c} \mathbf{S} f \, d\mathbf{c}$ can already be inserted. Furthermore, evaluating the last integrals yields

$$\begin{aligned} & \partial_t \langle C_\alpha \rangle + \langle V_i \rangle \partial_{x_i} \langle C_\alpha \rangle - D_{ij}^{\text{ens}} \partial_{x_i} \partial_{x_j} \langle C_\alpha \rangle \\ &= c_\alpha \chi(c_\alpha - \langle C_\alpha \rangle) f|_{\Omega_c} - \chi(\langle C_\alpha \rangle - \langle C_\alpha \rangle) f \\ & \quad - c_\alpha S_\alpha f|_{\Omega_c} + \langle S_\alpha \rangle. \end{aligned} \quad (4.7)$$

The first three terms on the right hand side vanish, assuming that the function c_α has compact support in Ω_c . Thus, the transport equation for the mean concentration is

$$\partial_t \langle C_\alpha \rangle + \langle V_i \rangle \partial_{x_i} \langle C_\alpha \rangle - D_{ij}^{\text{ens}} \partial_{x_i} \partial_{x_j} \langle C_\alpha \rangle = \langle S_\alpha \rangle. \quad (4.8)$$

It can be seen that the mixing term does not influence the mean concentration, as it cancels itself out.

The variance is defined by (4.2). Thus, as with the derivation of the mean concentration, the starting point is again the PDF transport equation (4.3), but now it is multiplied by \mathbf{c}^2 and integrated over the whole concentration space ([Schüler et al., 2016](#)). The order of integration and derivation is swapped and the product rule is applied to the right hand side:

$$\begin{aligned} & \partial_t \int_{\Omega_c} c_\alpha^2 f \, d\mathbf{c} + \langle V_i \rangle \partial_{x_i} \int_{\Omega_c} c_\alpha^2 f \, d\mathbf{c} - D_{ij}^{\text{ens}} \partial_{x_i} \partial_{x_j} \int_{\Omega_c} c_\alpha^2 f \, d\mathbf{c} \\ &= \int_{\Omega_c} \{ \partial_{c_\alpha} [c_\alpha^2 \chi(c_\alpha - \langle C_\alpha \rangle) f] - 2c_\alpha \chi(c_\alpha - \langle C_\alpha \rangle) f \} \, d\mathbf{c} \\ & \quad - \int_{\Omega_c} [\partial_{c_\alpha} (c_\alpha^2 S_\alpha f) - 2c_\alpha S_\alpha f] \, d\mathbf{c}. \end{aligned} \quad (4.9)$$

The first and third term on the right hand side both vanish for the same reason as in the derivation of the mean concentration. The definition of the mean concentration (4.1) can be inserted into the second term on the right hand side:

$$\begin{aligned} & \partial_t \int_{\Omega_c} c_\alpha^2 f d\mathbf{c} + \langle V_i \rangle \partial_{x_i} \int_{\Omega_c} c_\alpha^2 f d\mathbf{c} - D_{ij}^{\text{ens}} \partial_{x_i} \partial_{x_j} \int_{\Omega_c} c_\alpha^2 f d\mathbf{c} \\ &= -2\chi \left[\int_{\Omega_c} c_\alpha^2 f d\mathbf{c} - \langle C_\alpha \rangle^2 \right] + 2 \int_{\Omega_c} c_\alpha S_\alpha f d\mathbf{c}. \end{aligned} \quad (4.10)$$

The term inside the squared brackets on the right hand side could already be replaced by the concentration variance (4.2), but to do this for every term, the transport equation of $\langle \mathbf{C} \rangle^2$ needs to be subtracted from equation (4.10). Therefore, the equation of the squared mean concentration needs to be derived first. This is done by multiplying equation (4.8) by $\langle \mathbf{C} \rangle$, yielding

$$\langle C_\alpha \rangle \partial_t \langle C_\alpha \rangle + \langle C_\alpha \rangle \langle V_i \rangle \partial_{x_i} \langle C_\alpha \rangle - \langle C_\alpha \rangle D_{ij}^{\text{ens}} \partial_{x_i} \partial_{x_j} \langle C_\alpha \rangle = \langle C_\alpha \rangle \langle S_\alpha \rangle. \quad (4.11)$$

By making extensive use of the product rule, it follows

$$\begin{aligned} & \partial_t \langle C_\alpha \rangle^2 - \langle C_\alpha \rangle \partial_t \langle C_\alpha \rangle + \langle V_i \rangle \partial_{x_i} \langle C_\alpha \rangle^2 - \langle C_\alpha \rangle \langle V_i \rangle \partial_{x_i} \langle C_\alpha \rangle \\ & - D_{ij}^{\text{ens}} \left[\partial_{x_i} (\langle C_\alpha \rangle \partial_{x_j} \langle C_\alpha \rangle) - \partial_{x_i} \langle C_\alpha \rangle \partial_{x_j} \langle C_\alpha \rangle \right] = \langle C_\alpha \rangle \langle S_\alpha \rangle. \end{aligned} \quad (4.12)$$

The dispersion term is further modified by using the product rule:

$$\begin{aligned} & D_{ij}^{\text{ens}} \left[\partial_{x_i} (\langle C_\alpha \rangle \partial_{x_j} \langle C_\alpha \rangle) - \partial_{x_i} \langle C_\alpha \rangle \partial_{x_j} \langle C_\alpha \rangle \right] \\ &= D_{ij}^{\text{ens}} \left[\partial_{x_i} \left(\partial_{x_j} \langle C_\alpha \rangle^2 - \langle C_\alpha \rangle \partial_{x_j} \langle C_\alpha \rangle \right) - \partial_{x_i} \langle C_\alpha \rangle \partial_{x_j} \langle C_\alpha \rangle \right] \\ &= D_{ij}^{\text{ens}} \left[\partial_{x_i} \partial_{x_j} \langle C_\alpha \rangle^2 - \langle C_\alpha \rangle \partial_{x_i} \partial_{x_j} \langle C_\alpha \rangle - 2 \partial_{x_i} \langle C_\alpha \rangle \partial_{x_j} \langle C_\alpha \rangle \right]. \end{aligned} \quad (4.13)$$

Hence, equation (4.12) is transformed into

$$\begin{aligned} & \partial_t \langle C_\alpha \rangle^2 + \langle V_i \rangle \partial_{x_i} \langle C_\alpha \rangle^2 - D_{ij}^{\text{ens}} \partial_{x_i} \partial_{x_j} \langle C_\alpha \rangle^2 + 2D_{ij}^{\text{ens}} \partial_{x_i} \langle C_\alpha \rangle \partial_{x_j} \langle C_\alpha \rangle \\ & - \langle C_\alpha \rangle \partial_t \langle C_\alpha \rangle - \langle C_\alpha \rangle \langle V_i \rangle \partial_{x_i} \langle C_\alpha \rangle + \langle C_\alpha \rangle D_{ij}^{\text{ens}} \partial_{x_i} \partial_{x_j} \langle C_\alpha \rangle = \langle C_\alpha \rangle \langle S_\alpha \rangle. \end{aligned} \quad (4.14)$$

Comparing the second line of equation (4.14) with equation (4.11), it is seen that it is identical to $-\langle C_\alpha \rangle \langle S_\alpha \rangle$ and the transport equation of $\langle C \rangle^2$ is

$$\begin{aligned} & \partial_t \langle C_\alpha \rangle^2 + \langle V_i \rangle \partial_{x_i} \langle C_\alpha \rangle^2 - D_{ij}^{\text{ens}} \partial_{x_i} \partial_{x_j} \langle C_\alpha \rangle^2 \\ & + 2D_{ij}^{\text{ens}} \partial_{x_i} \langle C_\alpha \rangle \partial_{x_j} \langle C_\alpha \rangle - 2 \langle C_\alpha \rangle \langle S_\alpha \rangle = 0. \end{aligned} \quad (4.15)$$

Now, equation (4.15) can be subtracted from equation (4.10) and the mean $\langle C_\alpha S_\alpha \rangle = \int_{\Omega_c} c_\alpha S_\alpha f d\mathbf{c}$ can be inserted:

$$\begin{aligned}
& \partial_t \left[\int_{\Omega_c} c_\alpha^2 f d\mathbf{c} - \langle C_\alpha \rangle^2 \right] + \langle V_i \rangle \partial_{x_i} \left[\int_{\Omega_c} c_\alpha^2 f d\mathbf{c} - \langle C_\alpha \rangle^2 \right] \\
& - D_{ij}^{\text{ens}} \partial_{x_i} \partial_{x_j} \left[\int_{\Omega_c} c_\alpha^2 f d\mathbf{c} - \langle C_\alpha \rangle^2 \right] \\
& = 2D_{ij}^{\text{ens}} \partial_{x_i} \langle C_\alpha \rangle \partial_{x_j} \langle C_\alpha \rangle - 2\chi \left[\int_{\Omega_c} c_\alpha^2 f d\mathbf{c} - \langle C_\alpha \rangle^2 \right] \\
& + 2(\langle C_\alpha S_\alpha \rangle - \langle C_\alpha \rangle \langle S_\alpha \rangle). \tag{4.16}
\end{aligned}$$

Finally, the definition of the concentration variance (4.2) is inserted and the last term on the right hand side is identified as the covariance between the concentration and the reaction rate $\text{cov}(C_\alpha, S_\alpha) = \langle C_\alpha S_\alpha \rangle - \langle C_\alpha \rangle \langle S_\alpha \rangle$, which yields the transport equation for the variance:

$$\begin{aligned}
& \partial_t \sigma_{c_\alpha}^2 + \langle V_i \rangle \partial_{x_i} \sigma_{c_\alpha}^2 - D_{ij}^{\text{ens}} \partial_{x_i} \partial_{x_j} \sigma_{c_\alpha}^2 \\
& = 2D_{ij}^{\text{ens}} \partial_{x_i} \langle C_\alpha \rangle \partial_{x_j} \langle C_\alpha \rangle - 2\chi \sigma_{c_\alpha}^2 + 2\text{cov}(C_\alpha, S_\alpha). \tag{4.17}
\end{aligned}$$

It can be seen that the concentration variance is transported by the mean velocity $\langle \mathbf{V} \rangle$ and by the ensemble dispersion coefficients \mathbf{D}^{ens} exactly like the mean concentration. But in contrast to the transport equation for the mean concentration (4.8) it has additional source and sink terms on the right hand side. The source term creates variance at mean concentration gradients and couples the two equations (4.8) and (4.17) weakly, as the coupling is only in one direction. The reaction term in equation (4.3) is transformed into the covariance between the concentration and the reaction rate. For this study, the most interesting term of equation (4.17) is the second one on the right hand side. This sink term destroys variance by small-scale fluctuations. It is not closed and the same variance decay coefficient χ as in the mixing term of the transport equation of the full PDF (4.3) appears here. This link makes it possible to test different propositions of the variance decay coefficient as a closure assumption for the transport equation for the concentration variance. Subsequently, the new proposition can be transferred to the PDF equation. The big advantage of testing different closures for the variance is that this equation is easier to handle. On the one hand, the variance equation has an analytical solution expressed by a time integral (see Section 4.2.3) which can be readily evaluated by numerical quadratures. And on the other hand, PDF equations are high-dimensional, with independent variables in both the physical and the concentration space and they have to be solved numerically.

Analytical Solutions of the Moment Equations

With an analytical solution of the concentration variance transport equation, new mixing models can easily be examined and compared to Monte

Carlo reference simulations. In order to make the analytical solutions for the first two moments easier, it is assumed that the ensemble dispersion coefficients \mathbf{D}^{ens} are constant. The asymptotic value is therefore used. This assumption was already justified in Section 4.2.1. Furthermore, only one species is considered and the reaction term is set to zero, yielding

$$\partial_t \langle C \rangle + \langle V_i \rangle \partial_{x_i} \langle C \rangle - D_{ij}^{\text{ens}} \partial_{x_i} \partial_{x_j} \langle C \rangle = 0. \quad (4.18)$$

Analytical Solution of the Mean Concentration Equation

An analytical solution of the passive transport equation for the mean concentration (4.18) can be found, for example, by transforming it into the frequency domain, which makes it an ordinary differential equation. Following *Kapoor and Gelhar (1994b)*, a multivariate Gaussian distribution with zero mean and a diagonal covariance matrix $2D_{ii}^{\text{ens}}t_0$ as the initial condition is prescribed. It can be interpreted as a function which evolved from a Dirac delta function for a time span t_0 according to equation (4.18) without the advection term. The solution is then given by

$$\langle C \rangle(\mathbf{x}, t) = \prod_{i=1}^d (4\pi D_{ii}^{\text{ens}}(t + t_0))^{-1/2} \exp\left(-\frac{(x_i - \langle V_i \rangle t)^2}{4D_{ii}^{\text{ens}}(t + t_0)}\right), \quad (4.19)$$

where d is the spatial dimension.

Analytical Solution of the Concentration Variance Equation

Deriving an analytical solution of the concentration variance evolution equation is more involved than deriving a solution of the mean concentration equation. This derivation is similar to the one presented by *Kapoor and Gelhar (1994b)*, but the derivation presented here uses more standard techniques and is more straightforward. Furthermore, a time dependency of the variance decay coefficient $\chi(t)$ is considered here (*Schüler et al., 2016*).

The variance evolution equation for passive transport is equation (4.17) with the covariance term set to zero

$$\partial_t \sigma_{c_\alpha}^2 + \langle V_i \rangle \partial_{x_i} \sigma_{c_\alpha}^2 - D_{ij}^{\text{ens}} \partial_{x_i} \partial_{x_j} \sigma_{c_\alpha}^2 = 2D_{ij}^{\text{ens}} \partial_{x_i} \langle C_\alpha \rangle \partial_{x_j} \langle C_\alpha \rangle - 2\chi \sigma_{c_\alpha}^2 \quad (4.20)$$

and is an inhomogeneous linear partial differential equation and as such a fundamental solution (also known as Green's function) is formulated. The general solution of equation (4.20) can then be calculated by the convolution of Green's function with the inhomogeneity $2D_{ij}^{\text{ens}} \partial_{x_i} \langle C \rangle \partial_{x_j} \langle C \rangle$. This way, an analytical solution can be found without making any approximations or assumptions. Because the convolution transforms into a simple multiplication, it is transformed into Fourier space. Eventually, the solution of the mean concentration (4.19) is needed. This is where the time shift t_0 becomes

important, because without it, a singularity would appear in the limit $t \rightarrow 0$, as the Gaussian solution would tend to a Dirac delta function in this short time limit. By applying this time shift, the solution stays Gaussian and the singularity vanishes.

The differential operator $L(\mathbf{x}, t)$ is defined by

$$L\sigma_c^2 = \partial_t \sigma_c^2 + \langle V_i \rangle \partial_{x_i} \sigma_c^2 - D_{ij}^{\text{ens}} \partial_{x_i} \partial_{x_j} \sigma_c^2 - 2\chi \sigma_c^2 = 0, \quad (4.21)$$

with the inhomogeneity

$$g(\mathbf{x}, t) = 2D_{ij}^{\text{ens}} \partial_{x_i} \langle C \rangle \partial_{x_j} \langle C \rangle. \quad (4.22)$$

Then, the concentration variance transport equation (4.20) can be rewritten as

$$L(\mathbf{x}, t) \sigma_c^2(\mathbf{x}, t) = g(\mathbf{x}, t). \quad (4.23)$$

The fundamental solution (or Green's function) $G(\mathbf{x} - \mathbf{x}', t, t')$ is defined as the solution of the differential operator $L(\mathbf{x}, t)$ with delta functions as the inhomogeneity:

$$L(\mathbf{x}, t) G(\mathbf{x} - \mathbf{x}', t, t') = \delta(\mathbf{x} - \mathbf{x}') \delta(t - t'). \quad (4.24)$$

The fundamental solution is translation invariant in space, because the operator L has constant coefficients with respect to \mathbf{x} . The general solution of equation (4.20) is given by

$$\sigma_c^2(\mathbf{x}, t) = \sigma_{c_h}^2(\mathbf{x}, t) + \int_0^t \int_{\Omega_x} G(\mathbf{x} - \mathbf{x}', t, t') g(\mathbf{x}', t') d\mathbf{x}' dt', \quad (4.25)$$

where $\sigma_{c_h}^2(\mathbf{x}, t)$ is the solution of equation (4.20) without the inhomogeneity. But because it is assumed that the initial condition is known exactly, the variance at time $t = 0$ is $\sigma_c^2(\mathbf{x}, t = 0) = 0$. Thus, without the inhomogeneity, which acts as the only source term, the solution of the homogeneous partial differential equation is $\sigma_{c_h}^2(\mathbf{x}, t) = 0$ for all times. Therefore, the solution of the homogeneous equation can be dropped.

If Green's function is known, the solution of equation (4.20) can be calculated from equation (4.25), which is a convolution of Green's function and the inhomogeneity in physical space:

$$\begin{aligned} \sigma_c^2(\mathbf{x}, t) &= \int_0^t \int_{\Omega_x} G(\mathbf{x} - \mathbf{x}', t, t') g(\mathbf{x}', t') d\mathbf{x}' dt' \\ &= \int_0^t (G * g)(\mathbf{x}, t, t') dt' \\ &= \int_0^t \mathcal{F}^{-1} \left[\tilde{G}(\mathbf{k}, t, t') \tilde{g}(\mathbf{k}, t') \right] dt', \end{aligned} \quad (4.26)$$

where \mathcal{F}^{-1} denotes the inverse Fourier transform with the independent variable $\mathbf{k} \in \Omega_k$ being defined in the frequency space. A tilde denotes the Fourier transform of a function. Hence, \tilde{G} and \tilde{g} need to be calculated in order to obtain the solution σ_c^2 .

Fourier transforming both sides of equation (4.24) gives an inhomogeneous ordinary differential equation in the frequency domain:

$$(\partial_t + I \langle V_i \rangle k_i + D_{ij}^{\text{ens}} k_i k_j + 2\chi(t)) \tilde{G}(\mathbf{k}, t, t') = \delta(t - t'), \quad (4.27)$$

with I being the imaginary unit. This ordinary differential equation can be solved by separation of variables for a solution of the homogeneous equation, which can be used as a starting point to guess a particular solution of the inhomogeneous solution, yielding

$$\tilde{G}(\mathbf{k}, t, t') = \Theta(t - t') \exp \left(- (D_{ij}^{\text{ens}} k_i k_j + I \langle V_i \rangle k_i) (t - t') - 2 \int_{t'}^t dt'' \chi(t'') \right), \quad (4.28)$$

where Θ is the Heaviside step function. In order to transform the inhomogeneity (4.22), the transformed mean concentration $\langle C \rangle$ from equation (4.19) needs to be plugged in:

$$\tilde{g}(\mathbf{k}, t) = \mathcal{F} [2D_{ij}^{\text{ens}} \partial_{x_i} \langle C \rangle \partial_{x_j} \langle C \rangle] = \frac{-2D_{ij}^{\text{ens}}}{(2\pi)^{d/2}} k_i \langle \tilde{C} \rangle * k_j \langle \tilde{C} \rangle. \quad (4.29)$$

At this point, the time shift t_0 is needed. Otherwise, a singularity for $t = 0$ would cause problems, as the Gaussian distribution would tend to a Dirac delta function for small times. The Fourier transformed mean concentration is

$$\langle \tilde{C} \rangle = \frac{1}{(2\pi)^{d/2}} \exp(-D_{ij}^{\text{ens}} k_i k_j (t + t_0) - I k_i \langle V_i \rangle t). \quad (4.30)$$

With this solution, the Fourier transformed inhomogeneity can be calculated:

$$\tilde{g}(\mathbf{k}, t) = \frac{D_{ij}^{\text{ens}}}{2(2\pi)^d} \frac{1}{(2D_{ij}^{\text{ens}}(t + t_0))^{d/2}} \left[\frac{d}{D_{ij}^{\text{ens}}(t + t_0)} - k_i k_j \right] \exp \left(-\frac{1}{2} D_{ij}^{\text{ens}} (t + t_0) k_i k_j - I \langle V_i \rangle k_i t \right). \quad (4.31)$$

Finally, the transformed Green's function (4.28) and the transformed inhomogeneity (4.31) are inserted into equation (4.26):

$$\sigma_c^2(\mathbf{x}, t) = \frac{D_{ij}^{\text{ens}}}{2(2\pi)^{3d/2}} \int_0^t dt' \frac{\Theta(t - t')}{[2D_{ij}^{\text{ens}}(t' + t_0)]^{d/2}} \int_{\Omega_k} d\mathbf{k} \left[\frac{d}{D_{ij}^{\text{ens}}(t' + t_0)} - k_i k_j \right] \exp \left(-\frac{1}{2} D_{ij}^{\text{ens}} (2t - t' + t_0) k_i k_j + I(x_i - \langle V_i \rangle t) k_i - 2 \int_{t'}^t dt'' \chi(t'') \right), \quad (4.32)$$

By completing the square for the variable \mathbf{k} , the Fourier integrand is lead back to a Gaussian function which can be integrated. Because the ensemble dispersion tensor is diagonal, the expression can be simplified by only considering the diagonal elements. Now, only a final time integral remains to be calculated:

$$\begin{aligned} \sigma_c^2(\mathbf{x}, t) = & \sum_{i=1}^d 2D_{ii}^{\text{ens}} \int_0^t dt' \prod_{j=1}^d \frac{\exp\left(-\frac{(x_j - \langle V_j \rangle t)^2}{2D_{jj}^{\text{ens}}(2t + t_0 - t')}\right)}{\left[(2\pi D_{jj}^{\text{ens}})^2(2t + t_0 - t')(t' + t_0)\right]^{1/2}} \\ & \left[\frac{t - t'}{2D_{ii}^{\text{ens}}(2t + t_0 - t')(t' + t_0)} + \frac{(x_i - \langle V_i \rangle t)^2}{(2D_{ii}^{\text{ens}}(2t + t_0 - t'))^2} \right] \\ & \exp\left(-2 \int_{t'}^t dt'' \chi(t'')\right). \end{aligned} \quad (4.33)$$

This integral can either be evaluated analytically by using a long-time approximation or by applying numerical methods. The time integral is rather well behaved and can easily be solved, for example by adaptive numerical quadrature algorithms. *Kapoor and Gelhar (1994b)* have further tackled this integral with $\chi = \text{const}$ by applying some long term approximations and came up with a closed analytical solution. But because the short time behaviour is of interest in this work, solution (4.33) will be considered. The variance decay coefficient χ appears in the argument of the last exponential function. Hence, new mixing models can be verified with this equation if, for example, compared to Monte Carlo reference solutions.

Time Dependent Extension of the IEM Model

The IEM model describes the decrease of the concentration PDF too slow, as already pointed out in Sections 2.5.3 and 3.5. It was developed for simulating turbulent flows. One major difference between turbulent flows and flows in porous media is the time scale on which mixing takes place. In the turbulent regime, it is often taken as a constant. And even there, a mixing time scale as a variable parameter has already been taken into account (*Sabel'nikov et al., 2006; Jones et al., 2012; Dodoulas and Navarro-Martinez, 2013*).

The original IEM model for turbulent flows approximates the conditional dissipation rate by equation (4.4). The variance decay coefficient χ is proportional to the inverse mixing time scale. In classical PDF approaches, the latter is usually assumed to be proportional to the turbulence time scale (*Pope, 1985; Celis and Figueira da Silva, 2015*). In large eddy simulations (LES), the mixing time scale is often estimated as a velocity (*Dodoulas and Navarro-Martinez, 2013*) or as a diffusion time scale (*Colucci et al., 1998*). *Colucci et al. (1998)*, for instance, used the subgrid length scale λ , which defines the transition from resolved to unresolved scales and the subgrid

diffusion coefficient, which corresponds to an isotropic ensemble dispersion coefficient D^{ens} in groundwater flows. Following this approach, the variance decay coefficient can be formulated as

$$\chi = k_\chi \frac{D^{\text{ens}}}{\lambda^2}. \quad (4.34)$$

The dimensionless model parameter k_χ is usually in the range of $0.6 \leq k_\chi \leq 3.1$ (Pope, 1985; Colucci *et al.*, 1998).

For groundwater systems, characterised by the anisotropic local dispersion coefficients D_{ij} , Kapoor and Gelhar (1994a) arrived at a very similar equation for the variance decay coefficient, by introducing the Taylor microscales Δ_{c_i} , which characterise the gradients of the concentration fluctuations along the i th coordinate. The resulting variance decay coefficient is

$$\chi = \sum_{i,j=1}^d \frac{D_{ij}}{\Delta_{c_i} \Delta_{c_j}}. \quad (4.35)$$

However, the Taylor microscales could only be fitted to measurements, as a closed formula was not given.

It is recalled that the IEM model was developed to approximate the second derivative of the conditional dissipation rate with respect to c (4.4). The conditional dissipation rate is defined by

$$\mathcal{M} = \langle D_{ij} \partial_{x_i} C \partial_{x_j} C | c \rangle, \quad (4.36)$$

with $\langle A|B \rangle = \langle AB \rangle / \langle B \rangle$ denoting the conditional expectation of A given B . The conditional dissipation rate \mathcal{M} depends on the squared concentration gradients, which clearly evolve in time. But the IEM model has no way of accounting for this evolution. It only takes the difference between the current concentration and the local mean concentration into account. As already mentioned in Section 3.5, a more accurate mixing model would account for larger dissipation rates at early times and smaller dissipation rates at later times, as the concentration gradients decrease. For turbulent reactive flows, a dependence of χ on the Reynolds number of the subgrid scale flow was already proposed (Jones *et al.*, 2012; Dodoulas and Navarro-Martinez, 2013). Furthermore, Sabel'nikov *et al.* (2006) modelled the mixing frequency as a stochastic process in order to account for the entire range of time scales in the mixing process. They named their model “extended interaction by exchange with the mean” (EIEM). The idea of using a variable variance decay coefficient $\chi(t)$ is elaborated and a new time dependent extension of the model, adapted to the transport processes in groundwater, is proposed.

Like Andrićević (1998), the concentration gradients are approximated using an evolving effective spatial scale $\lambda_c(t)$. This assumption implies that the squared concentration gradients evolve inversely proportional to that

squared characteristic length scale $(\nabla C)^2 \sim \lambda_c(t)^{-2}$ as the plume spreads and its fringes and fluctuations smooth out. Since the concentration fluctuations are smoothed out by the local dispersion with the characteristic scale $\lambda_c(t) = \sqrt{2Dt}$, it is assumed that the decay of the conditional dissipation rate (4.36) is proportional to $\mathcal{M} \sim \lambda_c(t)^{-2}$. In order to improve the IEM model, this dependency on $\lambda_c(t)$ is included into the variance decay coefficient (4.34).

Furthermore, the ensemble dispersion coefficient \mathbf{D}^{ens} accounts for an artificial dispersion which is caused by centre of mass fluctuations of the solute plume from realisation to realisation. The effective dispersion coefficient \mathbf{D}^{eff} excludes this artificial dispersion and converges to \mathbf{D}^{ens} in the long-time limit for velocity fields with short range correlations (Dentz *et al.*, 2000; Suciú, 2014). Because the mixing in turbulent flows is so much faster than it is in groundwater flows, the difference does not matter for turbulent flows. Therefore, the mathematically simpler to handle ensemble dispersion coefficient is used in studies concerning flows in the turbulent regime (Pope, 1985; Colucci *et al.*, 1998). But in groundwater flows the difference is significant and because the centre of mass fluctuations do not influence the dissipation, the effective dispersion coefficient \mathbf{D}^{eff} describes the correct behaviour for the mixing model. With these physical arguments and choosing $k_\chi = 2$ from the middle of the interval of reported values, following time-dependent variance decay coefficient is proposed:

$$\chi(t) = \sum_{i,j=1}^d \frac{D_{ij}^{\text{eff}}(t)}{D_{ij}t}. \quad (4.37)$$

In order to show the similarities between this newly proposed variance decay coefficient and the previous ones, it is assumed that the correlation length of the log conductivity field λ_Y and the local dispersion coefficient D are both isotropic, which yields the dispersive time scale $\tau_D = \lambda_Y^2/D$. With this relationship, the variance decay coefficient can be transformed to

$$\chi(t) = \sum_{i,j=1}^d \frac{D_{ij}^{\text{eff}}(t)\tau_D}{\lambda_Y^2 t}. \quad (4.38)$$

Equation (4.38) generalises equation (4.34) to a time-variable characteristic length scale and to anisotropic effective dispersion coefficients. Compared to the coefficient (4.35) introduced by Kapoor and Gelhar (1994a), the new variance decay coefficient (4.38) depends on the effective dispersion coefficients instead of the local dispersion coefficients. Furthermore, the unclosed Taylor microscale was replaced by the correlation length and a dimensionless time factor τ_D/t is included.

As shown in Figure 4.2, this variance decay coefficient has larger values than the constant one at early times, which causes a stronger dissipation.

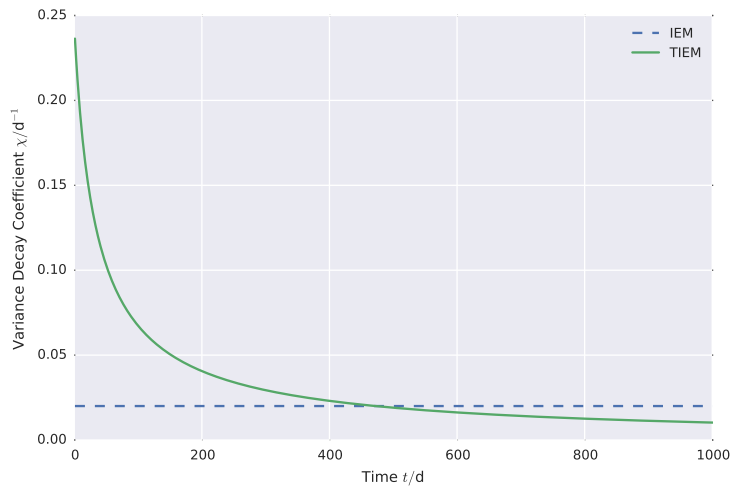


Figure 4.2: An illustration of the different time behaviours of the IEM and the TIEM variance decay coefficients. The TIEM model causes strong dissipation at early times, but for long times it causes less dissipation than the IEM model.

But then it drops below the constant variance decay coefficient and approaches $\lim_{t \rightarrow \infty} \chi(t) = 0$. In order to distinguish this model from other extensions of the IEM model, it is named the “time dependent interaction by exchange with the mean model” (TIEM).

With this extension, the simplicity and low computational costs of the IEM model are preserved, while at the same time, it incorporates the time dependent physical processes causing the dissipation.

Simulations

Variance Modelling

In order to verify the TIEM model independently, simulations with two different numerical models were performed. A sequential standard particle tracking model is implemented following *Dentz et al. (2002)* and the global random walk (GRW) algorithm (*Vamos et al., 2003*), presented in Section 1.4, is used as an independent model. The mean concentration and the concentration variance are derived from both numerical simulations and compared to the analytical solutions (4.19) and (4.33) with the IEM and TIEM mixing models.

Simulation setup

Both numerical transport simulations are calculated for the same conditions as the PDF simulations from Section 2.5. Thus, a two-dimensional heterogeneous velocity field which is modelled as a solution of the linearised Darcy and continuity equations by the Kraichnan algorithm (*Kraichnan, 1970*). The mean flow velocity is prescribed as $\langle \mathbf{V} \rangle = (1, 0)^T \text{m d}^{-1}$ and an isotropic Gaussian covariance structure with a correlation length of $\lambda = (1, 1)^T \text{m}$ and a variance of $\sigma^2 = 0.1$ is chosen for the underlying conductivity field. The flow fields are generated by using 6400 Fourier modes for the randomisation method (*Suciu et al., 2016; Heße et al., 2014*), in order to capture the self-averaging behaviour of the transport process over hundreds of correlation lengths (*Eberhard et al., 2007*).

The simulations are performed with an isotropic local dispersion coefficient of $D = 0.01 \text{m}^2 \text{d}^{-1}$, which results in a Péclet number equal to 100 with the above parameters for the mean velocity and the correlation length. The particles are injected instantaneously and distributed uniformly on a rectangle with side lengths $1.62 \text{m} \times 1.62 \text{m}$. This initial distribution of particles approximates the analytical solution (4.19) for $t = 0$ and $t_0 = 10 \text{d}$. Both numerical models use a time step of $\Delta t = 0.5 \text{d}$.

For the standard particle tracking simulation, the particles, transported by the velocity field and dispersed by heterogeneities, are modelled according to the Itô equations

$$dX_i(t) = V_i(\mathbf{X})dt + \sqrt{2D}dW_i(t), \quad (4.39)$$

where $W_i(t)$ are independent standard Wiener processes (*Suciu et al., 2015a*). An extended Runge-Kutta scheme (*Drummond et al., 1984*) with an accuracy of order $(\Delta t)^{3/2}$ is used to discretise the stochastic equations (4.39).

1000 realisations with 150000 particles in each of them are calculated to create a statistical ensemble. It takes about 1100 min to compute one realisation on a single core of the EVE cluster at the UFZ Leipzig.

The GRW-algorithm takes a different approach. It uses a superposition of many weak solutions of Itô equations projected onto a regular grid. The particles solving the Itô equations are spread on the grid globally according to the drift and diffusion coefficients of the equation. By construction, this algorithm is free of numerical diffusion and can be used for practically arbitrary numbers of particles without an impact on the computational costs. For more details about the GRW algorithm see Section 1.4. *Suciu et al. (2006, Appendix A1)* show how to implement an efficient GRW version of Monte Carlo simulations, whereas more technical details and the convergence behaviour of the schemes are presented by *Suciu (2014)* and *Suciu et al. (2013)*. The same physical parameters are used as for the standard particle tracking. The GRW simulations are performed on a grid with 4600×1800 cells with a resolution of $0.1 \text{m} \times 0.1 \text{m}$. A total of 10^{24} particles are used to represent

the behaviour of the concentration on the GRW lattice. The computation of the velocity field on the grid and the GRW transport simulation takes about 48 min for each realisation. The ensemble of realisations of the transport process is obtained by conducting independent simulations on 1000 cores, in a single job executed on the JURECA supercomputer at Research Centre Jülich.

A normalised two-dimensional histogram on grid cells with a size of $1\text{ m} \times 1\text{ m}$ is performed for both simulations to calculate concentrations from the particle distributions. Rather than representing a sampling volume which mimics experimental measurements, the cells are needed to estimate concentrations from particles distributions provided by the two numerical methods. Ensembles of simulated concentrations, along the mean flow direction, are used to estimate variances which are further compared to the analytical solution at the continuum scale given by equation (4.33).

A comparison of the two numerical approaches shows how much the number of particles required for accurate simulations of localised quantities reduces the computational performance in classical, sequential particle tracking methods. Fewer particles are needed to compute global quantities, such as spatial moments of the solute plume (e.g. *Dentz et al., 2002*). But for accurate estimations of the local variance of the solute concentration, 10^5 , or even more particles are required (see Figure 4.3). This results in a dramatic increase of computational time. Comparing the computing times normalised by the corresponding numbers of particles shows that GRW simulations are about 10^{20} times more efficient in estimating the same localised quantity.

Results

The impact of the TIEM model (4.37) on the analytical solution (4.33) of the concentration variance evolution equation (4.17) is investigated by comparing the results to the two numerical models described in Section 4.4.1. Because no mixing term appears in the evolution equation for the mean concentration (4.8), different mixing models do not influence the mean concentration behaviour. Thus, the results for the mean concentration will not be shown here.

When using it in the analytical solution, the IEM model has no space dependency. Therefore, it destroys the variance at a uniform rate over the whole plume. Hence, the well-known bimodal shape of the variance of a Gaussian-like mean concentration will remain unaltered and only the magnitude of the variance will change by introducing new mixing models which act globally.

In Figure 4.4, the concentration standard deviation σ_c computed from the GRW simulation is compared to the analytical solution (4.33) using the two different mixing models. For the ensemble and effective dispersion

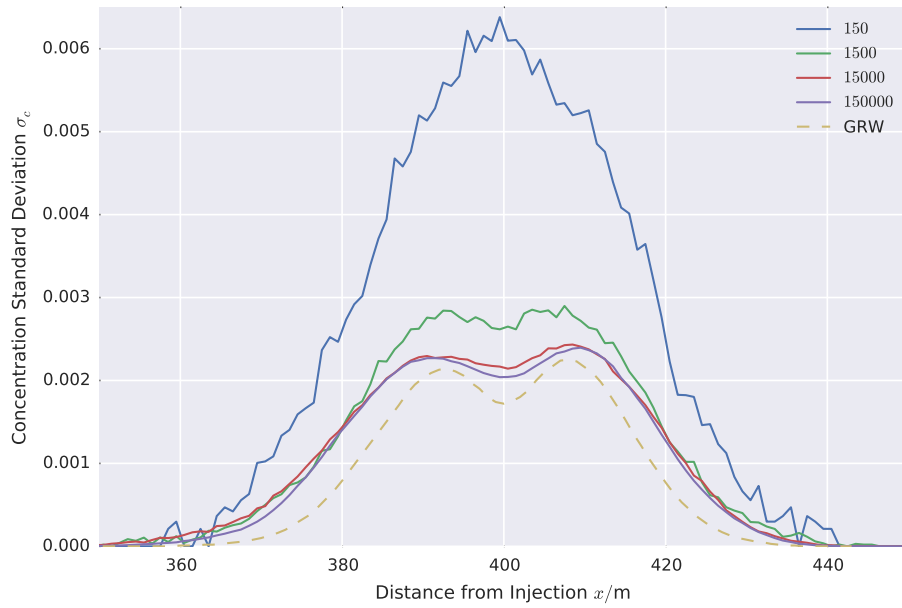


Figure 4.3: The concentration standard deviation calculated from standard particle tracking simulations with different amounts of particles per realisation compared to results from GRW simulations with 10^{24} particles per realisation.

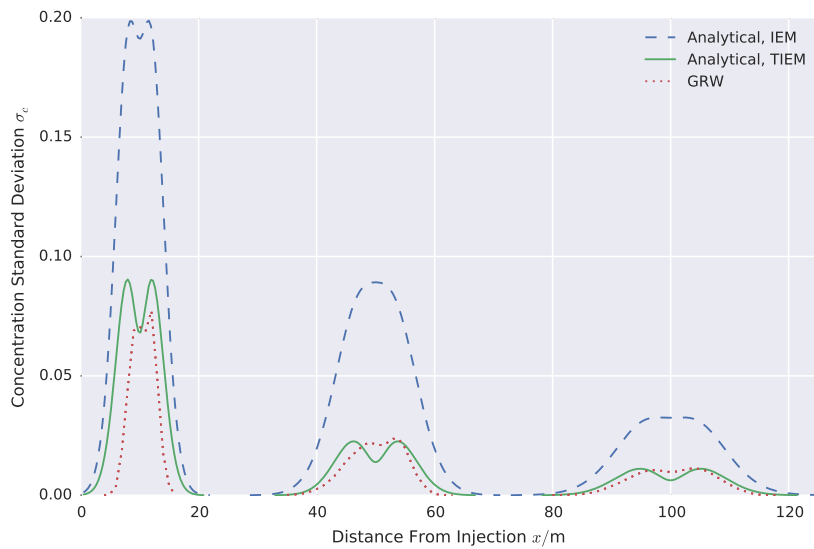


Figure 4.4: Analytical concentration standard deviations with the IEM and TIEM mixing models compared to concentration standard deviations computed from GRW simulations at times $t = 10$ d, 50 d, and 100 d.

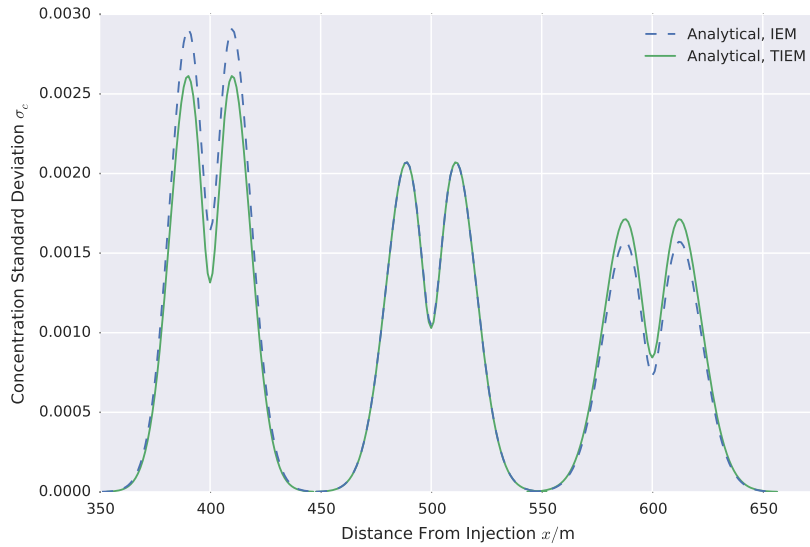


Figure 4.5: For $t > 500$ d, the TIEM solutions stays larger than the IEM solution.

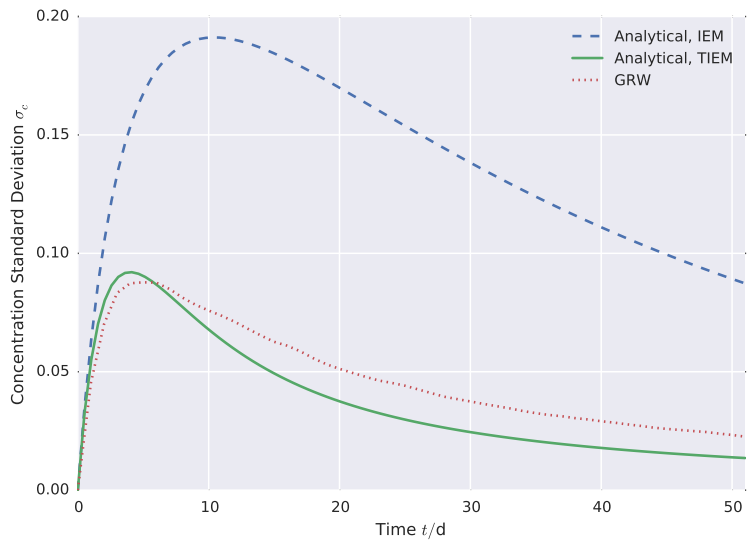


Figure 4.6: The concentration standard deviation at the centre of mass $\mathbf{x}_{cm} = \langle \mathbf{V} \rangle t$.

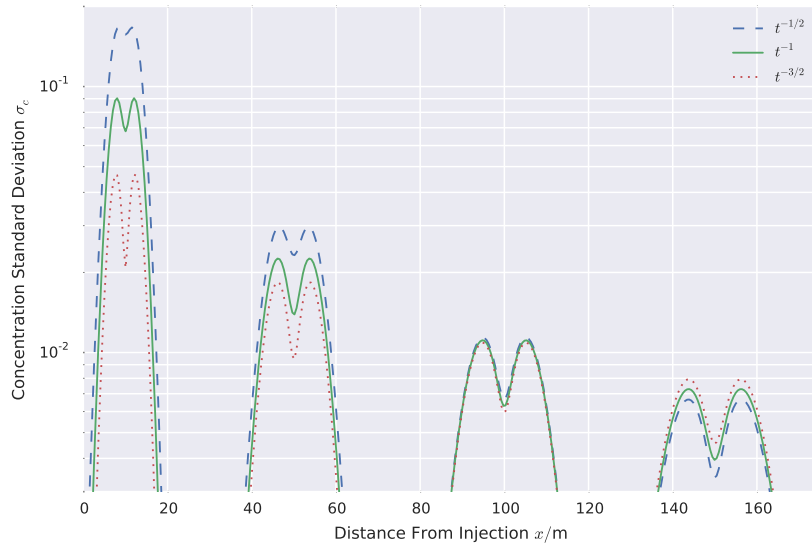


Figure 4.7: The analytical concentration standard deviation with different exponents a for t^a . The solution with $a = -1$ is the same as in Figure 4.4. A semi-log plot is used in order to make the differences at $t = 150$ d clearer.

coefficients, the results from [Dentz et al. \(2000\)](#) are used. The results from the particle tracking are omitted, because they are very similar to the GRW solutions and make the figure difficult to read. The different solutions are plotted at $t = 10$ d, 50 d, and 100 d after injection. Instead of the variance, its square root, the standard deviation, is plotted in Figure 4.4 for practical reasons.

The most obvious feature of the figure is the large peak of the analytical solution at short times with the IEM mixing model. This large peak shows the problem of the IEM model, namely that the variance destruction at short times due to small-scale fluctuations of the flow field is strongly underestimated. As seen from Figure 4.2, the TIEM model has a much larger variance decay coefficient at short times which manifests itself as a stronger decline of variance at these early times. In Figure 4.4, this behaviour can be seen in the analytical solution with the TIEM model, which matches the numerical simulation very well at intermediate and long times. At 500 d, the analytical solutions with the IEM and the TIEM models intersect. At even larger times, the TIEM solution stays greater than the IEM solution, as shown in Figure 4.5. On the other side of the time axis, at very early times, ranging from $t = 0$ d up to about $t = 15$ d there is still a gap between the numerical reference simulations and the TIEM model. But for $t = 10$ d the IEM model differs from the reference simulations by about 61%, compared to a difference of 18% with the TIEM model, which is a major improvement.

The time evolution of the concentration standard deviation at the centre of mass of the mean concentration plume $\mathbf{x}_{\text{cm}} = \langle \mathbf{V} \rangle t$ is shown in Figure 4.6, to highlight the influence of the time dependent mixing model at early times. It should be noted that the analytical solution pronounces the valley of the bimodal structure of the variance curve too much. Comparing the peaks of the analytical solution and of the GRW solution, the difference at early times is more pronounced and becomes increasingly smaller at intermediate and long times. The slight asymmetry in the numerical solutions is due to the non-ergodicity at early times.

Finally, the impact of different exponents of the explicit time dependency of the TIEM model (4.38) is tested. In Figure 4.7, the standard deviation curves with the exponents $t^{-1/2}$ and $t^{-3/2}$ are compared to the exponent t^{-1} , which follows from the arguments made in Section 4.3. It can be seen that the exponent of $-1/2$ causes the variance to be too large at early times, which then decreases so fast over time, that it is less than the reference solution for $t > \tau_D = 100$ d. Thus, even if the large values at early times would be adjusted by the constant factor k_χ in the TIEM model, the variance would quickly drop beneath the reference values. On the other hand, the exponent of $-3/2$ causes the variance to be too small at early times, which then decreases so slowly, that for $t > 100$ d, it is greater than the reference solution. These results further support the physical reasoning made in Section 4.3.

PDF Modelling

As already discussed in Section 2.4, Lagrangian particle methods used to solve PDF problems in the fields of combustion and turbulence are not well-suited for groundwater problems, where concentrations are strongly diluted (Suciu *et al.*, 2016, 2015b). Therefore, numerical simulations of the PDF equation with the new TIEM model are only performed with the GRW algorithm adapted to PDF simulations. The concentration PDF at the centre of mass of the plume is simulated based on the GRW setup described in Section 2.5 and by Suciu *et al.* (2015a, Sections 4 and 5). There, it is shown that the PDF equation for the concentration at the centre of mass of the plume integrated over the transversal direction can be formulated as a two-dimensional Fokker-Planck equation. This equation describes the cross-section of the concentration at the centre of mass, for which corresponding Itô equations are formulated:

$$dX(t) = \langle V_1 \rangle dt + \sqrt{2D_{11}^{\text{ens}}} dW(t) \quad (4.40)$$

$$dC(t) = Mdt, \quad (4.41)$$

These stochastic differential equations can be solved by Monte Carlo methods and thus by the GRW algorithm. The same parameters as for the simu-

lations described in Section 4.4.1 are used. A reference solution is calculated from Monte Carlo simulations (*Suciu et al., 2015a*).

The results are shown in Figure 4.8. Here, the cumulative distribution function $F(c; x, t)$ and therefore the integral of the PDF is shown, because in general the CDF is a smoother curve than the PDF and can thus be compared better. The CDF at the centre of mass is shown at $t = 30$ d, 50 d, and 100 d after injection (from right to left). It can be seen that the TIEM model is a major improvement over the IEM model. At early times, the IEM model predicts a CDF which is shifted far towards higher concentrations. The TIEM model is just slightly shifted, but the shape differs too with a longer tail towards low concentrations, similar to the IEM model. At $t = 50$ d both models perform acceptable. At $t = 100$ d the IEM model is even shifted too far towards lower concentrations, while the TIEM model is still close to the reference solution. The deviation of the IEM model from the reference solution indicates that the drift in concentration space (see equation (4.41)) is too slow at early times and too large at large times. By considering a time variable variance decay coefficient $\chi(t)$ (see Figure 4.2), the TIEM model proposed in this work provides a correction for the drift in concentration space. This leads to the observed improvements of the PDF simulations. *Sabel'nikov et al. (2006)* also extended the IEM model to incorporate a time dependency of the variance decay coefficient for turbulent reactive flows. Compared to direct numerical simulations, they too reported a good match at intermediate times, but an increasing mismatch for small and large times.

Conclusions and Future Perspectives

This chapter presents a new and time-dependent mixing model: an extended IEM model for groundwater, named TIEM. It is shown that the same mixing model is used for both the concentration variance evolution equation (4.17) and the concentration PDF evolution equation (4.3). This link is used to verify the new TIEM model (4.37) with the much simpler to handle variance equation. The verification is done by comparing an analytical solution of the variance equation (4.33), which depends on a mixing closure model, to two independent numerical models. The TIEM model shows a strong improvement over the IEM model. A significant deviation from the reference simulations can only be observed at times $t < 15$ d. And even for these very short times, the new model is a significant improvement.

Based on these promising results, the model is transferred to the PDF framework. The results obtained from the PDF simulations with the TIEM model are not quite as satisfying as the results from the variance simulations mentioned above. Although there are mismatches at early and also at later times, the new model is still a major improvement over the classical IEM

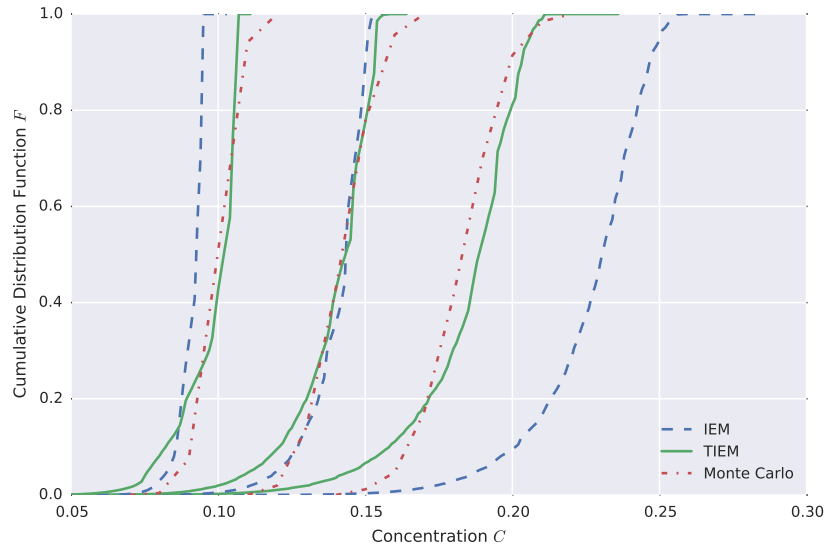


Figure 4.8: The CDF at the centre of mass of the solute plume at times $t = 30$ d, 50 d, and 100 d (from right to left) is calculated with two different IEM models and with dissipation rates extracted from simulated particle trajectories.

model. One possible way of further improving the IEM model is to derive a partial differential equation as a dynamic model for the variance decay coefficient (*Im et al., 1997; Pierce and Moin, 1998*). Such a model could include the actual and instantaneous length scales of the processes destroying the variance. This feature would make it possible to also apply the model to statistically non-homogeneous conductivity fields (*Pierce and Moin, 1998*), as needed if the fields are to be conditioned on measurements.

The GRW-simulations, together with the TIEM model, can easily be extended to three-dimensional problems, to anisotropic dispersion coefficients, and to reactive transport. Especially the latter point is worth highlighting. The reaction terms can simply be plugged into the PDF equations (*Suciu et al., 2016*), which makes the PDF framework the method of choice for modelling complex reactive transport in groundwater.

The TIEM model explicitly takes into account the dimensionality of the transport problem through expression (4.38) of the variance decay coefficient. This shows that by increasing the dimension of the physical space the variance decay coefficient increases, which results in enhanced mixing. The TIEM model also depends on the Péclet number implicitly, through the dependence on the effective diffusion coefficient given in (4.38). The limit of an infinite Péclet number causes a singularity in (4.38). However, for vanishing local dispersion there is no mixing at all and the PDF equation

takes the form of a Fokker-Planck equation ([Venturi et al., 2013](#)). In case of passive transport as considered here, this Fokker-Planck equation reduces to equation (4.3) with the right hand side set to zero, which describes the PDF transport in physical space.

Unlike the approaches based on mapping random variables ([Dentz and Tartakovsky, 2010](#); [Cirpka et al., 2011](#); [de Barros and Fiori, 2014](#)), the derivation of the PDF equation (see Section 2.3) and the closure by IEM or TIEM mixing models are free of the low heterogeneity variance assumption. Another important difference is the way the influence of the sampling volume is taken into account. In mapping approaches ([de Barros and Fiori, 2014](#)), as well as in Monte Carlo simulations ([Srzie et al., 2013a,b](#)) the sampling volume is explicitly considered in the computation of the concentration. A sampling volume, associated with the spatial scale of the measurement, can be accounted for by a spatial filtering of the transport equations, similarly to the LES approach in turbulence ([Suciu et al., 2016](#)), which is presented in Chapter 3. The FDF, which describes the unresolved concentration fluctuations, verifies the PDF equation (4.3), with coefficients defined by spatial filtering and is solved by the GRW algorithm described in Section 4.4.2. The GRW solution also provides the filtered concentration, which corresponds to a spatial average over the sampling volume in this approach. In the limit of large filter widths, the filtered concentration tends to its ensemble average. For finite filter widths it is a random quantity. Its statistics can be inferred from a Monte Carlo ensemble of GRW-FDF solutions, obtained at low computational costs (e.g. computing time of the order of seconds ([Suciu et al., 2016](#))). The TIEM model for FDF simulations is easily obtained by adding the filter width at the denominators of the terms in expression (4.38).

Chapter 5

Summary and Outlook

Inherently connected to subsurface hydrology is the scarcity of data in conjunction with the high variability of physical properties influencing the groundwater and the transport of solutes. The uncertainty, which is always present when investigating transport in the subsurface, needs to be taken into account for risk assessments. Therefore, a geostatistical representation of the subsurface is created from all available measurements and knowledge. This representation includes the uncertainties and variabilities encountered. Now, the concentration PDF can be simulated. All necessary statistical information about the transport can be extracted from the PDF. However, these PDF methods rely on a statistically homogeneous conductivity field, which can thus not be conditioned on measurements. Moreover, PDF methods cannot take the support volume of different measuring techniques into account. An alternative to PDF approaches is therefore found by applying a spatial filter to the PDF equations, resulting in FDFs where the dynamics of the larger scales on a coarser grid are separated from subgrid effects, which are modelled. The aim of this research was to develop an FDF framework tailored towards the transport in groundwater.

The first step towards such a framework was to develop an efficient numerical solver for PDF equations. Because the simulation of concentration PDFs is computationally very expensive due to the highly dimensional nature of these functions, Lagrangian particle methods are the method of choice for solving them, as these methods scale better with increasing dimensionality. But they actually solve Fokker-Planck equations and not necessarily PDF equations. Therefore, consistency conditions were formulated that relate PDF equations to Fokker-Planck equations, which makes it possible to use particle methods to solve PDF equations. From these consistency conditions, a reverse Fokker-Planck approach was developed. The GRW algorithm was adapted to solve such Fokker-Planck equations and in turn solve the PDF equations of interest. The adapted GRW algorithm proves to be computationally very efficient for solving PDF equations.

The next step was to adapt FDF equations to groundwater transport. FDF equations have the same mathematical structure as PDF equations and are also derived in a very similar manner. The main difference is that the ensemble average of the fine-grained PDF is replaced by a spatial filter. The resulting FDF equation now contains spatial averages of the parameters, instead of their expectations. Consequently, the filtered parameters need to be calculated. The velocity field was coarse-grained by applying a spatial filter directly to the Kraichnan formula. The filtered formula can still be evaluated at every arbitrary point without the need to interpolate between values. Moreover, the coarse-graining procedure results in only one additional term per mode. These terms can even be calculated prior to any simulations and be saved. Single particle trajectories were computed on different filtered velocity fields with increasing filter sizes. The upscaled dispersion coefficients could be computed from the differences between the fine-grained and filtered dispersion coefficients. The conditional dissipation rate, governing the transport of the FDF in concentration space, was modelled by a mixing model. This model consists of a linear combination of two individual mixing models. The first one is a time series mixing model, which uses an ensemble of simulated time series to extract the necessary information. The second one is the IEM model, which has proven itself useful in turbulent reactive flows. With the so found parameters of the velocity, the dispersion, and the mixing, the FDF simulations could be performed. The results are promising, but also show that further research needs to be invested into finding mixing models adequately adapted to the transport in groundwater.

Therefore, a connection is identified between the PDF equation and the variance equation, which is derived from the PDF equation. This connection is created when the IEM model with an unknown parameter is applied to the PDF equation. Then the unknown parameter is transferred to the variance equation. Because the variance equation is much easier to handle, different time dependent parameters in the IEM model can be evaluated very efficiently. By using physical arguments and by testing it with the variance equation, the TIEM model is found. Subsequently, it is transferred to PDF equations. The new TIEM model performs much better than the traditional IEM model, but still leaves room for improvement.

This work presents the first results on the way towards FDF methods applied to transport in groundwater. Future research should focus on finding better mixing models. One possible way of finding better mixing models by linking the PDF equations to the variance equation is shown in this work. Furthermore, the upscaling of the dispersion coefficients by analysing single particle trajectories is only possible under restricting assumptions. A more general way needs to be found. This research relied on statistically homogeneous conductivity fields. Thus, there is no way to incorporate measurements, as this is done by conditioning random conductivity fields on the given measurements, which destroys the statistical homogeneity. One way of upscaling

dispersion coefficients in statistically non-homogeneous conductivity fields is to apply numerical volume averages. Another way could be multiscale finite element methods. However, more research is needed to suggest an appropriate upscaling procedure.

The research presented here contributes towards the development of an integrated risk assessment framework applicable to human health risks and ecological risks through contaminations in hydrological systems.

Bibliography

- Alzraiee, A. H., D. Baú, and A. Elhaddad (2014), Estimation of heterogeneous aquifer parameters using centralized and decentralized fusion of hydraulic tomography data from multiple pumping tests, *Hydrol. Earth Syst. Sci. D.*, *11*(4), 4163–4208, doi:10.5194/hessd-11-4163-2014.
- Andričević, R. (1998), Effects of local dispersion and sampling volume on the evolution of concentration fluctuations in aquifers, *Water Resour. Res.*, *34*(5), 1115–1129, doi:10.1029/98WR00260.
- Andričević, R., and V. Cvetković (1996), Evaluation of Risk from Contaminants Migrating by Groundwater, *Water Resour. Res.*, *32*(3), 611–621, doi:10.1029/95WR03530.
- Attinger, S. (2003), Generalized coarse graining procedures for flow in porous media, *Comput. Geosci.*, *7*(4), 253–273.
- Attinger, S., M. Dentz, H. Kinzelbach, and W. Kinzelbach (1999), Temporal behaviour of a solute cloud in a chemically heterogeneous porous medium, *J. Fluid Mech.*, *386*, 77–104.
- Bear, J. (1972), *Dynamics of Fluids in Porous Media*, American Elsevier.
- Bear, J., and H.-D. A. Cheng (2010), *Modeling Groundwater Flow and Contaminant Transport*, Springer, Dordrecht Heidelberg London New York.
- Bear, J., D. Zaslavsky, and S. Irmay (1968), *Physical Principles of Percolation and Seepage*, UNESCO.
- Beckie, R., A. A. Aldama, and E. F. Wood (1996a), Modeling the large-scale dynamics of saturated groundwater flow using spatial-filtering theory: 2. Numerical evaluation, *Water Resour. Res.*, *32*(5), 1281–1288.
- Beckie, R., A. A. Aldama, and E. F. Wood (1996b), Modeling the large-scale dynamics of saturated groundwater flow using spatial-filtering theory: 1. Theoretical development, *Water Resour. Res.*, *32*(5), 1269–1280.

- Bellin, A., and D. Tonina (2007), Probability density function of non-reactive solute concentration in heterogeneous porous formations, *J. Contam. Hydrol.*, *94*(1-2), 109–125, doi:10.1016/j.jconhyd.2007.05.005.
- Bilger, R. W. (1976), The structure of diffusion flames, *Combust. Sci. Technol.*, *13*(1-6), 155–170, doi:10.1080/00102207608946733.
- Borghini, R. (1988), Turbulent Combustion Modelling, *Prog. Energy Combust. Sci.*, *14*, 245–292.
- Bronstein, I. N., K. A. Semendjajew, G. Musiol, and H. Mühlig (2006), *Taschenbuch der Mathematik*, 6 ed., Harri Deutsch, Frankfurt.
- Burr, D. T., E. A. Sudicky, and R. L. Naff (1994), Nonreactive and reactive solute transport in three-dimensional heterogeneous porous media: Mean displacement, plume spreading, and uncertainty, *Water Resour. Res.*, *30*(3), 791–815, doi:10.1029/93WR02946.
- Celis, C., and L. F. Figueira da Silva (2015), Lagrangian Mixing Models for Turbulent Combustion: Review and Prospects, *Flow, Turbul. Combust.*, *94*(3), 643–689, doi:10.1007/s10494-015-9597-1.
- Cirpka, O. A., F. P. J. de Barros, G. Chiogna, and W. Nowak (2011), Probability density function of steady state concentration in two-dimensional heterogeneous porous media, *Water Resour. Res.*, *47*(11), 1–14, doi:10.1029/2011WR010750.
- Colucci, P. J., F. A. Jaber, P. Givi, and S. B. Pope (1998), Filtered density function for large eddy simulation of turbulent reacting flows, *Phys. Fluids*, *10*(2), 499–515, doi:10.1063/1.869537.
- Dagan, G. (1982), Stochastic Modeling of Groundwater Flow by Unconditional and Conditional Probabilities 1. Conditional Simulation and the Direct Problem, *Water Resour. Res.*, *18*(4), 813–833, doi:10.1029/WR018i004p00835.
- Dagan, G. (1994), Upscaling of dispersion coefficients in transport through heterogeneous formations, *Comput Methods Water Resour X*, *1*, 431–9.
- Darcy, H. (1856), *Les fontaines publiques de la ville de Dijon*, Victor Dalmont, Paris.
- de Barros, F. P. J., and A. Fiori (2014), First-order based cumulative distribution function for solute concentration in heterogeneous aquifers: Theoretical analysis and implications for human health risk assessment, *Water Resour. Res.*, *50*(5), 4018–4037, doi:10.1002/2013WR015024.

- De Barros, F. P. J., and Y. Rubin (2011), Modelling of block-scale macrodispersion as a random function, *J. Fluid Mech.*, *676*, 514–545, doi:10.1017/jfm.2011.65.
- de Barros, F. P. J., D. Bolster, X. Sanchez-Vila, and W. Nowak (2011a), A divide and conquer approach to cope with uncertainty, human health risk, and decision making in contaminant hydrology, *Water Resour. Res.*, *47*(5), doi:10.1029/2010WR009954.
- de Barros, F. P. J., A. Fiori, and A. Bellin (2011b), A simple closed-form solution for assessing concentration uncertainty, *Water Resour. Res.*, *47*(12), 1–5, doi:10.1029/2011WR011107.
- Dentz, M., and D. M. Tartakovsky (2010), Probability density functions for passive scalars dispersed in random velocity fields, *Geophys. Res. Lett.*, *37*(24), 1–4, doi:10.1029/2010GL045748.
- Dentz, M., H. Kinzelbach, S. Attinger, and W. Kinzelbach (2000), Temporal behavior of a solute cloud in a heterogeneous porous medium 1 .Point-like injection, *Water Resour. Res.*, *36*(12), 3591–3604, doi:10.1029/2000WR900162.
- Dentz, M., H. Kinzelbach, S. Attinger, and W. Kinzelbach (2002), Temporal behavior of a solute cloud in a heterogeneous porous medium 3. Numerical simulations, *Water Resour. Res.*, *38*(7), 23–1–23–13, doi:10.1029/2001WR000436.
- Dodoulas, I. A., and S. Navarro-Martinez (2013), Large Eddy Simulation of Premixed Turbulent Flames Using the Probability Density Function Approach, *Flow, Turbul. Combust.*, *90*(3), 645–678, doi:10.1007/s10494-013-9446-z.
- Dopazo, C., and E. E. O’Brien (1974), An approach to autoignition of a turbulent mixture, *Acta Astronaut.*, *1*, 1239–1266, doi:10.1016/0094-5765(74)90050-2.
- Drummond, I. T., S. Duane, and R. R. Horgan (1984), Scalar diffusion in simulated helical turbulence with molecular diffusivity, *J. Fluid Mech.*, *138*, 75–91, doi:10.1017/S0022112084000045.
- Eberhard, J. P., N. Suci, and C. Vamoş (2007), On the self-averaging of dispersion for transport in quasi-periodic random media, *J. Phys. A: Math. Gen.*, *40*(4), 597, doi:10.1088/1751-8113/40/4/002.
- Efendiev, Y., and L. J. Durlofsky (2003), A Generalized Convection-Diffusion Model for Subgrid Transport in Porous Media, *Multiscale Model. Simul.*, *1*(3), 504–526, doi:10.1137/S1540345902413693.

- Efendiev, Y., and T. Y. Hou (2009), *Multiscale Finite Element Methods: Theory and Applications*, Springer, New York.
- Efendiev, Y., L. J. Durlofsky, and S. H. Lee (2000), Modeling of subgrid effects in coarse-scale simulations of transport in heterogeneous porous media, *Water Resour. Res.*, *36*(8), 2031–2041, doi:10.1029/2000WR900141.
- Fox, R. O. (2003), *Computational Models for Turbulent Reacting Flows*, Cambridge Series in Chemical Engineering, Cambridge University Press, New York.
- Gelhar, L. W. (1977), Effects of hydraulic conductivity variations on groundwater flows, in *Effects of hydraulic conductivity variations on groundwater flows*, pp. 409–431, Water Resources Publications, Fort Collins, Colo.
- Gelhar, L. W., and C. L. Axness (1983), Three Dimensional Stochastic Analysis of Macrodispersion in Aquifers, *Water Resour. Res.*, *19*(1), 161–180, doi:10.1029/WR019i001p00161.
- Haworth, D. C. (2010), Progress in probability density function methods for turbulent reacting flows, *Prog. Energy Combust. Sci.*, *36*, 168–259.
- Haworth, D. C., and S. B. Pope (2011), Transported Probability Density Function Methods for Reynolds-Averaged and Large-Eddy Simulations, in *Turbulent Combustion Modeling*, no. 95 in Fluid Mechanics and Its Applications, pp. 119–142, Springer Netherlands.
- Heinz, S. (2007), Unified turbulence models for LES and RANS, FDF and PDF simulations, *Theor. Comput. Fluid Dyn.*, *21*(2), 99–118, doi:10.1007/s00162-006-0036-8.
- Herz, M. (2014), Mathematical Modelling and Analysis of Electrolyte Solutions, Ph.D. thesis, Friedrich-Alexander-Universität Erlangen-Nürnberg.
- Heße, F., F. Radu, M. Thullner, and S. Attinger (2009), Upscaling of the advection–diffusion–reaction equation with Monod reaction, *Adv. Water Resour.*, *32*(8), 1336–1351, doi:10.1016/j.advwatres.2009.05.009.
- Heße, F., V. Prykhod’ko, S. Schlüter, and S. Attinger (2014), Generating random fields with a truncated power-law variogram. A comparison of several numerical methods with respect to accuracy and reproduction of structural features., *Environ. Model. Softw.*, *55*, 32–48, doi:10.1016/j.envsoft.2014.01.013.
- Im, H. G., T. S. Lund, and J. H. Ferziger (1997), Large eddy simulation of turbulent front propagation with dynamic subgrid models, *Phys. Fluids*, *9*(12), 3826–3833, doi:10.1063/1.869517.

- Jaberi, F. A., P. J. Colucci, S. James, P. Givi, and S. B. Pope (1999), Filtered mass density function for large-eddy simulation of turbulent reacting flows, *J. Fluid Mech.*, *401*, 85–121.
- Jones, W., A. Marquis, and V. Prasad (2012), LES of a turbulent premixed swirl burner using the Eulerian stochastic field method, *Combust. Flame*, *159*(10), 3079–3095, doi:10.1016/j.combustflame.2012.04.008.
- Kapoor, V., and L. W. Gelhar (1994a), Transport in three-dimensionally heterogeneous aquifers: 1. Dynamics of concentration fluctuations, *Water Resour. Res.*, *30*(6), 1775–1788, doi:10.1029/94WR00076.
- Kapoor, V., and L. W. Gelhar (1994b), Transport in three-dimensionally heterogeneous aquifers 2. Predictions and observations of concentration fluctuations, *Water Resour. Res.*, *30*(6), 1789–1801, doi:10.1029/94WR00075.
- Kapoor, V., and P. K. Kitanidis (1997), Advection-diffusion in spatially random flows: Formulation of concentration covariance, *Stoch. Hydrol. Hydraul.*, *11*(5), 397–422, doi:10.1007/BF02427926.
- Klimenko, A. Y. (2007), On simulating scalar transport by mixing between Lagrangian particles, *Phys. Fluids*, *19*(3), 031,702, doi:10.1063/1.2711233.
- Klimenko, A. Y., and R. W. Bilger (1999), Conditional moment closure for turbulent combustion, *Prog. Energy Combust. Sci.*, *25*(6), 595–687, doi:10.1016/S0360-1285(99)00006-4.
- Kloeden, P. E., and E. Platen (1999), *Numerical Solutions of Stochastic Differential Equations*, Springer, Berlin.
- Kraichnan, R. H. (1970), Diffusion by a Random Velocity Field, *Phys. Fluids*, *13*(1), 22–31, doi:10.1063/1.1692799.
- Kurbanmuradov, O. A., and K. K. Sabelfeld (2010), Stochastic Flow Simulation and Particle Transport in a 2d Layer of Random Porous Medium, *Transp. Porous Media*, *85*(2), 347–373, doi:10.1007/s11242-010-9567-y.
- Lundgren, T. S. (1969), Model Equation For Nonhomogeneous Turbulence, *Phys. Fluids*, *12*(3), 485–497.
- McDermott, R., and S. Pope (2007), A particle formulation for treating differential diffusion in filtered density function methods, *J. Comput. Phys.*, *226*(1), 947–993, doi:10.1016/j.jcp.2007.05.006.
- Meyer, D. W., P. Jenny, and H. A. Tchelepi (2010), A joint velocity-concentration PDF method for tracer flow in heterogeneous porous media, *Water Resour. Res.*, *46*(12), 1–17, doi:10.1029/2010WR009450.

- Minier, J.-P., and E. Peirano (2001), The pdf approach to turbulent poly-dispersed two-phase flows, *Phys. Rep.*, *352*(1-3), 1–214, doi:10.1016/S0370-1573(01)00011-4.
- Minier, J.-P., S. Chibbaro, and S. B. Pope (2014), Guidelines for the formulation of Lagrangian stochastic models for particle simulations of single-phase and dispersed two-phase turbulent flows, *Phys. Fluids*, *26*(11), 113,303, doi:10.1063/1.4901315.
- Morales-Casique, E., S. P. Neuman, and A. Guadagnini (2006a), Nonlocal and localized analyses of nonreactive solute transport in bounded randomly heterogeneous porous media: Computational analysis, *Adv. Water Resour.*, *29*(9), 1399–1418, doi:10.1016/j.advwatres.2005.10.014.
- Morales-Casique, E., S. P. Neuman, and A. Guadagnini (2006b), Non-local and localized analyses of non-reactive solute transport in bounded randomly heterogeneous porous media: Theoretical framework, *Adv. Water Resour.*, *29*(8), 1238–1255, doi:10.1016/j.advwatres.2005.10.002.
- Mustata, R., L. Valiño, C. Jiménez, W. P. Jones, and S. Bondi (2006), A probability density function Eulerian Monte Carlo field method for large eddy simulations: Application to a turbulent piloted methane/air diffusion flame (Sandia D), *Combust. Flame*, *145*(1-2), 88–104, doi:10.1016/j.combustflame.2005.12.002.
- Möbus, H., P. Gerlinger, and D. Brüggemann (2001), Comparison of Eulerian and Lagrangian Monte Carlo PDF methods for turbulent diffusion flames, *Combust. Flame*, *124*(3), 519–534, doi:10.1016/S0010-2180(00)00207-8.
- Pasetto, D., A. Guadagnini, and M. Putti (2011), POD-based Monte Carlo approach for the solution of regional scale groundwater flow driven by randomly distributed recharge, *Adv. Water Resour.*, *34*(11), 1450–1463, doi:10.1016/j.advwatres.2011.07.003.
- Pierce, C. D., and P. Moin (1998), A dynamic model for subgrid-scale variance and dissipation rate of a conserved scalar, *Phys. Fluids*, *10*(12), 3041–3044, doi:10.1063/1.869832.
- Pope, S. B. (1976), The Probability Approach to the Modelling of Turbulent Reacting Flows, *Combust. Flame*, *27*, 299–312.
- Pope, S. B. (1981), A Monte Carlo method for the PDF equations of turbulent reactive flow, *Combust. Sci. Technol.*, *25*, 159–174.
- Pope, S. B. (1985), PDF Methods for Turbulent Reactive Flows, *Prog. Energy Combust. Sci.*, *11*(2), 119–192, doi:10.1016/0360-1285(85)90002-4.

- Pope, S. B. (2000), *Turbulent Flows*, Cambridge University Press, Cambridge.
- Popov, P. P., and S. B. Pope (2014), Implicit and explicit schemes for mass consistency preservation in hybrid particle/finite-volume algorithms for turbulent reactive flows, *J. Comput. Phys.*, *257*, 352–373, doi:10.1016/j.jcp.2013.09.005.
- Raman, V., and H. Pitsch (2007), A consistent LES/filtered-density function formulation for the simulation of turbulent flames with detailed chemistry, *Proc. Combust. Inst.*, *31*(2), 1711–1719, doi:10.1016/j.proci.2006.07.152.
- Renard, P., and G. d. Marsily (1997), Calculating equivalent permeability: a review, *Adv. Water Resour.*, *20*(5-6), 253–278, doi:10.1016/S0309-1708(96)00050-4.
- Rubin, Y., A. Sun, R. Maxwell, and A. Bellin (1999), The concept of block-effective macrodispersivity and a unified approach for grid-scale and plume-scale-dependent transport, *J. Fluid Mech.*, *395*, 161–180.
- Sabel’nikov, V., M. Gorokhovski, and N. Baricault (2006), The extended IEM mixing model in the framework of the composition PDF approach: applications to diesel spray combustion, *Combust. Theory Modell.*, *10*(1), 155–169, doi:10.1080/13647830500348109.
- Sabel’nikov, V., and O. Souldard (2005), Rapidly decorrelating velocity-field model as a tool for solving one-point Fokker-Planck equations for probability density functions of turbulent reactive scalars, *Phys. Rev. E*, *72*(1), doi:10.1103/PhysRevE.72.016301.
- Sanchez-Vila, X., A. Guadagnini, and D. Fernández-García (2009), Conditional Probability Density Functions of Concentrations for Mixing-Controlled Reactive Transport in Heterogeneous Aquifers, *Math. Geosci.*, *41*(3), 323–351, doi:10.1007/s11004-008-9204-2.
- Schwarze, H., U. Jaekel, and H. Vereecken (2001), Estimation of macrodispersion by different approximation methods for flow and transport in randomly heterogeneous media, *Transp. Porous Media*, *43*(2), 265–287, doi:10.1023/A:1010771123844.
- Schwede, R. L., O. A. Cirpka, W. Nowak, and I. Neuweiler (2008), Impact of sampling volume on the probability density function of steady state concentration, *Water Resour. Res.*, *44*(12), doi:10.1029/2007WR006668.
- Schüler, L., N. Suciú, P. Knabner, and S. Attinger (2016), A time dependent mixing model to close PDF equations for transport in heterogeneous aquifers, *Adv. Water Resour.*, under review.

- Srzic, V., R. Andricevic, H. Gotovac, and V. Cvetkovic (2013a), Collapse of higher-order solute concentration moments in groundwater transport, *Water Resour. Res.*, *49*(8), 4751–4764, doi:10.1002/wrcr.20371.
- Srzic, V., V. Cvetkovic, R. Andricevic, and H. Gotovac (2013b), Impact of aquifer heterogeneity structure and local-scale dispersion on solute concentration uncertainty: Impact of Aquifer Heterogeneity on Concentration Uncertainty, *Water Resour. Res.*, *49*(6), 3712–3728, doi:10.1002/wrcr.20314.
- Suciu, N. (2014), Diffusion in random velocity fields with applications to contaminant transport in groundwater, *Adv. Water Resour.*, *69*, 114–133, doi:10.1016/j.advwatres.2014.04.002.
- Suciu, N., and C. Vamoş (2009), Ergodic Estimations of Upscaled Coefficients for Diffusion in Random Velocity Fields, in *Monte Carlo and Quasi-Monte Carlo Methods 2008*, edited by P. L’Ecuyer and A. Owen, Springer Berlin Heidelberg, Berlin, Heidelberg.
- Suciu, N., C. Vamoş, J. Vanderborght, H. Hardelauf, and H. Vereecken (2006), Numerical Investigations on Ergodicity of Solute Transport in Heterogeneous Aquifers, *Water Resour. Res.*, *42*(4), 1–17, doi:10.1029/2005WR004546.
- Suciu, N., C. Vamoş, F. A. Radu, H. Vereecken, and P. Knabner (2009), Persistent memory of diffusing particles, *Phys. Rev. E*, *80*(6), doi:10.1103/PhysRevE.80.061134.
- Suciu, N., F. A. Radu, A. Prechtel, F. Brunner, and P. Knabner (2013), A coupled finite element–global random walk approach to advection-dominated transport in porous media with random hydraulic conductivity, *J. Comput. Appl. Math.*, *246*, 27–37, doi:10.1016/j.cam.2012.06.027.
- Suciu, N., F. A. Radu, S. Attinger, L. Schüler, and P. Knabner (2015a), A Fokker-Planck approach for probability distributions of species concentrations transported in heterogeneous media, *J. Comput. Appl. Math.*, *289*, 241–252, doi:10.1016/j.cam.2015.01.030.
- Suciu, N., L. Schüler, S. Attinger, C. Vamoş, and P. Knabner (2015b), Consistency issues in PDF methods, *An. St. Univ. Ovidius Constanta, Ser. Mat.*, *23*(3), 187–208, doi:10.1515/auom-2015-0055.
- Suciu, N., L. Schüler, S. Attinger, and P. Knabner (2016), Towards a filtered density function approach for reactive transport in groundwater, *Adv. Water Resour.*, *90*, 83–98, doi:10.1016/j.advwatres.2016.02.016.
- Tennekes, H., and J. L. Lumley (1972), *A First Course in Turbulence*, MIT Press, Cambridge, Mass.

- United Nations (2010), The human right to water and sanitation, *Resolution 64/292*.
- Valiño, L. (1998), A field Monte Carlo formulation for calculating the probability density function of a single scalar in a turbulent flow, *Flow, Turbul. Combust.*, *60*(2), 157–172, doi:10.1023/A:1009968902446.
- Vamoş, C., and M. Crăciun (2010), Separation of components from a scale mixture of Gaussian white noises, *Physical Review E*, *81*(5), doi:10.1103/PhysRevE.81.051125.
- Vamoş, C., N. Suciu, and H. Vereecken (2003), Generalized random walk algorithm for the numerical modeling of complex diffusion processes, *J. Comput. Phys.*, *186*(2), 527–544, doi:10.1016/S0021-9991(03)00073-1.
- Vamoş, C., M. Crăciun, and N. Suciu (2015), Automatic algorithm to decompose discrete paths of fractional Brownian motion into self-similar intrinsic components, *Eur. Phys. J. B*, *88*(10), doi:10.1140/epjb/e2015-60515-5.
- Venturi, D., D. Tartakovsky, A. Tartakovsky, and G. Karniadakis (2013), Exact PDF equations and closure approximations for advective-reactive transport, *J. Comput. Phys.*, *243*, 323–343, doi:10.1016/j.jcp.2013.03.001.
- Villermaux, J., and J. C. Devillon (1972), Représentation de la coalescence et de la redispersion des domaines de ségrégation dans un fluide par un modèle d’interaction phénoménologique., in *Proceedings of the 2nd International symposium on chemical reaction engineering*, pp. 1–13, Elsevier New York.
- Wacławczyk, M., J. Pozorski, and J.-P. Minier (2008), New Molecular Transport Model for FDF/LES of Turbulence with Passive Scalar: Special Issue THMT06, *Flow, Turbul. Combust.*, *81*(1-2), 235–260, doi:10.1007/s10494-007-9112-4.
- Wang, H., P. P. Popov, and S. B. Pope (2010), Weak second-order splitting schemes for Lagrangian Monte Carlo particle methods for the composition PDF/FDF transport equations, *Journal of Computational Physics*, *229*(5), 1852–1878, doi:10.1016/j.jcp.2009.11.012.
- Wen, X.-H., and J. J. Gómez-Hernández (1996), Upscaling hydraulic conductivities in heterogeneous media: An overview, *J. Hydrol.*, *183*(1), ix–xxxii.
- WWAP (2012), *The United Nations World Water Development Report 4: Managing Water under Uncertainty and Risk*, no. Vol. 1 in World Water Assessment Programme, Unesco, Paris.

Yee, E., and R. Chan (1997), Comments on "Relationships between higher moments of concentration and of dose in turbulent dispersion", *Boundary Meteorol*, 82(2), 341–351, doi:10.1023/A:1000254829126.

Zetkser, I. S., and L. G. Everett (2004), *Groundwater resources of the world and their use*, UNESCO, Paris.

Acknowledgements

First, I would like to offer my special thanks to my advisor Prof. Dr. Sabine Attinger for the continuous support of my research and for giving me the opportunities to expand my scientific horizon. Her scientific visions have guided me throughout my research. My sincerest gratitude also goes to my advisor PD Dr. Nicolae Suciuc whose great knowledge is only surpassed by the patience with which he guided me. Our discussions have always been thought-provoking. *Multumesc foarte mult.*

Besides my advisors, I thank the CHS department for many different things besides all the interesting discussions we had. I am particularly grateful for the assistance given by following colleagues. Falk Heße always had a sympathetic ear for me, even for the most peculiar questions. Whenever I had problems solving an integral, Alraune Zech was on the spot with a solution. Sebastian Müller's great understanding of many mathematical topics has helped me more than once. Martin Schrön gave me a taste of his mastery over graphics editors. At the beginning of my PhD, Jude Musuza has helped me out when I sometimes felt lost in the bureaucratic machinery and he gave me a kickstart with his numerical code. Vladyslav Prykhodko always had patience with me, when I had yet another question to him. David Schäfer who, as a big fan and advocate of parallelism, indeed parallelised parts of my numerical code with great success. He is the first person I met who might one day understand the deeper magic of Python. And Thomas Grau for proof reading and telling me that my text is too emotional.

Many thanks also go to Ben Langenberg and Christian Krause for their excellent support not only regarding EVE, but for all kind of help regarding computers. I thank Maria König for taking a look at my research from an outside perspective and for keeping me in-line with my ice cream diet. And I thank Sébastien Fries for sharing the same passion for my work and for his persistence.

I wish to thank Mark Schlutow for the many coffees and the long discussions about PDF methods when they were still new to me and full of seemingly unsolvable puzzles.

Very special thanks go to my family. My parents Hanna and Peter Schüler have supported this work indirectly by giving me the best possible start in life. They have always encouraged me to follow my way. Although a wise man once told us that water and electricity do not get along well

together, I think that my brother Malte Schüler and I proof him wrong. I can always count on his honest opinion, when a “real” physicist broadens his mind.

Finally, I want to express my deepest gratitude to Veronika Zeiner who not only directly helped me a lot with this work, but who also helped me keep my motivation high and with whom I can always enjoy life. Thank you!

Selbstständigkeitserklärung

Ich erkläre, dass ich die vorliegende Arbeit selbstständig und unter Verwendung der angegebenen Hilfsmittel, persönlichen Mitteilungen und Quellen angefertigt habe.

Leipzig, 9. Juni 2016

Lennart Schüler